DIPARTIMENTO DI SCIENZE DELLA VITA

DOTTORATO DI RICERCA IN SCIENZE DELLA VITA

XXXIII CICLO

Coordinatore: Prof. Massimo Valoti

"Ultrastructural and immunolocalization studies on the interactions occurring between IntraFlagellar Transport components and the ciliary tip structures during IFT trains turnaround in *Chlamydomonas* flagella"

Settore Scientifico Disciplinare: BIO/05

Relatore: Prof. Pietro Lupetti

Correlatore: Prof.ssa Caterina Mencarelli

Tesi di: Ambra Pratelli

Anno Accademico 2020/2021

Table of Contents

Abstract

Cilia and flagella are dynamic organelles of the eukaryotic cell that undergo cycles of assembly/disassembly, in a manner that is coordinated in time with the cell cycle. Cilia are composed by more than 600 peptides and their turnover occurs at the plus distal end of the axoneme; since these organelles lack the machinery required for protein synthesis, a bidirectional transport process known as the IntraFlagellar Transport (IFT) is required to provide flagellar precursors and remove turnover products.

IFT is carried on by macromolecular complexes (the IFT particles) which are arranged in polymers (the IFT trains) in the space between the microtubular doublets and the flagellar membrane. IFT trains operate as platforms for cargoes and are moved bidirectionally by specific molecular motors, kinesin-2 as the anterograde motor and dynein-1b as the retrograde motor. Anterograde and retrograde IFT trains possess distinct architectures but, up to now, a high-resolution 3D-model is available only for the anterograde trains, while much less is known on the ultrastructure of retrograde trains.

At the distal tip of the organelle, the anterograde transport (from the cell body up to the ciliary distal end or tip) is converted into the retrograde transport (from the tip back to the cell body). Such a turnaround process is strictly required for the correct functioning of the IFT process. So far, however, very little is known about the morpho-functional organization of the tip district, where IFT turnaround takes place. In particular, nothing is known on the interactions that might occur between IFT proteins and the distal tip structures.

This doctoral work has been aimed at contributing new information for the comprehension of the IFT turnaround process in the model organism *Chlamydomonas reinhardtii*.

We started our studies from the observation that thin sections of flat-embedded flagella often show anterograde IFT trains that contact the distal end of the central pair microtubules (CP), suggesting the direct involvement of CP capping structures (terminal plates and the ring above) in the IFT turnaround process. We confirmed the interaction of anterograde trains with the CP distal end by electron-tomographic reconstruction of flat-embedded flagellar tips. This approach revealed that anterograde trains split into three components after having reached the end of the A tubule, with the outer part of the train that remains associated with the membrane, the inner part, closer to the microtubule surface, that continues its travel and bends to contact the CP plates, and an intermediate part that stops before reaching the tip. The latter region was interpreted as the part of the train consisting of inactive dynein-1b, which is known to dissociate from the anterograde train before its activation and recruitment for the retrograde transport.

Then, we sought to obtain further information on the ultrastructural organization of the distal CP segment. We were able to identify a ladder-like structure (LLS) which is distinctive of this region, is intercalated between the two CP tubules, and is resistant to the cold treatments used to depolymerize tubulin.

In order to confirm the association between IFT anterograde trains and the capping CP structures, whole cells were treated with inhibitors of Ca^{++}-dependent protein kinases before flagellar demembranation and negative staining. These inhibitors block the release of kinesin-2 from the anterograde trains and, consequently, IFT turnaround at the tip. As expected, we observed a massive accumulation of IFT particles around the CP terminus.

Successively, we analyzed by immunoelectronmicroscopy the specific distribution of the three protein complexes present within the IFT particles. At this purpose, we carried out a series of immunolabeling experiments on grid-absorbed demembranated cells or on sections of resin-embedded samples, using antibodies directed against subunits of the IFT-A complex (IFT139), and of the two IFT-B subcomplexes IFT-B1 (IFT74 and IFT81) and IFT-B2 (IFT172 and IFT57).

Our findings suggest that at the tip the IFT-A complex is closely associated with the membrane. On the contrary, both IFT-B1 and IFT-B2 antibodies labelled the distal CP region, though, interestingly, with distinct spatial distributions. IFT-B2 labeling was restricted to approximately the distal 200 nm-segment of the CP, which contains the LLS, and gold particles were never found more distally, above the terminal plates, while IFT-B1 labeling extend also to the ring. The whole set of immunoelectronmicroscopy data indicates that the IFT-B1 and IFT-B2 subcomplexes differentially interact with the distal CP region and its capping structures, and suggests that the IFT-B1 subcomplex might be a main component of the CP capping structures. Accordingly, in our negatively stained samples the cap was shown to consist of thin elongated elements, frequently with a sort of small knob at their mid region; these elements fit quite well with the available IFT-B 3D model. The possibility that IFT-B1 proteins are involved in the formation of the CP cap was confirmed by the analysis of a series *Chlamydomonas* mutants with defective IFT, which related the presence of the CP cap to the establishment of a fully cycling IFT process.

Our data sustain a model of IFT turnaround in which *i)* the IFT-A complex turns around quickly, remaining associated with the membrane, *ii)* IFT-B1 and IFT-B2 follow a more complex pathway, during which they separate and differentially interact with the CP distal segment, *iii)* IFT-B1 directly contribute to the formation of the CP cap. The LLS component, which is ectopically assembled also in mutant strains devoid of the CP tubules, is likely to act as an anchoring structure for IFT-B2 during IFT turnaround.

1. Introduction

1.1 Cilia and Flagella: an introduction

Cilia and flagella (homologous microtubule-based organelles) are thin thread-like extensions protruding from the surface of most eukaryotic cells, in organisms ranging from protists to humans.

These specialized organelles are optimized to interact with the space surrounding the cell: they are structurally resilient but also flexible and dynamic, and they have peculiar lipid and protein composition, differentiated from that of the cell body. These features enable them to perform distinctive functions, including sensory reception, cell signaling, and motility.

From a historical perspective, cilia are among the earliest observed organelles; they were discovered in the 17th century by van Leeuwenhoek (1677) and noted for their remarkable motility properties. In the late 1800s, the Swiss anatomist Karl Zimmermann supposed a sensory role for these protrusions but, afterward his observations, studies on these organelles went through a long stop. After a century, a revival of interest occurred when an immotile cilium was observed emerging from the surface of mammalian cells, which was defined as the primary cilium (Sorokin, 1962, 1968).

The advent of electron microscopy (EM) provided new opportunities for the analysis of ciliary architecture. In 1954, a comparative analysis carried out by Fawcett and Porter on thin sections of samples from mollusks, amphibians, mice and humans revealed that cilia and flagella share an internal cytoskeletal structure - the axoneme - built of a ring of nine doublet “filaments” and a central pair of singlet “filaments” (fig.1). Also, this study showed that cilia originate from complex elongated basal corpuscles, or basal bodies, from which ciliary rootlets (striated fibers) extend downward into the cytoplasm, likely to anchor them (Fawcett and Porter, 1954). Since then, most studies focused on motile cilia, which showed an obvious function. In contrast, the immotile primary cilium was believed for a long time to be a vestigial organelle with dispensable role (Currie and Wheatley, 1966; Wheatley, 1969).

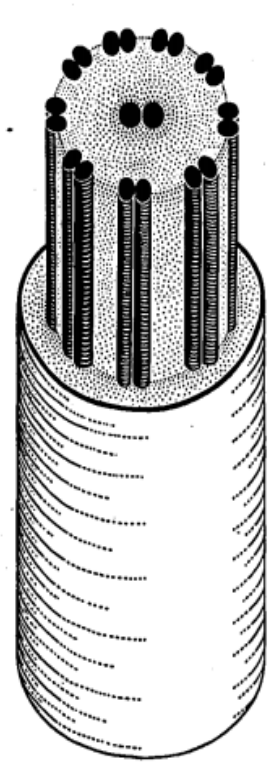

Figure 1: Schematic of the ciliary architecture, as first proposed by Fawcett. In his electronmicroscopy studies, the Author described the presence in cilia of nine longitudinal pairs of "filaments" arranged around two single filaments located in the center of the structure (modified from Fawcett, 1954).

As a matter of fact, the primary cilium mediates several cellular processes, that are critical for both the embryonic development and tissues homeostasis (reviewed by Satir and Christensen, 2007; Goetz and Anderson, 2010; Daems et al., 2020); however, this organelle acquired fame only in the late 1990s, after the discovery of the IntraFlagellar Transport (IFT) by Kozminski and Rosenbaum, in 1993. IFT was first described as an ongoing transport of particles occurring along *Chlamydomonas* flagella, and was later shown to be a highly specialized, microtubule-dependent transport system for the delivery of protein precursors to the flagellar compartment, a process that is essential for the assembly and maintenance of all eukaryotic cilia, both motile and immotile (Cole et al.,1998; Pazour et al., 1998).

As the relationship between ciliary structural anomalies and some human genetic diseases became more and more evident, the crucial functional role of primary cilia was definitely established.

The first evidence was reported by Pazour et al. (2000), who showed how the pathogenesis of polycystic kidney disease is related to the assembly of shorter, defective primary cilia in the kidney epithelial cell. This study paved the way to the comprehension of the molecular defects that - affecting ciliary structure and function - underly several human diseases, now collectively known

as ciliophaties (Brown and Witman, 2014; Braun and Hildebrandt, 2017; Wallmeier et al., 2020).This term defines a wide spectrum of diseases sharing a group of common clinical features, such as blindness, obesity, cognitive impairment, skeletal anomalies, chronic respiratory problems, infertility, *situs inversus* and polycystic kidneys. The number of established ciliopathies as well as of the candidate genes involved therein are still rising (reviewed by Reiter and Leuroux, 2017), adding further corroboration to the currently accepted view of cilia and flagella as "cellular antennae" that mediate and integrate several signal transduction modules crucial for a variety of cellular functions (Brown and Zhang, 2020).

1.2 Ciliary Organization

Regardless of the diversity that can be observed among the numerous known types of specialized cilia, the overall ciliary architecture and a majority of ciliary protein components have been highly conserved during eukaryotic evolution (reviewed by Satir et al., 2008).

At the ultrastructural level, cilia and flagella consist of three main segments, namely, the basal body (BB), the transition zone (TZ), and the axoneme, enclosed by the ciliary membrane (fig. 2).

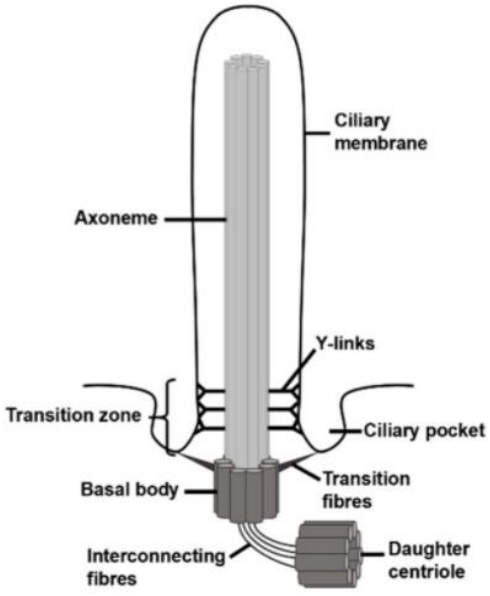

Figure 2: The cilium consists of three principal domains, the basal body, the transition zone and the axoneme (modified from Wiegering et al., 2019).

1.2.1 The Basal Body (BB) and the Ciliogenesis

In 1954, Fawcett and Porter were the first to report centrioles and BB as two ultrastructurally identical and related organelles, which convert each other during the cell cycle, so that basal bodies are essentially membrane-docked centrioles. The centrosome of each cell contains an older 'mother' centriole and a 'daughter' centriole that has been newly generated just before the preceding mitosis; the two centrioles differ for the presence of two sets of appendages on the mother centriole, the so-called distal and subdistal appendages (fig. 3) (Paintrand et al., 1992). In quiescent or interphase (G1 phase) cells, the centrosome migrates to the cell surface; meanwhile, the distal and subdistal appendages on the mother centriole act as sites for the anchoring of a primary ciliary vesicle and, successively, assist with plasma membrane docking (fig. 3) (Sorokin, 1962; reviewed by Izawa et al., 2015).

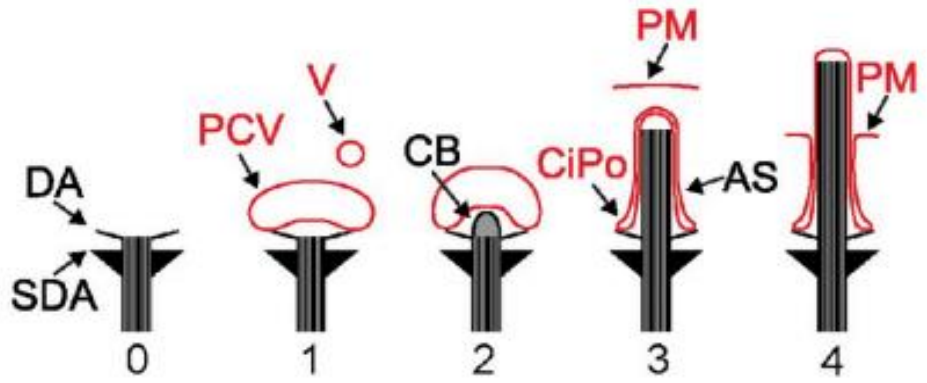

Figure 3: Scheme illustrating the different stages of early ciliogenesis. The M-centriole with its distal (DA) and subdistal appendages (SDA) is shown (0). Early stages involve the docking of primary ciliary vesicles (PCVs) at the M-centriole (1), while nearby secondary vesicles (V) are subjected to a subsequential fusion with the PCVs. Accumulation of electron-dense material at the distal end of the M-centriole builds the so-called ciliary bud (CB), which invaginates the PCV (2). The axonemal shaft (AS) grows out and the ciliary pocket (CiPo) forms (3). During the last event, the cilia membrane fuses with the apical plasma membrane (PM) (4). M-centriole and axonemal shaft are illustrated in black, and membrane structures are shown in red (modified from Schmidt et al., 2012).

Upon completion of these events, the mother centriole is structurally and functionally transformed into the basal body of the cilium, but still remains connected to the daughter centriole by filaments at its proximal end; thus, the daughter centriole is oriented roughly perpendicular to the basal body (fig. 2) (Bahe et al., 2005). Once docked to the plasma membrane, the basal body functions as the microtubule organizing center for the cilium, serving as a template for the assembly of microtubular doublets. During this process, the basal body and its appendages (now named as the transition fibers) are also involved in docking the protein components of IFT before their entering into the ciliary compartment.

In addition, structures linking the BB to the plasma membrane control the exchange of membrane and soluble proteins between the two compartments (reviewed by Garcia-Gonzalo and Reiter, 2012).

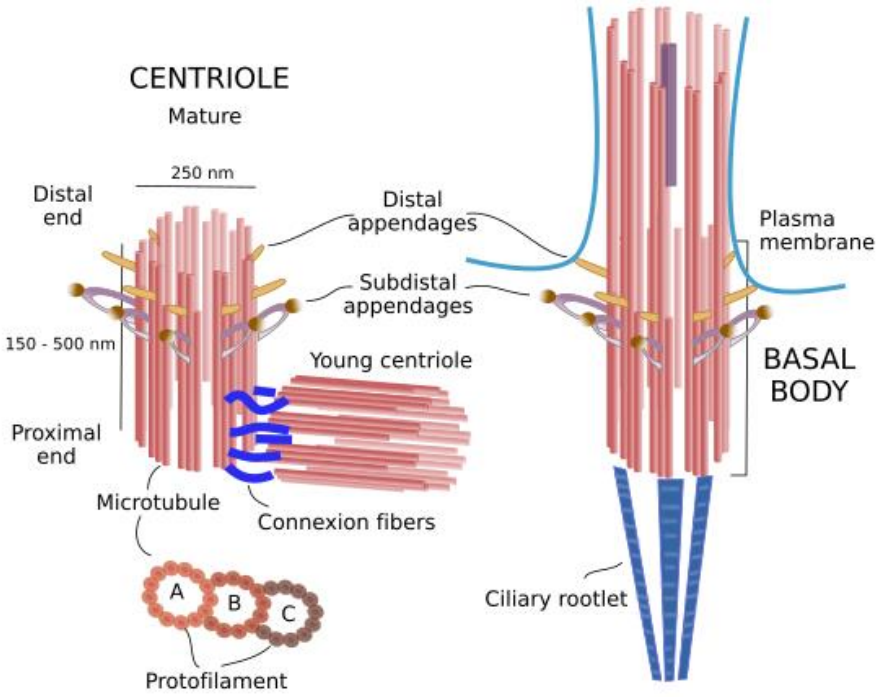

Figure 4: Structural organization of centrioles, barrel-shaped structures involved in ciliogenesis. The mother centriole docks to the plasma membrane and originates the flagellum (from Megias et al., 2019).

Ciliogenesis is a finely regulated and elaborated process that involves several cellular processes, from gene transcription and protein synthesis, to the delivery of ciliary precursors up to the tip, from microtubule dynamics to signal transduction (reviewed by Santos and Reiter, 2008; Ishikawa and Marshall, 2011; Kobayashi and Dynlacht, 2011).

There is a well-established link between ciliary dynamics and cell cycle progression; in fact, in proliferating tissues, cilia are resorbed as cells enter the cell cycle (Tucker et al., 1979).

In most cells the cilium is resorbed before mitosis, allowing the two centriole pairs (resulting from the duplication of the mother and the daughter centriole during the S phase) to detach from the cell cortex and move to the spindle poles, which they help to organize and position (Tucker et al., 1979). Cilia are then re-formed after re-entry of each daughter cell into the G_1 phase, when the BB is established by plasma membrane docking of the mother centriole (Anderson, 1972; Ishikawa et al., 2005; Tanos et al., 2013). Some conditions, such as progression through G2 or differentiation into an unciliated cell type, cause ciliary disassembly. However, the pathways regulating cilium disassembly are less well characterized (reviewed by Wang and Dynlacht, 2018).

The main steps of centriole to basal body conversion, cilia elongation and resorption along the cell cycle are schematized in fig. 5.

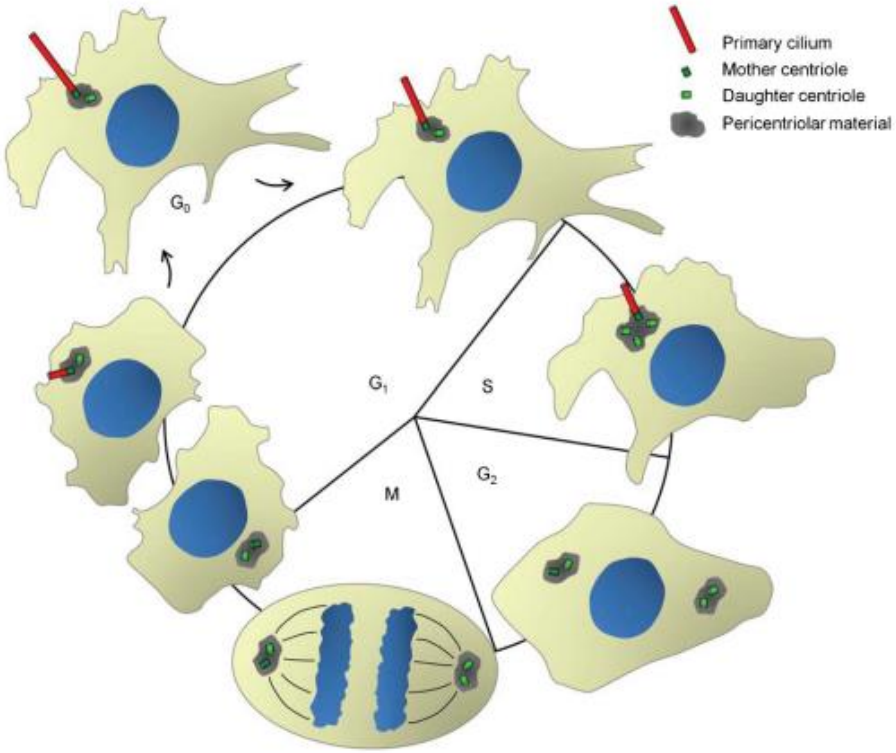

Figure 5: Cilia and the cell cycle. Assembly and disassembly of primary cilia are tightly coordinated with the cell cycle (from Pedersen et al., 2012).

1.2.2 The Transition Zone

The region comprised between the distal end of the basal body C-tubules and the beginning of the axonemal central pair tubules is referred to as the transition zone (TZ), a ciliary subdomain that plays a fundamental role in the compartmentalization of the cilium. The TZ operates as a gate between the cell and the cilium and strictly controls inbound as well as outbound ciliary trafficking, by selecting specific proteins for entry into the cilium and avoiding the entrance of others (reviewed by Reiter et al., 2012; Jensens and Leroux, 2017).

The TZ architecture is characterized by the presence of microtubule-ciliary membrane connectors, usually the Y-links, so called for their peculiar shape, and by the ciliary necklace, a specialized membrane domain characterized by rows of membrane particles encircling the base of the axoneme. In comparison to the basal body and the axoneme, the ultrastructure of the TZ may present considerable variations in different species, and further additional components may occur (Jana et al., 2018). Genetic interaction studies in *C. elegans*, along with the biochemical analysis of

protein-protein interactions in mammalian systems, revealed the presence of three main TZ protein modules, the MKS, NPHP and CEP290 modules. TZ modules are composed of soluble and membrane-associated proteins which cooperate to the assembly and establishment of TZ gating functions (fig. 6); each TZ module is composed of multiple proteins that can be co-purified and are interdependent for their localization to the TZ (Chih et al., 2011; Garcia-Gonzalo et al., 2011; Sang et al., 2011; Okazaki et al., 2020).

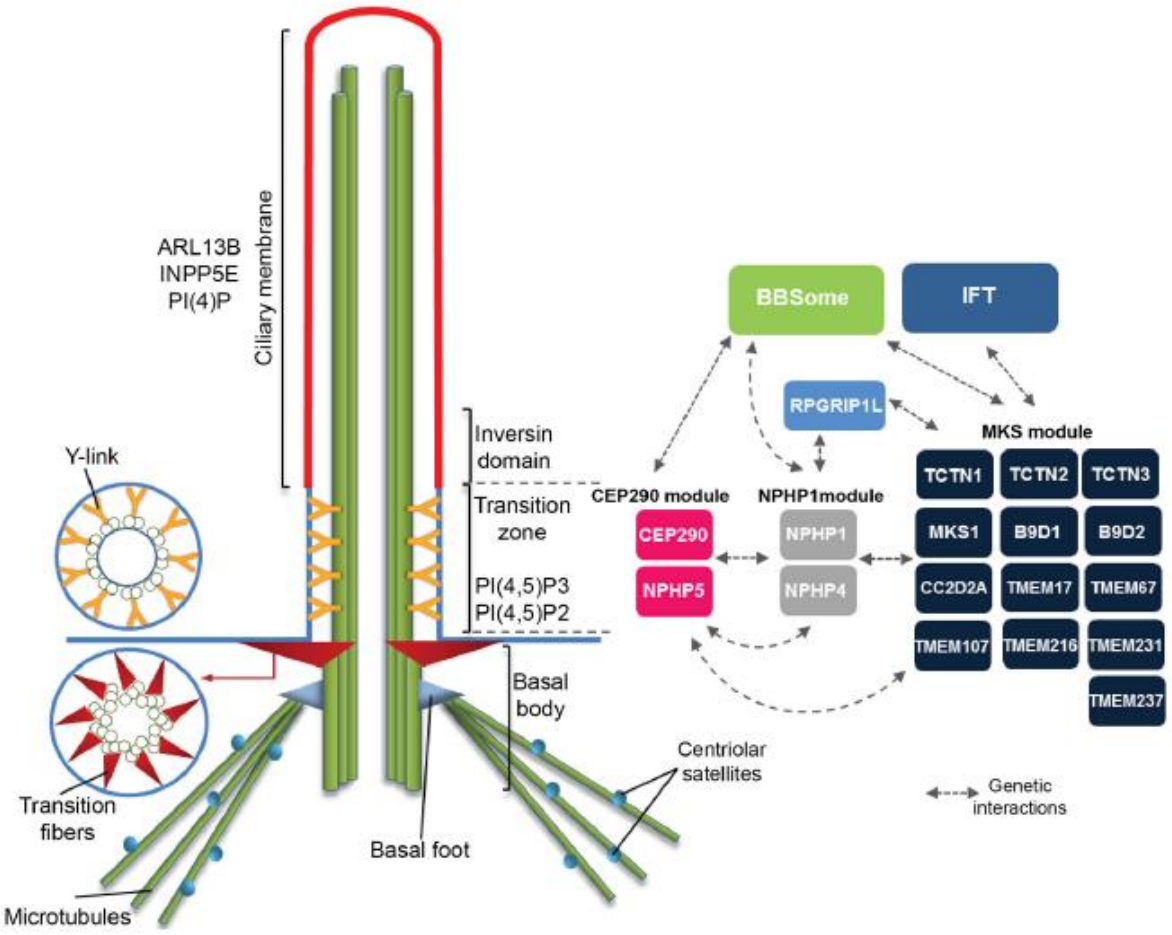

Figure 6: The figure shows the protein modules present at the transition zone and their interactions. The ciliary membrane is a specialized membrane domain, enriched in specific proteins (e.g. ARL13B) and lipid species (e.g. PI(4)P) (from Gonçalves and Pelletier, 2017).

Proteomic analysis of TZ isolated from the model organism *C. reinhardtii* identified most of the components that had been previously described in other species (e.g., NPHP4 and CEP290) and six proteins of the Endosomal Sorting Complexes Required for Transport (ESCRT), which could function in membrane sealing during flagellar and TZ shedding (Diener et al., 2015). The role of ESCRT proteins in ciliary membrane dynamics has been implicated also in the formation of ciliary ectosomes (Diener et al., 2015; Long et al., 2015).

The evolutionary conservation of the TZ proteins was analyzed in a subsequent study by Dean et al. (2016) on *Trypanosoma* TZ proteome; these authors established that 34% and 36% of TZ proteins have human or *Chlamydomonas* orthologs, respectively, and revealed that some of these proteins play essential roles in flagellum biogenesis and motility.

Recently, the TZ has been shown to act also as a lipid gate, in maintaining a definite ciliary membrane phosphoinositide (PI) composition (fig. 6; see also below).

1.2.3 The Axoneme

Eukaryotic cilia and flagella are essentially divided into two groups, motile or not motile, that are characterized by distinct structural organization (fig. 7).

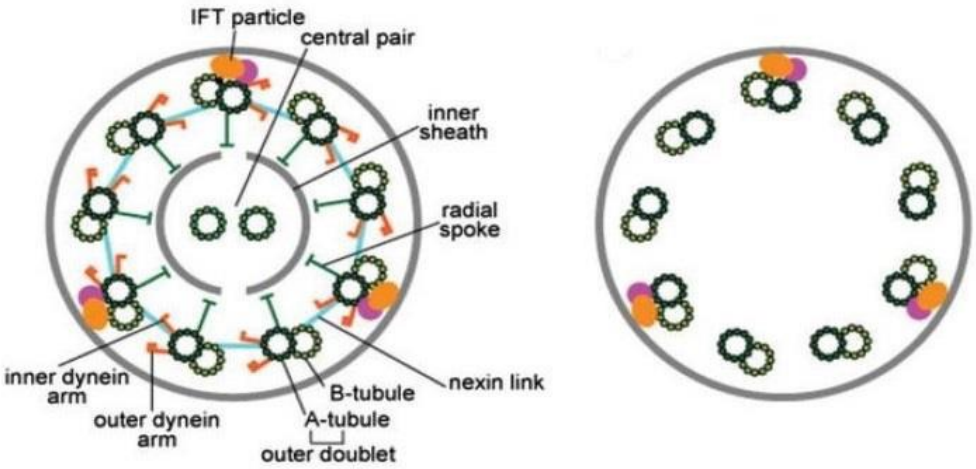

Figure 7: The axonemal 9+2 and 9+0 architectural patterns. Compared with the '9+2' organization, the '9+0' axoneme lacks the central pair as well as all the accessory structures required for motility, like the dynein arms and the radial spokes (from Nakayama and Katoh, 2020).

Motile cilia are most commonly characterized by the so-called "9+2" axoneme, consisting of 9 microtubular doublets (MTDs) that surround two central pair (CP) singlet microtubules; each doublet consists of one complete microtubule (the A-tubule) and an incomplete one (the B-tubule). In addition to the presence of the CP, motile cilia and flagella also exhibit a series of structural components which are all involved in motility; these are the outer and inner dynein arms (ODAs, IDAs), the associated nexin links (or dynein-regulatory complex), and the radial spokes (RS), all located on the A-tubule, as well as projections on the two CP tubules. The whole set of projections

is present along most of the axoneme, being missing only in its most distal region, where only the A-tubules occur (fig. 8).

Motility is thought to be induced by a signal transduction pathway that originates from the CP and is transmitted by the RS to IDAs, with ODAs being only a sort of accelerator, not essential for the determination of bending waveform. In fact, mutants lacking the RS or the CP are all paralyzed under physiological stimuli for beating conditions, and many IDAs mutants have abnormal beating, or are unable to beat (reviewed by Kamiya, 2002), while mutants missing ODAs swim slowly and with a reduced frequency, but show an almost normal flagellar waveform (Oda et al., 2013).

The tubulin of the outer doublets is usually subjected to various post-translational modifications, including acetylation, polyglutamylation, and polyglycylation, which are known to be important for the assembly, stability and motility of cilia (Orback and Howard, 2019).

Non-motile cilia typically lack any structural component related to motility, including the CP, and hence exhibit a “9+0” axonemal pattern. These organelles are also called “primary cilia”, a term first coined by Sorokin (1968) in his studies on ciliogenesis during pulmonary development.

Primary cilia are essentially sensory organelles, which act as signaling centers for various pathways, including Hedgehog, Notch, Wnt, and growth factor signaling (Falk et al., 2015). Modified primary cilia are present in peculiar and highly specialized postmitotic cells; these include, e.g., the connecting cilium of photoreceptors, which detects light, and olfactory cilia, which detect odorants (reviewed by Berbari et al., 2009).

In their recent EM analysis, Kiesel et al. (2020) noticed that the “9+0” canonical architecture of primary cilia is initially present at the proximal end of the organelle but, gradually, microtubules migrate toward the center of the axoneme and between 2 and 5 μm distal to the BB most B-tubules terminate. Therefore, the distal three-quarters of the axoneme are composed of singlets and the axoneme diameter reduces to about one half (Kiesel et al., 2020).

Although cilia had been historically classified as either motile or immotile sensory cilia, several exceptions are known. In fact, many protists possess flagella that function in both motility and sensory reception (reviewed by Fliegauf and Omran, 2006). Additionally, vertebrates have partially motile 9+0 cilia paving the embryonic node, that retain a few dynein arms randomly distributed along the doublets and are thus able to generate the fluid movement essential for left-right body axis determination in developing embryos (Nonaka et al., 1998). Also, the mature kinocilia occurring in the inner ear of mammals and fish are considered immotile, but have 9+2 structures (Flock and Duvall, 1965; reviewed by Dabdoub and Kelley, 2005).

1.2.4 The Ciliary Tip

The ciliary tip is probably the most enigmatic flagellar district; yet, this compartment is the site where several processes that are critical for cilia assembly and function occur.

Most cilia and flagella tend to narrow towards their distal end, presenting a slightly pointed tip. This region is characterized by a progressive modification of the 9+2 or 9+0 axoneme pattern, the peripheral microtubule doublets become singlets, due to the termination of the B-tubule, so that the distal district contains only the A-tubules; all the different types of projections that are associated with the A-tubules and the CP in 9+2 axonemes are missing at the ciliary tip.

The CP is usually observable until the end of the flagellum, and terminates in complex capping structures, located between the CP and the membrane, that are still very poorly characterised and may exhibit different structures in different cell types and animal species (reviewed by Soares et al., 2019).

The ultrastructural characterization of the distal tip components has in fact encountered several difficulties, so that, since the first observations carried out around 80s in the two protists *Chlamydomonas* and *Tetrahymena*, no further accurate study has been reported and our knowledge on this ciliary district has not been significatively improved.

The first electron microscopy images of the most distal region of *Chlamydomonas* flagella were reported by Ringo (1967) in a detailed study of thin sections of resin-embedded samples. The author reported the presence of an electrondense “tip sheet” intercalated between the two CP tubules, as well as of components located between the CP and the tip membrane (figure 8); however, these observations could not allow to clearly understand the structural organization of the latter components. These could be more clearly visualized some years later by negative staining of demembranated *Chlamydomonas* flagella (Dentler and Rosenbaum, 1977), and of *Tetrahymena* cilia (Dentler, 1980). This methodological approach allowed the observation of the whole distal domain components. The two protist species exhibit quite similar structures associated with the distal CP tip, which were described by Dentler (1980) as composed of two plates oriented perpendicularly to the microtubule longitudinal axis, and of an overlying spherical bead about 50 nm in diameter; thin links connect the two plates and other links anchor the bead to the membrane (fig. 9). Also, the A-tubules of the outer doublets of the axoneme terminate in a pair of filaments, known as distal filaments, emerging from a plug-like structure that is inserted into the lumen of the A-tubule (fig. 9).

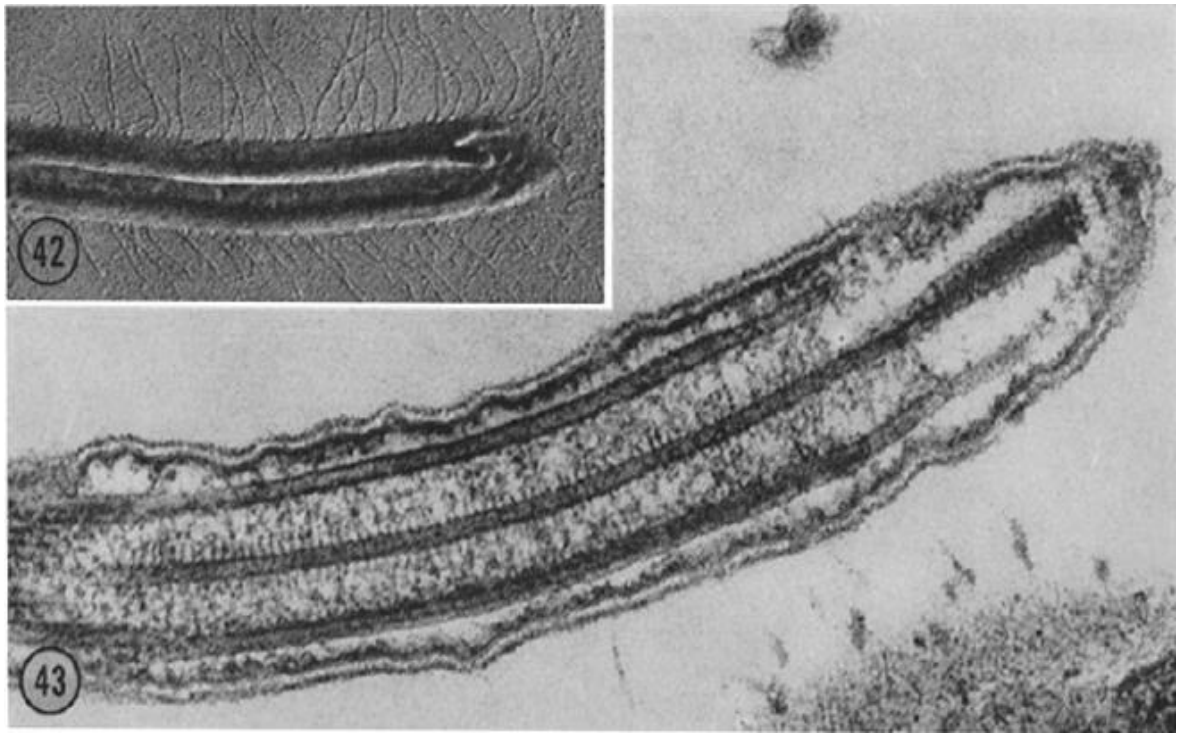

Figure 8: *Chlamydomonas* flagellar tip ultrastructure. For images like the one shown in the top panel (left side) cells were prepared by freeze-drying and shadowed with platinum-carbon. The bottom panel shows a thin section from a resin-embedded sample, in which the peculiar organization of the flagellar tip is evident (modified from Ringo, 1967).

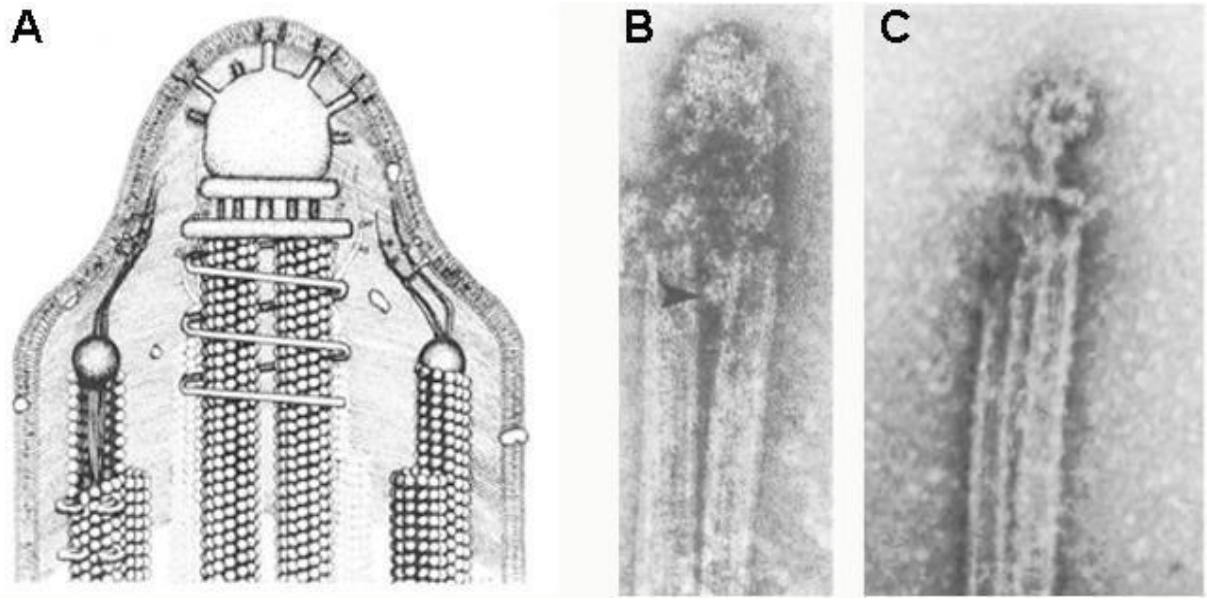

Figure 9: The capping structures occurring at the distal end of the CP microtubules (A) as schematized by Dentler (1980); in B and C these are visualized after negative staining of demembranated *Chlamydomonas* flagella and *Tetrahymena* cilia, respectively (modified from Dentler 1980, 1984).

In other ciliary types, the distal structures have been observed only on sections of resin-embedded samples, an approach that cannot provide a good resolution of the tip components; essentially, some ciliary types from different organisms exhibit an amorphous electron-dense material that encloses the distal ends of doublet and central microtubules (schematized in fig. 10).

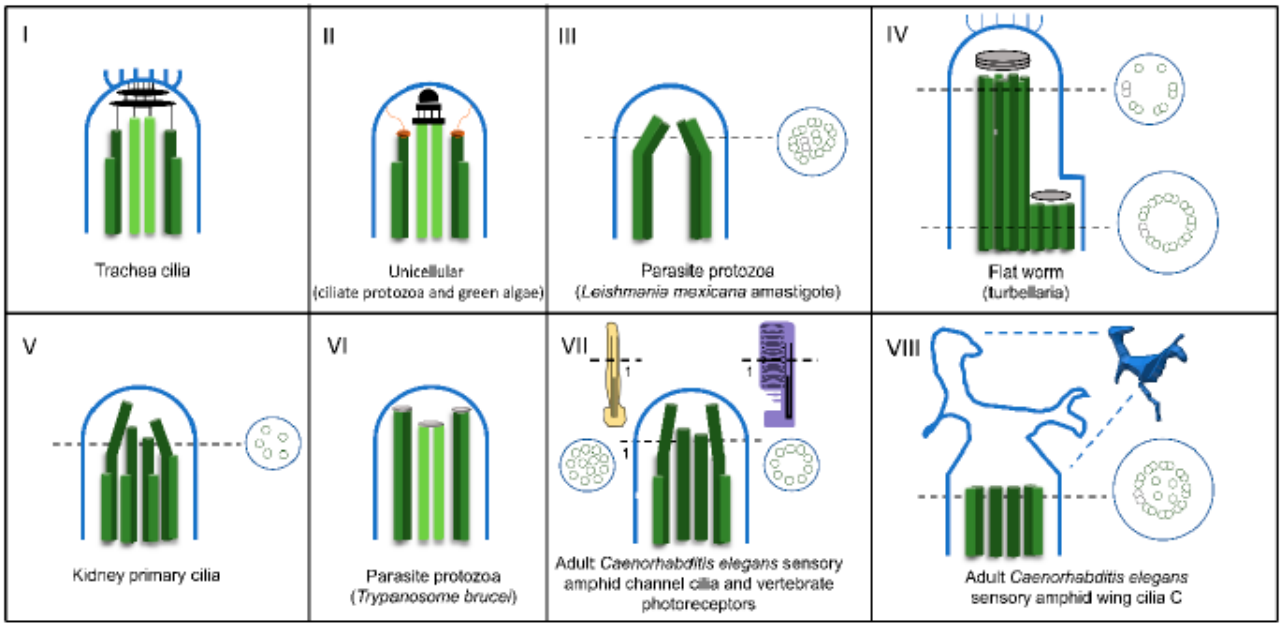

Figure 10: Schematic representation of known ciliary tip structures (from Soares et al., 2019).

In mammalian epithelial cilia, as those of oviduct and respiratory epithelia, the CP amorphous cap is connected to a structure -the ciliary crown- constituted by a cluster of fibrils emanating from the ciliary membrane at the very tip of the organelle (Dirksen and Satir, 1972; Cordier, 1975; Jeffery and Reid, 1975). Similar structures occur in the cilia of other vertebrates and invertebrates (reviewed by Soares et al., 2019). Interestingly, it was observed that the cilia crown was absent from the mouse developing oviduct cilia, appearing only when their growth is complete (Dirksen and Satir, 1972; Kuhn and Engleman, 1978). These findings may imply that the tip structure modifies along ciliary maturation, and not only among mature cilia form different organisms.

Primary cilia distal tips seem to lack cap structures or even any electron-dense material (reviewed by Pedersen et al., 2012; Sun et al., 2019; Kiesel et al., 2020). In primary cilia of cultured cells, the 9+0 architecture is restricted to the proximal ciliary segment, then is gradually replaced by an unordered bundle of microtubules decreasing in number towards the tip, so that these cilia progressively narrow to show only a few singlet microtubules at their distal tip (Kiesel et al., 2020).

As to the function of CP capping components, it was proposed that they might be involved in regulating the assembly of CP microtubules, or in providing further reinforcement to the axoneme during flagellar beating (Dentler and LeCluyse, 1982).

Compared to other ciliary domains, very little is known about the molecular composition of the tip. This limited knowledge is probably to be ascribed to the lability of these structures that makes their purification and biochemical characterization difficult (Dentler and Rosenbaum, 1977; Miller et al., 1990; reviewed by Fisch and Dupuis-Williams, 2011).

Proteins that have been assigned to the tip district have been all localized here by immunofluorescence microscopy and have not been related to any defined structural component. The first protein related to the tip was a *Tetrahymena* protein of 97 kDa, detected with autoantibodies of patients with CREST (Calcinosis/Raynaud's phenomenon/Esophageal dysmotility/Sclerodactyly/Telangiectasis), used as kinetochore markers (Miller et al., 1990); these first results suggested the hypothesis that caps and kinetochores might have similar regulatory mechanisms for microtubule polymerization/depolymerization. However, the identity of the *Tetrahymena* protein(s) recognized by these sera remains unknown.

A number of proteins resident at the ciliary tip have been identified and can be clustered in distinct functional groups: 1) molecular chaperones, 2) regulators of microtubule dynamics at the distal plus end, 3) kinesin proteins, 4) cap structural proteins (reviewed by Soares et al., 2019).

1. Molecular chaperones have been identified in the cilium compartment, some of which accumulate at the tip; among these, Hsp70 (Heat shock 70 kDa protein) is present in *Chlamydomonas* flagella (Bloch and Johnson, 1995), and TCP-1 (CCT) in *Tetrahymena* mature cilia (Seixas et al., 2003, 2010). The evidence concerning CCT is in agreement with studies carried out in sea urchin embryonic cells and rabbit tracheal cilia (Stephens and Lemieux, 1999). CCT is involved in the correct folding a wide range of newly synthesized proteins including tubulin and actin (Seixas et al., 2003). The occurrence of molecular chaperones at the flagellar tip supports the hypothesis that the cap might be involved in axoneme assembly, and/or in protein quality control during the turnover of ciliary proteins, including tubulin.

2. One class of proteins that play key role at the distal flagellar compartment is that of microtubule plus-end tracking proteins (+TIPs), which accumulate at the growing end (+, plus end) of microtubules to regulate their dynamics, and mediate interactions with other cellular components. End-binding proteins (EBs) operate mainly as scaffolding proteins at the microtubule plus-end, where they show a comet-like distribution and form a docking site for the association of other +TIPs, thereby regulating local protein composition and microtubule dynamics.

In *Chlamydomonas*, the EB1 orthologue (CrEB1) was found to localize to the tip of full-length, growing and shortening flagella, and to the proximal part of basal bodies. At the flagellar tip, CrEB1 has been implicated in IFT turnaround, along with IFT172 (Pedersen et al., 2003). Similarly, EB1 is also present at *Giardia* flagellar tips (Dawson et al., 2007). In metazoan, EB3 localizes at the tip of motile cilia (SchrØder et al., 2011; Larsen et al., 2013); it is also found in the outer segment of isolated mouse photoreceptors, suggesting that it localizes to the tip of different cilia types (Liu et al., 2007).

One of the main EB-interacting proteins is CEP104 (Centrosomal protein of 104 kDa). In mammals, CEP104 is a multidomain protein with TOG and jelly-roll domains (Al-Jassar et al., 2017; Yamazoe et al., 2020) that was identified as an EB-dependent microtubule plus-end-tracking protein (+TIPs) (Rezabkova et al., 2016); CEP104 is crucial for the conversion of the mother centriole to basal body (Satish-Tammana et al., 2013) and has been implicated in the initiation of ciliary growth by interacting with and removing from the distal end of the mother centriole the CP110-CEP97 complex, which prevents ciliary assembly (Jiang et al., 2012; Satish-Tammana et al., 2013; Rezabkova et al., 2016; Al-Jassar et al., 2017). Once flagella are assembled, CEP104 moves and localizes at the flagellar tip (Satish-Tammana et al., 2013). In *Chlamydomonas*, the orthologue of CEP104 is FAP256, and its depletion results in structural abnormalities of the flagellar tip, due to the absence of the singlet zone, with all the doublets and CP tubules ending together at the same level, and the CP missing the usual terminal plates (Satish-Tammana et al., 2013). The tip of the mutant strain appears blunt, more rounded, having lost the characteristic cone-shaped appearance (Satish-Tammana et al., 2013).

Remarkably, also *Tetrahymena* FAP256/CEP104-KO cells present a similar phenotype, with a reduction in the length of the distal segment due to the shortening of both the A-tubules and the central pair regions (Louka et al., 2018). Thus, in both protists, the shortening of the CP region is concomitant with the loss of the ciliary cap (Satish-Tammana et al., 2013; Breslow et al., 2018; Kar et al., 2018; Louka et al., 2018).

Available data support the idea that FAP256/CEP104 i) positively control the A-tubule length, and, when defective, induces the blunt tip phenotype of *Chlamydomonas* FAP256 mutants and, ii) also acts as a platform for the assembly of the cap, probably through an interaction with EB proteins.

3. Other tip-binding proteins that are likely to regulate microtubule dynamics at the distal tip include kinesin-13, that causes a structural conformational change in the tubulin dimers promoting their disassembly in an ATP dependent manner (Desai et al., 1999). In flagella of the parasite protist *Giardia intestinalis*, kinesin-13 localizes with EB1 at the distal tip and a strain

mutated in its coding gene shows a prominent increase in flagellar length (Miller et al., 1990). In agreement, in *Leishmania major,* kinesin-13 overexpression induces flagellar shortening whereas its knockdown yields long flagella (Blaineau et al., 2007). In *Chlamydomonas*, on the other hand, kinesin-13 plays a role during flagellar regeneration and shortening but does not seem to be involved in flagellar length control (Piao et al., 2009).

Another kinesin-like protein, KIF19 (KIF19A), a member of the kinesin-8 class, seems to be involved in cilia length control; it possesses both a microtubule plus-end directed motility and a microtubule depolymerizing activity that acts in a length-dependent mode (Gupta et al., 2006; Varga et al., 2006). In the mouse, KIF19A localizes to ciliary tips and depolymerizes microtubules from their plus ends, being a key regulator of motile cilia length (Niwa et al., 2012).

4. Until now, the only structural protein identified as a tip component is Sentan (Kubo et al., 2008). As mentioned above, human respiratory and oviductal cilia have amorphous caps and a ciliary crown. In these cilia, Sentan localizes exclusively between the ciliary membrane and the peripheral singlet microtubules at the distal narrowed ciliary portion, suggesting that it is involved in bridging singlets to the ciliary membrane. It is noteworthy that Sentan seems to be a specific component of tracheal and oviductal motile cilia tips, since it is not detectable in kidney and RPE1 cells' primary cilia, and it is not expressed in testis. Thus, the tip may also contain cell-type specific proteins.

An interesting report by Satish Tammana et al. (2013), conducted on *Chlamydomonas* flagella by using comparative, quantitative proteomics based on the fact that tip proteins will be approximately twice as concentrated in half-length compared with full-length flagella, identified some hypothetical tip proteins, including small GTP-ase proteins.

How proteins that show a very restricted tip localization, e.g. proteins like CEP104 that are specifically associated only with singlets (the A-tubules or the CP tubules) recognize their microtubule interaction site is not clear. It has been proposed that tubulin post-translational modifications, that are differentially distributed among distinct microtubules (Kubo et al., 2008) may provide specific binding sites within the axoneme. For example, glycylated tubulin isoforms are excluded from mammalian ciliary tip (Dossou et al., 2007).

Molecular information on tip protein constituents is still extremely limited, and, in particular, no information is available on proteins involved in the formation of the capping structures.

1.3 The IntraFlagellar Transport (IFT)

Cilia are composed by more than 600 proteins, the so called "ciliome" (Pazour et al., 2005; Inglis et al., 2006; Ishikawa et al., 2012) and their turnover occurs at the plus, distal end of the axoneme. These organelles lack the machinery required for protein synthesis, and a bidirectional transport process known as the IntraFlagellar Transport (IFT) is required to provide flagellar precursors and remove turnover products, thus ensuring assembly, disassembly and maintenance of flagellar homeostasis (reviewed by Webb et al., 2020).

First discovered in the green alga *Chlamydomonas reinhardtii* (Kozminski et al., 1993, 1995) IFT is carried out by multi-megadalton polymers, termed IFT "trains", which are moved along the microtubule doublets, in the space between the axoneme and the flagellar membrane, by the activity of two motor proteins, the anterograde (base to tip) kinesin-2 and the retrograde (tip to base) dynein-1b (fig.11).

IFT trains act as platforms for cargo loading and transport. Initially named as "rafts", they were confirmed to be the vehicles of transport by correlative light and electron microscopy (Kozminski et al., 1995). Each IFT train consists of multiple IFT particles, which in their turn are formed by two multiprotein complexes, IFT-A and IFT-B, that arrange linearly to form structures 300-800 nm long (fig.11).

In vivo, IFT trains assemble at the flagellar base, near the transition fibers that connect the BB to the membrane (Cole et al., 1998; Deane et al., 2001; Rogowski et al., 2013; Wood and Rosenbaum 2014; reviewed by Wingfield et al., 2018). After this first stage of assembly, IFT trains pass through the transition zone, a structural and functional filter operating as a gate or diffusion barrier that keeps separated the cellular cytosol and the flagellar compartment (see above) (reviewed by Nachury and Mick, 2019). Once they have reached the flagellar tip, the anterograde trains are thought to dissociate and successively rearrange into retrograde trains (Pedersen et al., 2006); at the same time, kinesin-2 is inactivated by an event of phosphorylation (Liang et al., 2014), dynein-1b is activated and the cargoes are released (reviewed by Lechtreck, 2015) (fig. 11).

Studies of *Chlamydomonas* flagella by correlative microscopy techniques (the combinatorial use of light fluorescence microscopy and electron microscopy) have shown that IFT particles move along the B-tubules in the anterograde direction, whereas they move along the A-tubules in the retrograde direction (Stepanek and Pigino, 2016; Vannuccini et al., 2016). Such a direction-specific use of the two doublet microtubules is expected to avoid any collision between trains traveling in opposite directions along MT doublets.

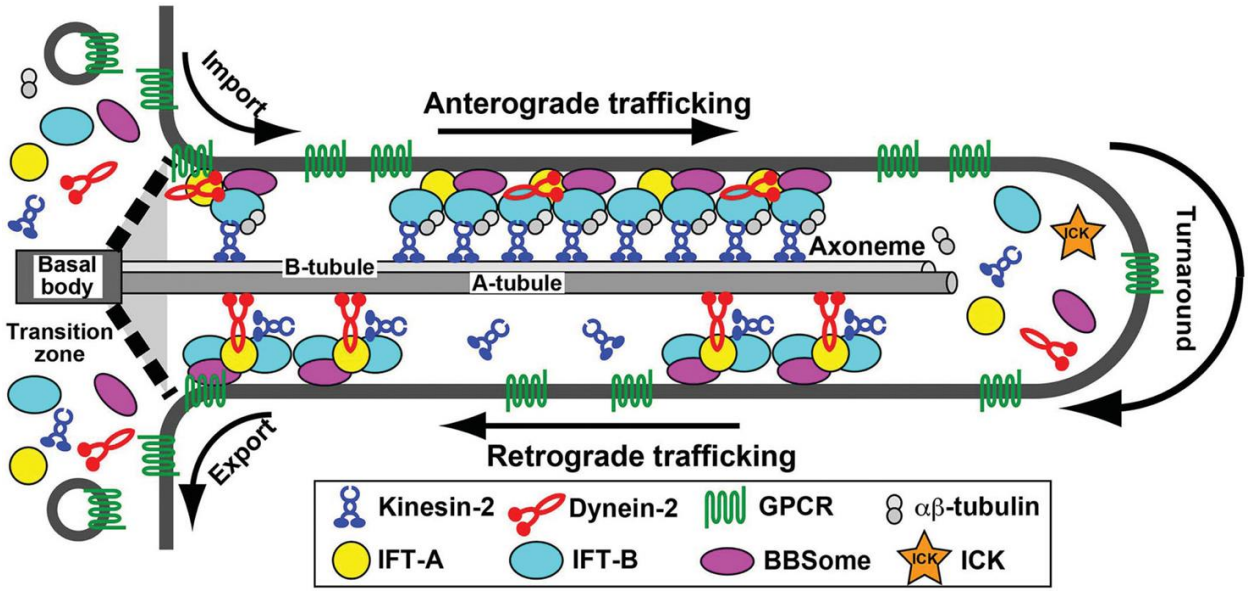

Figure 11: Schematic drawing of the IntraFlagellar Transport Process; its main components and steps are shown, from the initial docking at the BB, to the ciliary tip (anterograde trafficking) and vice-versa (retrograde trafficking) (modified from Nakayama and Katoh, 2020).

This scenario may not be the rule, and some variations are known. In the trypanosome flagellum, both anterograde and retrograde IFT transport takes place exclusively along two sets of microtubule doublets (Bertiaux et al., 2018). In addition, a recent cryo-electron tomographic analysis of mammalian primary cilia has shown that in the distal region of the axoneme, where the B-tubules are no longer present, anterograde IFT trains can move also on the singlet A-tubules (Kiesel et al., 2020).

Molecular size and complexity, along with the transient nature of the IFT machinery have made the comprehension of IFT structural organization as well as of the mechanisms controlling each step of the whole process a very demanding task. During last years a considerable information has been accumulated on several IFT proteins, however, several important aspects of the IFT process still remain unclear. We review in the next section the main molecular and structural data currently available on IFT components.

1.3.1 Multiprotein complexes involved in the IntraFlagellar Transport: the IFT-A, IFT-B, and BBSome complexes

Proteins participating in the assembly of IFT particles were first identified by comparing the sedimentation behavior and electrophoretic pattern of soluble flagellar extracts from

Chlamydomonas wild-type and *fla10* strains; the latter is a temperature-sensitive mutant carrying an aminoacid substitution in the kinesin-2 FLA10 subunit (Piperno and Mead, 1997; Cole et al., 1998).

Subsequently, IFT particles were biochemically purified and analyzed in various organisms, including *C. elegans*, zebrafish, and mammals, revealing a substantial level of evolutionary conservation (reviewed by Taschner and Lorentzen, 2016; Table 1).

IFT particles purified from *Chlamydomonas* flagella have been shown to dissociate under high ionic strength conditions, thus revealing the occurrence of two distinct multiprotein complexes, named IFT-A and IFT-B (Cole et al., 1998). The IFT-B complex is composed of 16 subunits (Table 1) and is thought to mediate the anterograde trafficking driven by the kinesin-2 motor; in fact, *Chlamydomonas* mutant strains defective in IFT-B subunits are no longer able to assemble flagella (reviewed by Taschner and Lorentzen, 2016). Among the cargo proteins of the IFT-B complex, the major one is the tubulin dimer, which is the building block of axonemal microtubules and is therefore essential for ciliogenesis (Bhogaraju et al., 2014).

		Alternative name in other organisms (if different)				
Complex	General	*Chlamydomonas reinhardtii*	*Trypanosoma brucei*	*Caenorhabditis elegans*	*Danio rerio*	Mammals
IFT-B						
IFT-B1	IFT88	-	-	OSM-5	Polaris	Polaris/Tg737
	IFT81	-	-	-	-	-
	IFT74	-	-	-	-	-
	IFT70	FAP259	PIFTB2	DYF-1	Fleer	TTC30A/B
	IFT56	DYF-13	PIFTC3	DYF-13	-	TTC26
	IFT52	BLD1	-	OSM-5	-	NGD5
	IFT46	-	-	DYF-6	-	-
	IFT27	-	-	(Absent)	-	RabL4
	IFT25	FAP232	-	(Absent)	-	HSPB11
	IFT22	FAP9	-	IFTA-2	-	RabL5
IFT-B2	IFT172	-	-	OSM-1	-	SLB
	IFT80	-	-	CHE-2	-	WDR56
	IFT57	-	-	CHE-13	-	Hippi
	IFT54	FAP116	-	DYF-11	Elipsa	Traf3IP1/MIP-T3
	IFT38	FAP22	PIFTA1	DYF-3	Qilin	Cluap1
	IFT20	-	-	-	-	-
IFT-A						
Core	IFT144	-	-	DYF-2	-	WDR19
	IFT140	-	-	CHE-11	-	WDTC2
	IFT122	FAP80	-	DAF-10	-	WDR10
Noncore	IFT139	-	-	-	-	THM1/TTC21B
	IFT121	-	PIFTD4	IFTA-1	-	WDR35
	IFT43	-	-	-	-	C14ORF179

Table 1: Nomenclature of *Chlamydomonas* IFT subunits and their orthologues identified in other species (Taschner and Lorentzen, 2016).

The IFT-A complex is composed of 6 subunits plus the adaptor protein TULP3 (fig. 12); it is believed to mediate retrograde trafficking driven by the dynein-1b complex (reviewed by Ishikawa and Marshall, 2011; Sung and Leroux, 2013; He et al., 2017), although there is no confirmed evidence for a direct interaction of IFT-A subunits with this motor.

Chlamydomonas IFT-A mutant strains are still able to assemble their flagella, though they show a distinctive phenotype characterized by an enlarged tip caused by the accumulation of IFT proteins (Piperno et al., 1998; Iomini et al., 2009). In addition to its role in retrograde trafficking, the IFT-A complex together with the adaptor TULP3 is also involved in the import of membrane proteins across the ciliary gate (Mukhopadhyay et al., 2010; Hirano et al., 2017; Ye et al., 2018; Han et al., 2019).

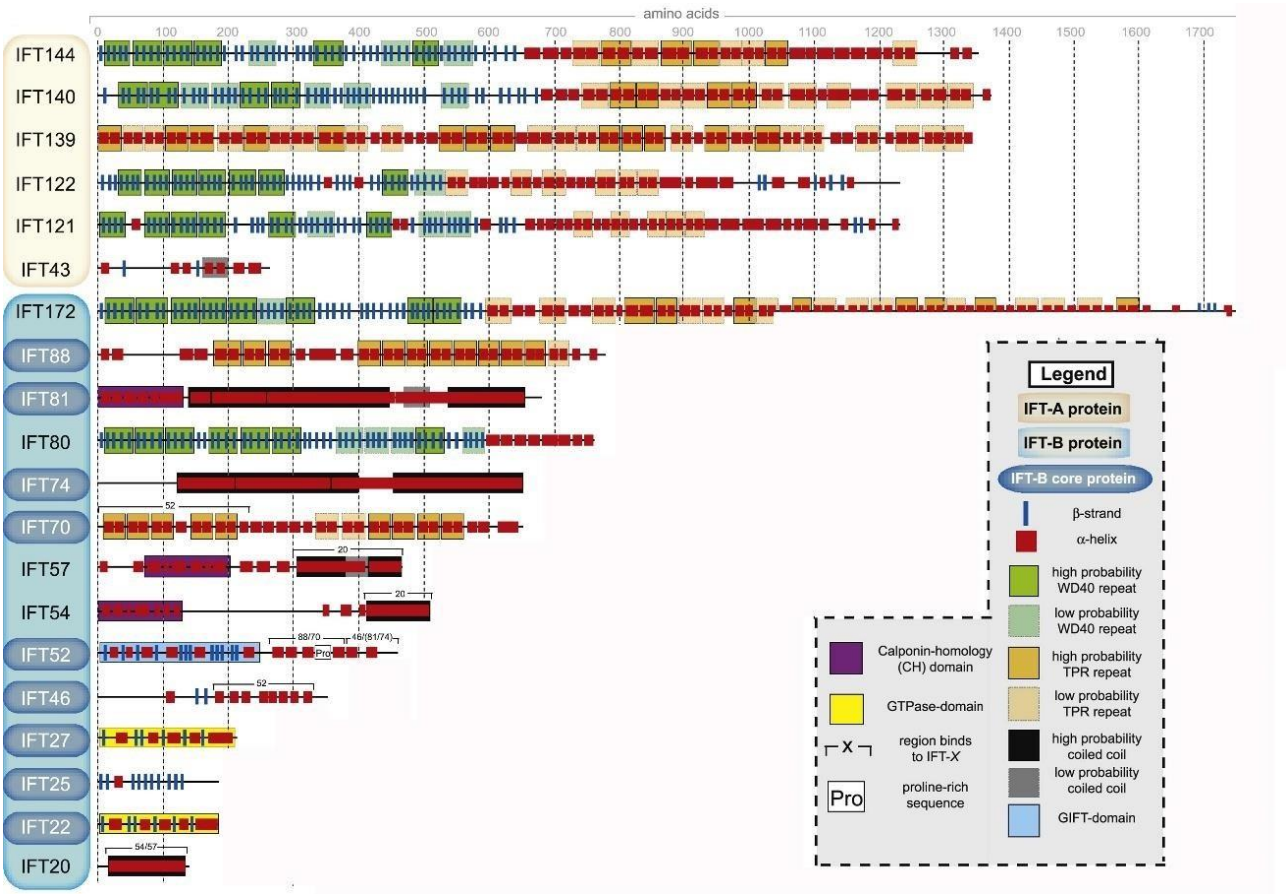

Figure 12: Domain organization of *Chlamydomonas* IFT proteins (modified from Taschner et al., 2012).

Most IFT proteins contain well-known protein–protein interaction motifs, including tetratricopeptide repeats (TPRs), WD-40 repeats, and coiled coils (Taschner et al., 2012); the occurrence of these sequence motifs is consistent with their capability to form large macromolecular complexes as well as to bind a variety of protein cargoes.

Yeast two-hybrid analysis and bacterial coexpressions/pulldowns experiments have clarified the specific protein-protein interactions occurring within the IFT-B and IFT-A complexes (Lucker et al., 2005; Kobayashi et al., 2007; Follit et al., 2009; Wang et al., 2009; Fan et al., 2010; Lucker et al., 2010; Bhogaraju et al., 2011; Zhao and Malicki, 2011; Howard et al., 2013; Swiderski et al., 2014).

More recently, these data have been integrated by information obtained using a new-developed visible-immunoprecipitation assay (VIP) (Katoh et al., 2015; Hirano et al., 2017; Takei et al., 2018; Kobayashi et al., 2021; reviewed in Nakayama and Katoh, 2020). The whole set of available data have allowed to design the overall architecture of the interactions occurring among IFT proteins (fig.13).

The 16-subunit IFT-B complex has been shown in *Chlamydomonas* to consist of a salt-stable subcomplex - the IFT-B1 core - which is based on substantial hydrophobic interactions and is crucial for ciliogenesis, and of other peripheral subunits, arranged into the IFT-B2 subcomplex (Taschner et al., 2014).

Several inter-subunit interactions have been mapped to specific protein domains of the IFT-B1 core (Taschner et al., 2011, 2014). In particular, the two IFT74 and IFT81 subunits, which are characterized by the presence of long alpha-helical domains able to form coiled coil structures, organize into an heterodimer (Wachter et al., 2019); this event is a prerequisite for the successive association of the IFT52/46 dimer and the IFT22 subunit (Taschner et al., 2014). IFT70 and IFT88, two tetratricopeptide repeat (TPR)-containing superhelical proteins, wrap around a largely unstructured, proline-rich region of IFT52 (Taschner et al., 2014) (fig. 13).

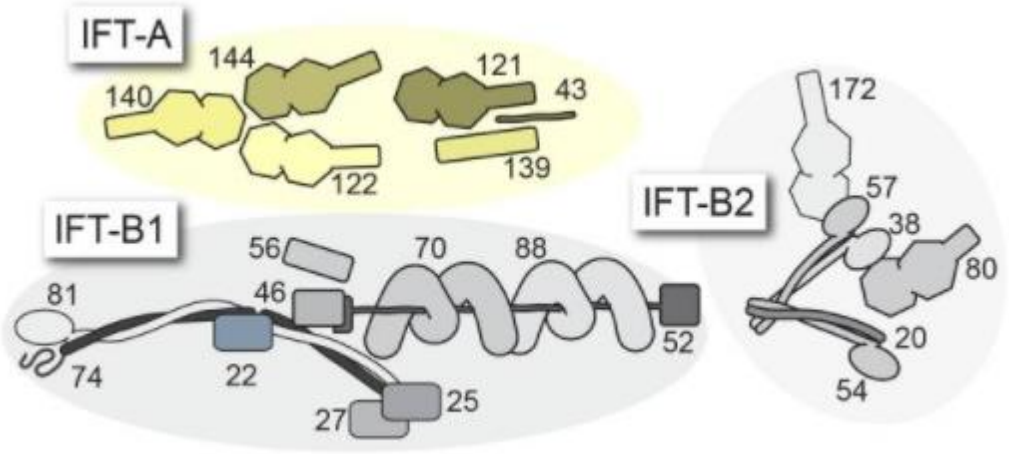

Figure 13: IFT subunits, which form the IFT-A, IFT-B1, and IFT-B2 sub-complexes (modified from Webb et al., 2020).

The crystal structures of several IFT-B1 proteins are available, allowing a more detailed knowledge of the IFT-B1 molecular organization (fig.14). Two sGTPases are part of this complex, the atypical small GTPase IFT27, that forms a dimer with the IFT25 subunit (Bhogaraju et al., 2011), and IFT22/RABL5. These sGTPases have been implicated not only in IFT trafficking in cooperation with the other subunits of the IFT-B complex, but also in promoting the exit of BBSome and associated cargoes from the cilium (IFT27; Liew et al., 2014) and in the recruitment of the BBSome on the IFT trains at the ciliary base (IFT22; Xue et al., 2020).

Two organizational principles occur within the IFT-B1 sub-complex. First, the heterodimeric coiled coil formed by IFT81/IFT74 (Wachter et al., 2019) scaffolds several domains involved in cargo binding, including the calponin-homology domain of IFT81, mediating tubulin binding (Bhogaraju et al., 2013a; Kubo et al., 2016); the Rab-like domains of IFT22 and IFT27 and the jelly-roll fold of IFT25, involved in the BBSome pathway (Liew et al., 2014); and the heterodimeric domains of IFT46 and IFT56 (implicated in axonemal dynein binding) (figg. 14, 15).

Second, IFT52 bridges multiple partners: its central region interacts with the tetratricopeptide repeat proteins IFT70 and IFT88, while its C-terminal domain binds IFT46, and its N-terminal GIFT domain associates with IFT-B2 (figg. 14, 15) (Taschner et al., 2014; 2016).

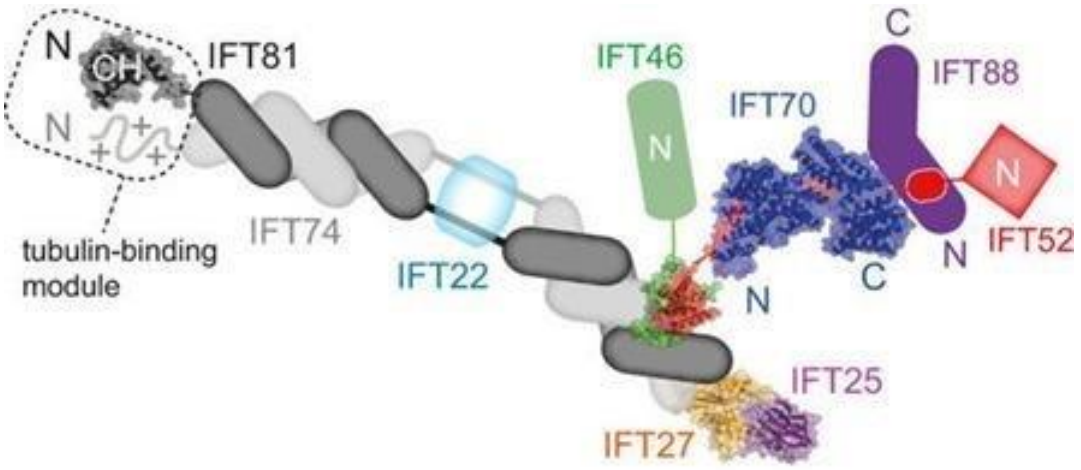

Figure 14: Schematic representation of IFT-B1 molecular organization; the precise positions of IFT27/25 and IFT52/46 on the C-terminal coiled-coil region of IFT81/74 are not known (from Taschner et al., 2014).

The six "peripheral" IFT-B subunits form a second, stable protein complex, named IFT-B2. in which the pairing of the two coiled coil proteins (IFT57/38) provides a central component that directly interacts via the N-terminal calponin-homology domains with IFT172, IFT80, and IFT54/20 (Katoh et al., 2015; Taschner et al., 2016) (figg. 13, 15). Within the IFT-B2 complex, IFT172 is the more weakly attached subunit (Cole et al., 1998; Pedersen et al., 2005; Taschner et al., 2016), suggesting that it might play a distinctive function.

The interacting surface between IFT-B1 and IFT-B2 is provided by the contribution of highly conserved residues occurring in the four subunits IFT88/IFT52 (on the IFT-B1 side) and the IFT57/38 on the IFT-B2 side (fig. 15) (Taschner et al., 2016).

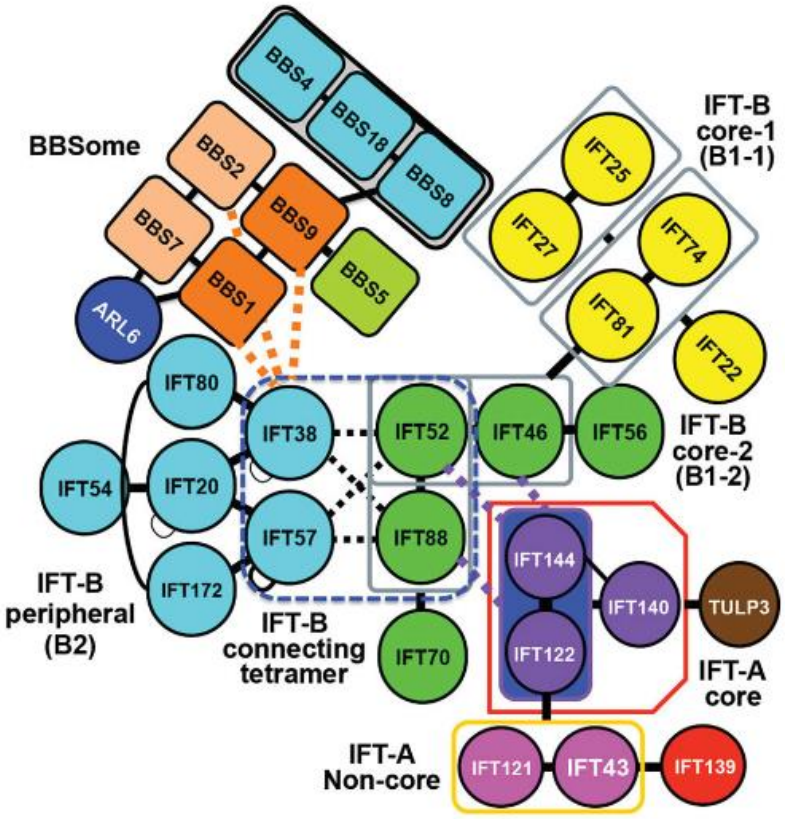

Figure 15: Maps of the protein interactions occurring among the IFT-A, IFT-B and the BBSome complexes (from Nakayama and Katoh, 2020).

The position of ciliary cargo-binding sites within the IFT-B complex has been defined only in very few cases. For instance, in *Chlamydomonas* IFT46 has been implicated in the specific transport of outer dynein arms (ODAs) via its amino-terminal domain, which is not required for IFT-B1 complex stability (Piperno et al., 1996; Qin et al., 2004; Taschner et al., 2014), while the transport of IDA motor complexes appears to require IFT56 (Ishikawa et al., 2014). Tubulin heterodimer - certainly the main IFT cargo that has to be transported for ciliary assembly - moves anterogradely with IFT trains in both *Chlamydomonas* and *C. elegans* (Hao et al., 2011; Craft et al., 2015) after its binding as a cargo to a module formed by the amino-terminal region of both IFT81 and IFT74, which contain, respectively, a calponin-homology (CH) domain, able to recognize tubulin dimers through conserved surface-exposed basic residues, and a highly positively charged amino terminus that strengthens dimer binding to the complex by forming electrostatic interactions with the negatively charged carboxy-terminal tubulin tails (Bhogaraju et al., 2013). Deletion of the amino-terminal region in either the IFT81 or the IFT74 subunit does not abolish ciliogenesis, but

slows it down (Brown et al., 2015; Kubo et al., 2016). This observation suggests that IFT81/74 may not be the only tubulin-binding site in the IFT complex. Recently, the CH domain of IFT54 has been also shown to bind tubulin (Taschner et al., 2016).

Less information is available on the molecular organization and specific roles of IFT-A subunits. Interestingly, four IFT-A subunits (IFT144, 140, 122, and 121) exhibit the same structural organization of membrane coat proteins, consisting of an amino-terminal WD40 ß-propellers and a solenoid carboxy-terminal tail (reviewed by Taschner et al., 2012); on this basis, it has been suggested that these IFT subunits might have evolved from a proto-coatomer protein (Jekely and Arendt, 2006; van Dam et al., 2013). This observation is particularly remarkable in light of the close apposition demonstrated for the IFT-A complex with the flagellar membrane (see below).

The IFT-A complex was shown to be important for the ciliary import of G-protein-coupled receptors (GPCRs), mediated by the protein TULP3 (Mukhopadhyay et al., 2010, 2013), as well as of the BBSome, which directly interact with the IFT144 subunit in mammalian cells (Wei et al., 2012). Accordingly, hypomorphic mutations in *C. elegans* IFT144/DYF-2 or BBS1, that disrupt this interaction, result in BBSome exclusion from cilia and a defective return of IFT-B proteins from the ciliary tip (Wei et al., 2012).

The third multiprotein complex involved in IFT is the above-mentioned BBSome, which is comprised by eight proteins (fig. 15) (Nachury et al., 2007; Loktev et al., 2008; Jin et al., 2010; Katoh et al., 2015) and move bidirectionally along axonemal microtubules in association with IFT particles (Ou et al., 2005; Lechtreck et al., 2009; Wei et al., 2012; Williams et al., 2014; Xue et al., 2020). Early studies suggested that this complex is required for the import of ciliary membrane proteins (Mykytyn et al., 2004; Su et al., 2014), but more recent studies have shown that it partecipates also in the export of ciliary membrane proteins, e.g. GPCRs, to the cytoplasm, by linking them to IFT particles (Eguether et al., 2014; Liew et al., 2014; Klink et al., 2017; Liu and Lechtreck, 2018; Wingfield et al., 2018; Ye et al., 2018; Nozaki et al., 2018, 2019).

The role of BBSome in membrane protein trafficking is also demonstrated by the phenotype of *Chlamydomonas* mutants that are defective in one of the BBS subunits; these mutant strains are in fact still able to assemble full-length motile flagella but have lost phototaxis and show an abnormal amount of several signaling proteins (Lechtreck et al., 2009). On this basis, the BBSome is generally considered to be a sort of adaptor for the transport of membrane proteins, However, further evidences have suggested that in *C. elegans* it is also required for the integrity of IFT particles, linking together IFT-A and IFT-B complexes (Ou et al., 2005), in the assembly of the IFT machinery at the ciliary base (Blacque et al., 2004), in IFT turnaround at the ciliary tip (Wei et

al., 2012), and in the negative regulation of the shedding of ciliary extracellular vesicles (Akella et al., 2020).

1.3.2 Molecular motors of IFT

The main IFT anterograde motor, the heterotrimeric kinesin-2, was first purified as a novel plus end-directed microtubule motor required for the assembly of cilia in sea urchin embryos (Morris and Scholey, 1997; Cole et al., 1998). Mutations in one of the ortholog motor subunits were shown to cause a cessation of IFT in *Chlamydomonas* flagella (Walther et al., 1994; Kozminski et al., 1995; Cole et al., 1998). The molecular architecture of kinesin-2 comprises two distinct motor subunits, KIF3A and KIF3B, and a non-motor accessory protein (KAP) that may serve as a cargo adaptor (Wedaman et al., 1996); in *Chlamydomonas*, these subunits are called respectively FLA8, FLA10, and FLA3, according to the name of the previously isolated mutant strains (Walther et al., 1994; Kozminski et al., 1995; Cole et al., 1998). The two motor subunits share the classic kinesin organization, with an N-terminal motor domain, coiled coil segments mediating heterodimerization, and a putatively disordered C-tail (fig. 16). The KAP/FLA3 subunit contains armadillo repeats and is dispensable for kinesin-2 motility *in vitro* but strictly required *in vivo* (Mueller et al., 2005); recently, it has been shown to help in relieving the motor from autoinhibition (Sonar et al., 2020).

The heterotrimeric kinesin-2 may not be the only IFT anterograde motor in other organisms. In fact, in *C. elegans* sensory cilia, it only drives IFT trains through the TZ and along the doublet microtubules of the proximal/middle segment of the axoneme (reviewed by Scholey, 2013; Prevo et al., 2015), while a second kinesin-2, the homodimeric OSM-3, is implicated in IFT transport along the singlet A-tubules of the distal segment (reviewed by Scholey, 2013; Prevo et al., 2015).

During IFT turnaround at the distal ciliary tip, kinesin-2 detaches from the anterograde train and is inhibited by folding of its tails onto the motor domain (Brunnbauer et al., 2010), to be then recycled back to the cell body by diffusion (Chien et al., 2017). The regulatory mechanisms that control the cyclic activation/inhibition of kinesin-2 are not yet completely clear, but are likely to involve multiple phosphorylation events; in fact, residues in the tail region of mammalian KIF3A and KIF3B are phosphorylated by the kinases ICK, PKA and CaMKII (fig. 16) (Chaya et al., 2014; Ichinose et al., 2015; Oh et al., 2019).

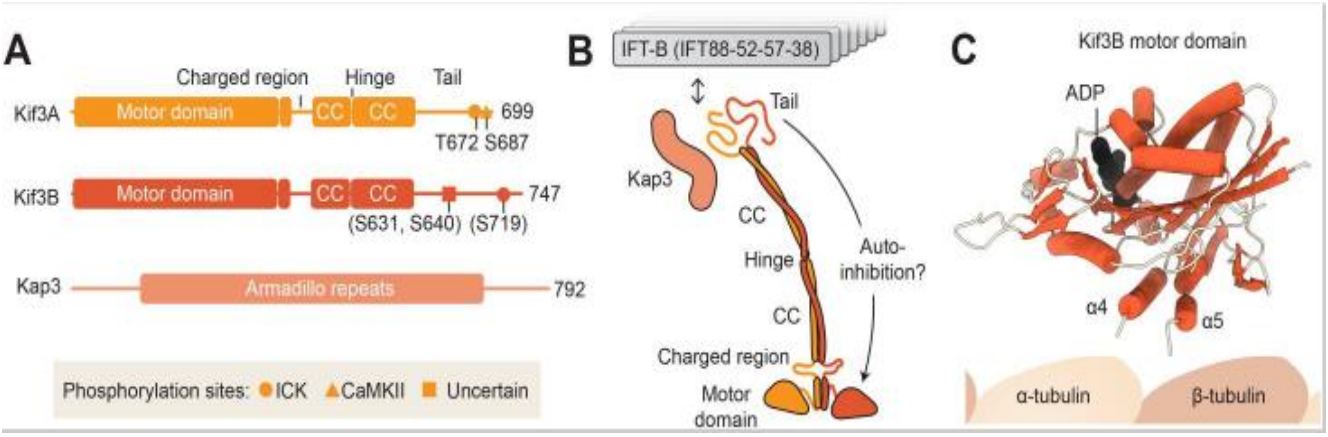

Figure 16: (A) Domain organization of human heterotrimeric kinesin-2, KIF3. Major phosphorylation sites in the human subunits are reported (putative sites in parenthesis). (**B**) Schematic drawing of KIF3 and its interaction with complex IFT-B (modified from Webb et al., 2020).

In *Chlamydomonas*, the calcium-dependent protein kinase CDPK-1 phosphorylates the conserved S663 residue on the motor subunit FLA8; phosphorylated FLA8 is no longer able to interact with the IFT-B complex, thus blocking IFT entry at the flagellar base and inducing IFT-B unloading at the flagellar tip (Liang et al., 2014). Therefore, FLA8 phosphorylation acts as a molecular switch to control IFT entry and turnaround (fig. 17).

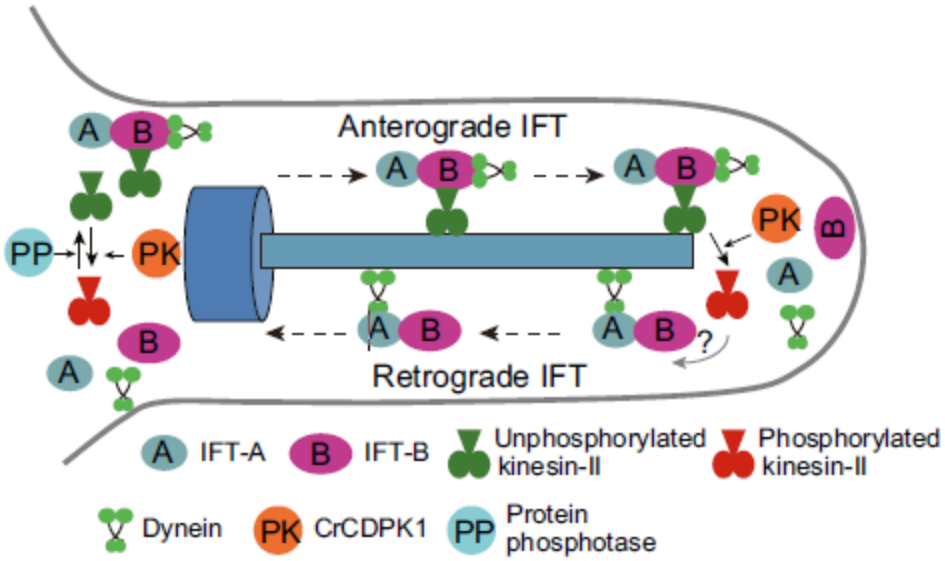

Figure 17: Model of IFT, showing the regulation by FLA8/KIF3B phosphorylation. At the ciliary base, the phosphorylation state of FLA8 is controlled by CrCDPK-1 and an unknown (till now) phosphatase (Liang et al., 2014).

Insights into the binding site of kinesin-2 to the IFT particles has been obtained using a visible immunoprecipitation (VIP) assay (Funabashi et al., 2018). The results indicated that kinesin-

2 interacts with the four-protein complex (IFT88/52/57/38) which provides the interface between IFT-B1 and IFT-B2, and that the tail of KIF3B is important for this interaction.

The retrograde motor, dynein-1b (also known as dynein-2), was first identified as a cytoplasmic dynein that is upregulated prior to ciliogenesis in sea urchin embryos (Gibbons et al., 1994) and was subsequently shown to be required for retrograde IFT in *Chlamydomonas* and *C. elegans* (Pazour et al., 1998; Porter et al., 1999; Signor et al., 1999). It consists of a large complex formed in mammals by at least 8 different proteins and built around two different >4000 aminoacid heavy chains, the N-terminal regions of which are involved in dimerization and binding of the associated intermediate and light subunits, while the C-terminal ring-shaped AAA regions contain the motor domains (reviewed by Hou and Witman, 2015) (fig.18).

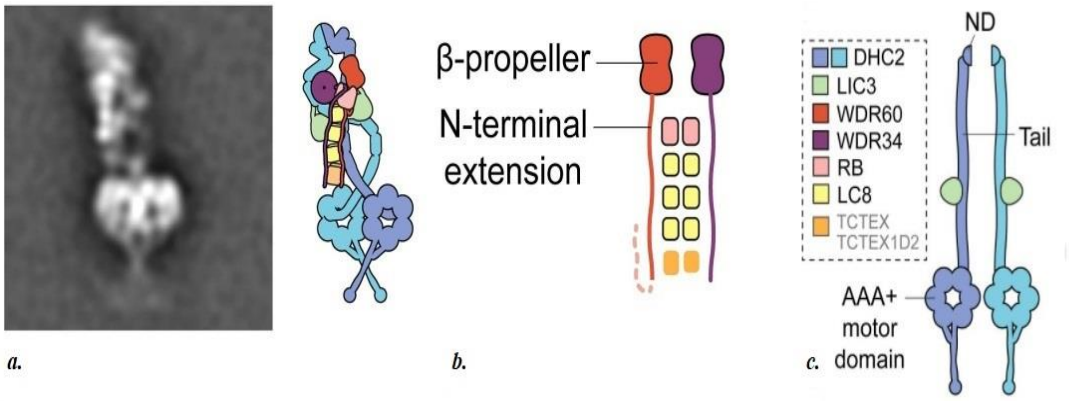

Figure 18: Human dynein-1b ultrastructural analysis. **a.** Negative staining class averages of the dynein-1b with the corresponding cartoon. **b-c.** Overview of the dynein-1b subunits (c) and their stoichiometry in the structure (b), colored according to the code in the upper left. The two copies of DHC2 are colored in different shades of blue for distinction. ND: N-terminal domain (modified from Toropova et al., 2019).

A quite detailed information is currently available on the structure that dynein-1b assumes when associated with the anterograde IFT trains (Toropova et al., 2019). This motor is transported anterogradely as a cargo in its autoinhibited form (Toropova et al., 2017), before becoming active at the tip for retrograde transport. In the inactive autoinhibited state, the two motor domains are stacked against each other, with their stalks pointing away from the microtubule surface; this conformation, which inhibits both the ATPase activity and motility, facilitates the transport of dynein-1b, being strictly tailored to the repeat of the IFT-B polymer (fig. 19).

Dynein-1b has been shown to bind to the IFT-B complex, but the precise molecular interactions involved are not completely clear. An intact IFT172 subunit is required for turnaround in both *Chlamydomonas* flagella and *Tetrahymena* cilia (Pedersen et al., 2005; Tsao and Gorovsky, 2008); Interestingly, *Chlamydomonas* dynein-1b heavy chain immunoprecipitated with IFT172 migrates differently by SDS-PAGE compared to that from crude extract, suggesting that it could be

differentially modified (Pedersen et al., 2005). In *Trypanosoma*, also the IFT27/IFT25 dimer is essential for retrograde cargo transport (Huet et al., 2014, 2019).

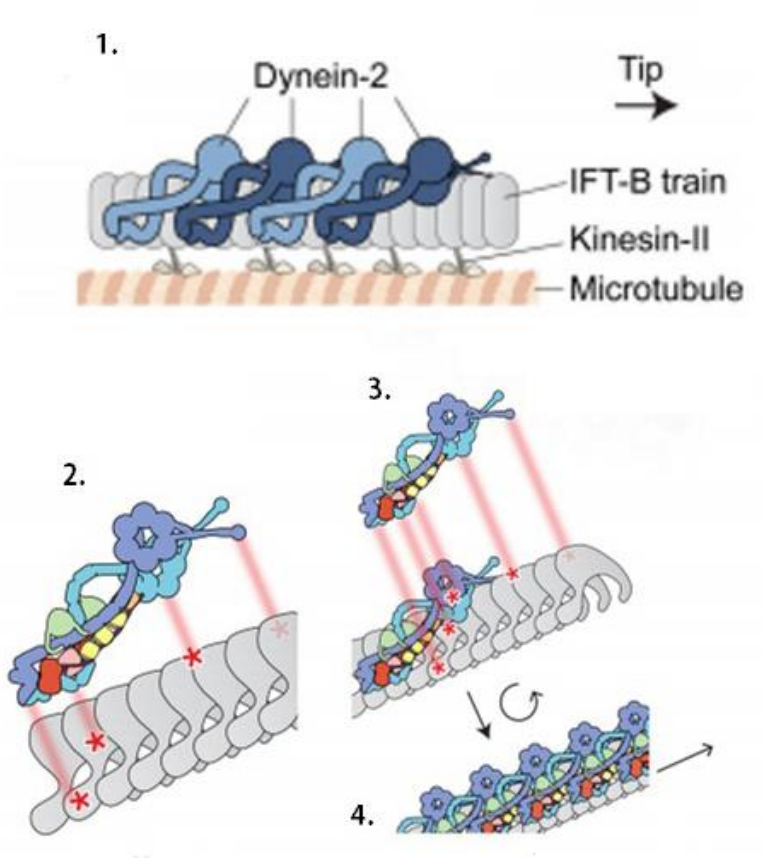

Figure 19: Dynein-1b structure matches the periodicity of the IFT anterograde train. Cartoon of the model of inactivated dynein-1b as a cargo of the anterograde IFT train (**1**). Each dynein-1b molecule recognizes the IFT-B periodicity in the train, spanning out every 7-8 repeats (**2**). Binding of one dynein-1b complex to the train creates extra binding surface for the next (**3**), enabling cooperative loading of dynein-1b along the train, before the assembly is completed and the train is imported into the cilium by kinesin-2 (**4**). (modified from Toropova et al., 2019).

Recently, new data have suggested an important role for the IFT54 subunit in both kinesin-2 and dynein-1b binding (Zhu et al., 2020). While it seems likely that its interaction with kinesin-2 has a stabilizing effect and reinforces the association of the anterograde motor with the IFT-B1/IFT-B2 connecting tetramer, the direct interaction of IFT54 with the dynein D1bLIC subunit occurs through a short aminoacid sequence, the deletion of which impairs the association of autoinhibited dynein-1b with the anterograde train and thus its transport to the ciliary tip.

It is thus likely that dynein-1b interacts with multiple IFT-B subunits. Indeed, cryo-ET data have revealed how dynein-1b binds to IFT-B complex within the anterograde train spanning seven to eight IFT-B repeats (Jordan et al., 2018; Toropova et al., 2019).

1.3.3 Architecture of IFT trains

Since the first electron microscopy observations carried out in *Chlamydomonas* flagella, IFT trains have been shown to exhibit distinct structural features on the basis of which two categories of trains were initially identified, that is, the less compact, more electron-transparent 'long' trains (mean length of ~700 nm, 40 nm repeat), and the thicker, more electron-opaque 'short' trains (mean length of ~250 nm, 16 nm repeat) (Pigino et al., 2009). On the basis of their different morphologies, the two classes of trains were suggested to play different functions. Given that long trains are the only category of IFT trains detected in *fla14* cells, where the function of the retrograde motor dynein-1b is impaired but anterograde transport is normal (Pazour et al., 1998), these trains were initially considered to be responsible for the anterograde trafficking, and the short trains had been suggested to be the retrograde ones (Pigino et al., 2009).

Later, the analysis of the distribution of the two categories of IFT trains during regeneration and resorption of *Chlamydomonas* flagella has revealed that the long trains are mainly formed during the early stages of flagellar assembly, while short trains are almost the only one type found in full-length flagella, suggesting that they are responsible for both anterograde and retrograde transport; also, electron tomography revealed the occurrence of two subtypes of short trains, each one with its own architecture (Vannuccini et al., 2016). This suggests that specific size and ultrastructure constraints act during the assembly of each type of train and that the function of each train is related to its specific ultrastructure.

The existence of two distinct types of short IFT trains, moving in opposite directions, was confirmed by Stepanek and Pigino (2016) (fig. 20) by using a time-resolved correlative fluorescence and three-dimensional electron microscopy approach (CLEM, Correlative Light Electron Microscopy). They also showed that the two types of short trains move along different microtubule tracks, the anterograde trains on the B-tubule and the retrograde ones on the A-tubule, thus avoiding collision.

A detailed 3D model for *Chlamydomonas* anterograde trains was obtained by cryoelectrontomographic analysis (Jordan et al., 2016), which confirmed them to be highly ordered assemblies ~312 nm long and 50 nm wide, formed by three different polymer-like components endowed with distinct periodicities, i.e., 6, 11 and 18 nm (fig. 21). Comparing the 3D models obtained from wt and mutant strains lacking either IFT-A or dynein-1b, the authors could assign IFT-A to the globular structures of the 11-nm repeat that are closely apposed to the membrane (consistent with the role of this complex in membrane proteins transport), IFT-B to the underlying

6-nm repeat structure, adjacent to the B-tubule surface, and the almost globular 18-nm repeat to inactive dynein-1b (fig. 21).

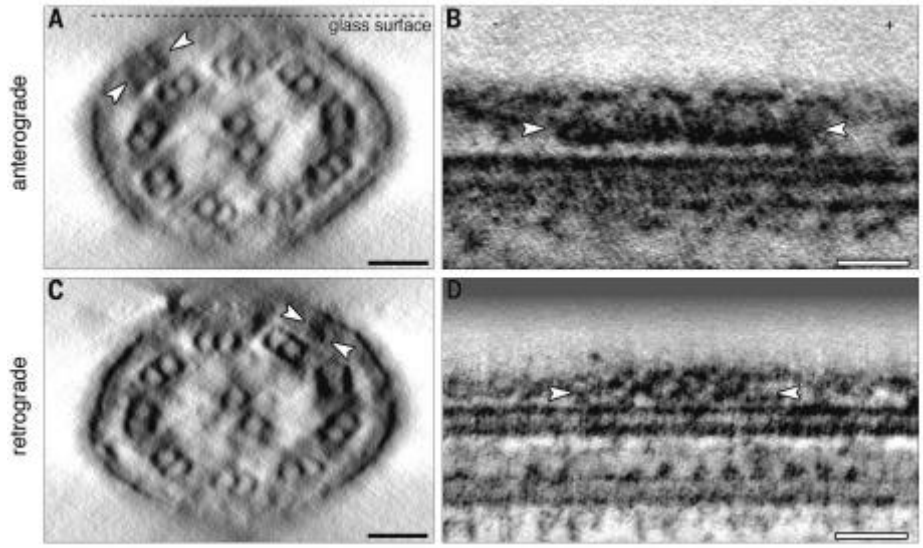

Figure 20: Morphology of the anterograde and retrograde classes of IFT trains. On the left, cross sections (**A, C**) and, on the right, longitudinal sections (**B, D**) of flat-embedded *Chlamydomonas* flagella. Trains are indicated by white arrowheads. The anterograde trains appeared as compact electron-dense structures with clearly defined boundaries (**B**). The structure of the retrograde trains appeared less condensed and less regular (**C** and **D**) (modified from Stephanek and Pigino, 2016). Scalebar = 50 nm.

IFT-A is often absent from both ends of the train, where only IFT-B is present, extending for ~9 nm. Thus, IFT-A may occur in substoichiometric amounts, while IFT-B represents the structural core of the anterograde train, consistent with genetic evidence that IFT-B is critical for IFT and cilium formation (Perkins et al., 1986; Cole et al., 1998; Pazour et al., 2000). IFT-B connects to the B-tubule through an elongated bridge, presumably the kinesin-2 motor.

In the same organism, retrograde trains have been shown to consist of elongated particles arranged to form a zig-zag pattern with a spacing of ~43 nm, associated with dynein-1b molecules repeating every ~80–90nm (fig. 20); however, a detailed 3D model is not yet available for these trains.

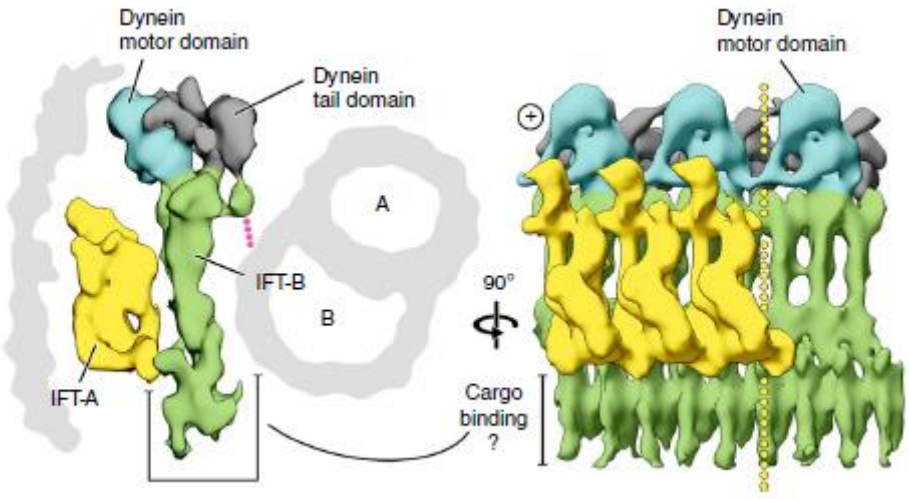

Figure 21: 3D model of the repeating units in the anterograde IFT train, obtained by Cryo-EM tomography. Anterograde IFT trains are composed of three different types of repeating units, indicated by different colors and each one endowed with its proper periodicity. Kinesin-2 is indicated by a pink broken line. Representative positions of a microtubule doublet and the membrane are outlined in grey. View of the train structure from the membrane side (looking towards the microtubule doublet) is on the right (modified from Jordan et al., 2018).

1.4 Ciliary Length Control

Once ciliogenesis takes place, cilia grow until they reach a predetermined canonical length. The mechanisms controlling ciliary length are not well understood but involve a balance of anterograde and retrograde traffic.

Also, the molecular pathways that sense length and regulate IFT injection in the flagellar compartment are not known, but might be investigated by using genetics to select mutants that alter the steady-state length.

In *Chlamydomonas reinhardtii* two genes have been identified that – when mutated - lead to longer flagella; these genes encode a member of the cyclin-dependent kinase (CDK) protein family, called LF2 (Tam et al., 2007), and a member of the mitogen-activated protein (MAP) kinase family, called LF4 (Berman at al., 2003).

LF4 is the main candidate to regulate IFT injection, since the analysis of a null mutant of the LF4 gene (which possesses twice longer than wild-type flagella) revealed that there is an increment of both IFT recruitment at basal bodies and injection into flagella (Ludington et al., 2013). LF2 is a cell cycle–related kinase that is required for LF4 phosphorylation. LF4 is likely to be a constitutively active kinase that is regulated by LF2 (Wang et al., 2019). Mammalian cilia show an apparently conserved genetic control of length (Omori et al., 2010; Ko et al., 2010).

Other studies have indirectly implied the glycogen synthase kinase 3β (GSK3β), and

calcium-mediated signaling pathways in the control of ciliary length (Wilson and Lefebvre 2004; Besschetnova et al., 2010). GSK3β might be the target of lithium, a flagellar length-increasing compound, but this is still hypothetical (Wilson and Lefebvre, 2004).

All cells may lose their cilia by either resorption and/or deflagellation. Resorption is the process by which the cilium is gradually disassembled, usually occurs before cell division and takes place at the distal end of the organelle. Deflagellation instead consists of the shedding of flagella that occurs at the distal end of the flagellar TZ in response to a wide range of stimuli (Blum, 1971; Lewin and Lee, 1985 reviewed by Quarmby, 2004).

Experiments in cultured mammalian cells suggest that cilia disassemble in a biphasic manner, with the first, major 'wave' occurring in the G1 phase shortly after mitogen stimulation of quiescent cells and a second wave prior to mitosis (Tucker et al., 1979; Pugacheva et al., 2007).

These studies identified several key regulators of cilium disassembly: the scaffolding protein HEF1 (also known as NEDD9) and calcium–calmodulin activated Aurora A kinase, which in turn phosphorylates and stimulates the histone deacetylase HDAC6, promoting the de-acetylation of modified, stabilized tubulins within the axoneme (Pugacheva et al., 2007; Plotnikova et al., 2012).

Cilium disassembly requires the destabilization and depolymerization of axonemal microtubules, and two members of the Kinesin-13 family of depolymerizing kinesins, Kif2a and Kif24, are involved in this process (Kobayashi et al., 2011; Kim et al., 2015; Miyamoto et al., 2015).

Cilia can also be removed by severing mechanisms subsequent to the reception of a number of stimuli. For example, in *Chlamydomonas*, the detachment of the axoneme from the basal body is facilitated by the action of a microtubule-severing enzyme, katanin (Lohret et al., 1998; Rasi et al., 2009). *Chlamydomonas* also loses its flagella in response to environmental or artificial stresses, including acidification, heat and mechanical shearing (reviewed by Blum, 1971; Cheshire and Keller, 1991). In addition to the mentioned stimuli the experiments conducted by Lohret et al. (1998), and Sanders and Salisbury (1989, 1994), indicate that calcium too can activate the deflagellation machinery.

1.5 Ciliary Signaling and Ciliopathies

Since the first studies that correlated ciliary defects to the onset of diseases, it has become widely accepted that vertebrate species use primary cilia to transduce a number of signaling pathways (reviewed by Wheway et al., 2019). The mechanisms by which cilia participate in signal transduction, however, are various and their specific details remain largely to be clarified.

At present, it is known that the primary cilium acts as an organelle with chemo- and mechanosensory capabilities, that is able to transfer signaling information from the extracellular environment to the inside of the cell to guarantee cell and tissue homeostasis.

The mechanosensory properties of the primary cilium regard its capability to sense extracellular fluid flow or tissue deformation: bending of the cilium initiates downstream mechanotransduction signaling cascades (McGlashan et al., 2006). Proteins like PC1, PC2, TRPV4, and AC6, that are localized in the cilium, have been related to mechanotransduction (Nauli et al., 2003; Kwon et al., 2010; Lee et al., 2015). The clearest example of such a role has been described in kidney development and function, which are dependent on the capability of kidney epithelial cell primary cilia to sense fluid flow through the developing nephrons and collecting ducts (Praetorius and Spring, 2003).

As to the chemosensory role of cilia, the most studied and representative example is the Hh signaling pathway that participates in the developmental patterning of many vertebrate tissues, (schematized in fig. 22); several other signaling pathways involve the primary cilium, e.g. GPCR signaling and Wnt signaling (reviewed by Anvarian et al., 2019).

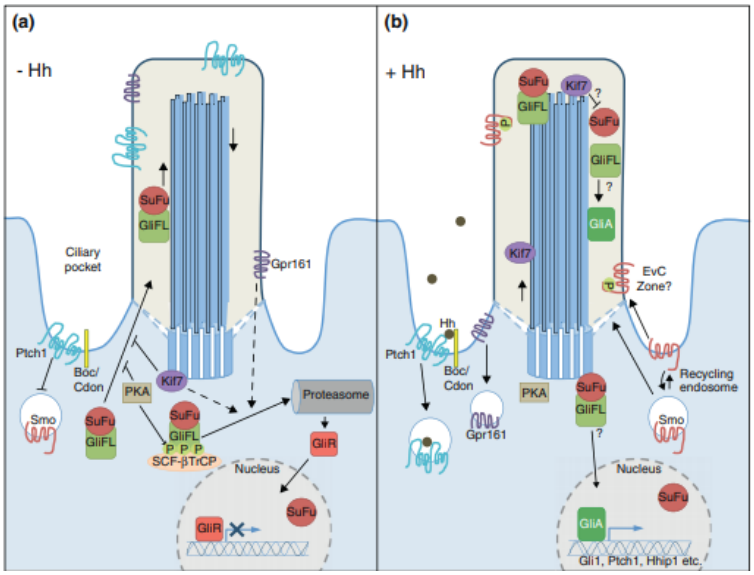

Figure 22: The mammalian Hh signaling pathway. (a) In the absence of the Hh ligand all of the events reported in the figure ensure silencing of the Hh pathway. (b) The Hh ligand binds to its receptor Ptch1 and co-receptors Boc/Cdon, activating the Hh pathway and the transcription of the target genes in the nucleus (from Nozawa et al., 2013).

Coherently into the nearly ubiquitous presence of cilia across tissues, and their crucial role in organogenesis and maintenance, it is not surprising that alterations in ciliary organization and/or function, consequent to genetic disorders, result in severe and invalidant diseases known as 'ciliopathies' (Brown and Witman, 2014). These are complex, inherited disorders that can affect almost any organ (fig. 23) (reviewed by Waters and Beales, 2011; Brown and Witman, 2014; reviewed by Powles-Glover, 2014; reviewed by Mitchinson and Valente, 2017), and manifest in a spectrum of hallmark phenotypes with variable penetrance and expressivity (reviewed by Tobin and Beales, 2009; reviewed by Reiter and Leroux, 2017). Although individually rare, there are 100 suspected or established cilia-related clinical synopses reported in the Online Mendelian Inheritance in Man database (https://omim.org/) with a collective incidence of 1:1000, which is comparable to the incidence of Down syndrome (reviewed by Davis and Katsanis, 2012).

Ciliopathies are usually classified into sensory (or primary) and motor ciliopathy syndromes. However, a wide range of genetic and phenotypic overlap exists between sensory and motor ciliopathy, with relevant genetic heterogeneity.

The first motor ciliopathy described in literature is Primary Cilia Dyskinesia (PCD) (Afzelius, 1976; reviewed by Ferkol and Leigh, 2012). PCD is a genetically heterogeneous disorder of motile cilia, caused by mutations of genes (mutations in at least 37 separate loci have been linked to the syndrome) affecting dynein motor structure or assembly, or other components of the ciliary axoneme (reviewed by Ferkol and Leigh, 2012; reviewed by Knowles et al., 2016; reviewed by Mitchinson and Valente, 2017). PCD is associated with chronic upper and lower respiratory tract disease, infertility, and organ laterality defects (usually *situs inversus*) in about 50% of cases (Werner et al., 2015; reviewed by Knowles et al., 2016).

Sensory ciliopathies extend beyond defects in interpreting environmental cues and comprise a spectrum of highly heterogeneous disorders (reviewed by Mitchinson and Valente, 2017). These were first thought to be organ-specific, but it is now clear that sensory ciliopathies involve many systems, with renal and liver disease often observed (reviewed by Tobin and Beales, 2009; reviewed by Ferkol and Leigh, 2012; reviewed by Powles-Glover, 2014). Among sensory ciliopathies, PKD (Polycistic Kidney Disease) is the most common and potentially lethal inherited human disease, caused mostly by mutations in the PKD1 and PKD2 genes, encoding polycystin-1 and -2, respectively (reviewed by Paul et al., 2014).

As whole-genome sequencing proceeds it is expected that new mutations associated with ciliopathies will be recognized. Baker and Beales predicted in 2009 that more than 72 syndromes were possible ciliopathies and, since then, some of their candidates have been confirmed to be indeed linked to ciliary dysfunction.

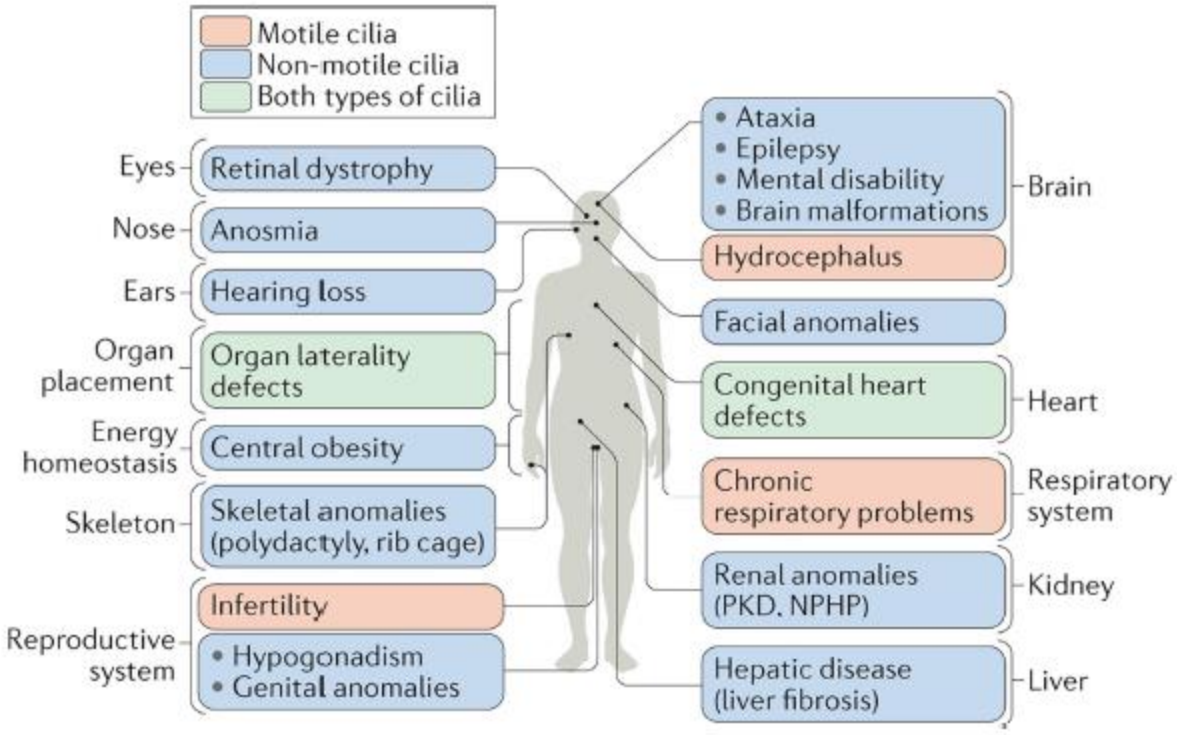

Figure 23: Defects in motile and/or non-motile cilia cause ciliopathies that can affect most human organ systems. The figure shows also the main phenotypic manifestations of the disease in each organ. NPHP, nephronophthisis; PKD, polycystic kidney disease (from Reiter and Leroux, 2017).

1.6 *Chlamydomonas* as a reference organism

The unicellular flagellated green alga *Chlamydomonas reinhardtii* is an excellent laboratory species: it grows vegetatively as a haploid cell, which allows mutant phenotypes to be expressed immediately, and, under optimal conditions, grows so quickly that its numbers can double approximately every 8 hours (Harris, 2001).

Chlamydomonas - from the Greek: *chlamys,* cloak or mantle, and *monas*, solitary - is the generic term used for a group of unicellular flagellates. Specifically, *Chlamydomonas* (*sensu stricto*) is comprised of three species (Pröschold et al., 2018). The majority of the contemporary *C. reinhardtii* laboratory strains were derived from a single zygote isolated from a potato field in Massachusetts in 1945 (Harris, 2001).

Structurally, *Chlamydomonas* has an oval-shaped cell body with a diameter of 5-10 µm. The two anterior flagella, with a 9+2 microtubule axonemal architecture, are critical for swimming in water, gliding on substrate and for mating processes (Harris, 2001). A single cup-shaped

chloroplast occupies a large proportion of the cell's volume. This organelle houses the photosynthetic machinery and contains the pyrenoid, a structure in which Rubisco is concentrated.

Close to the cell equator, at the edge of the chloroplast, is the eyespot. This primordial visual system allows the cells to orient their swimming toward or away from the light (phototaxis). Under hyposmotic conditions, the cytoplasmic water content is maintained by pumping water out of the cell through contractile vacuoles positioned at the cell's anterior (Komsic-Buchmann et al., 2014). Other features of the cell include a centrally located nucleus, a proteinaceous cell wall, Golgi bodies within the cup-shaped region formed by the chloroplast, and mitochondria (fig. 24).

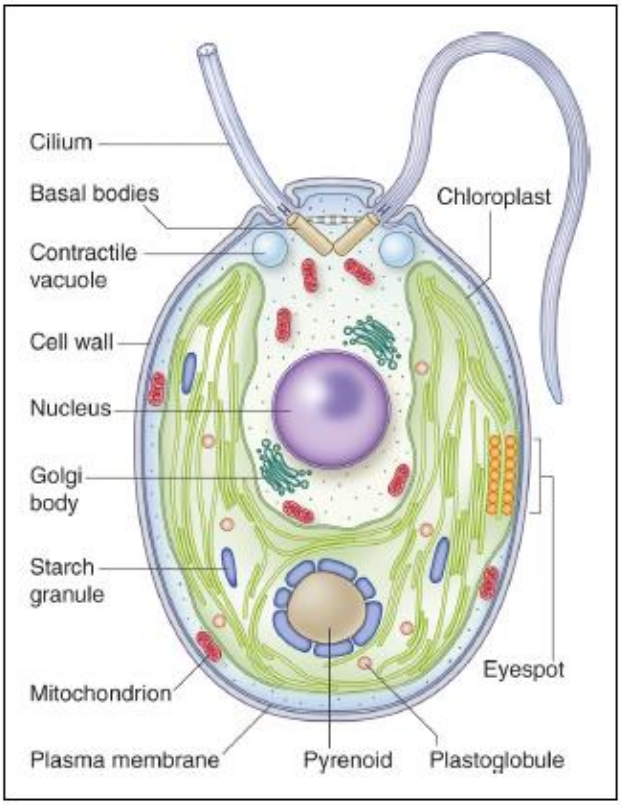

Figure 24: Drawing of a *C. reinhardtii* vegetative cell, reporting the structure of the cell body and its major features (from Sasso et al., 2018).

C. reinhardtii uses flagella to optimize light exposure during photosynthesis and for cell-cell recognition during mating. Forming zygotes likely allows cells to survive when conditions become austere (Harris, 2001; Goodenough et al., 2007). In the laboratory, vegetative growth occurs two mating types (mt^+ and mt^-), dividing by mitosis (Harris, 2001; Goodenough et al., 2007). Gametogenesis can be induced by nitrogen starvation (Treier et al., 1989) in specific light conditions; when nitrogen is added back to the medium, the zygotes germinate in the light, undergo meiosis and typically release four haploid cells that resume vegetative growth (fig. 25) (Harris, 2001).

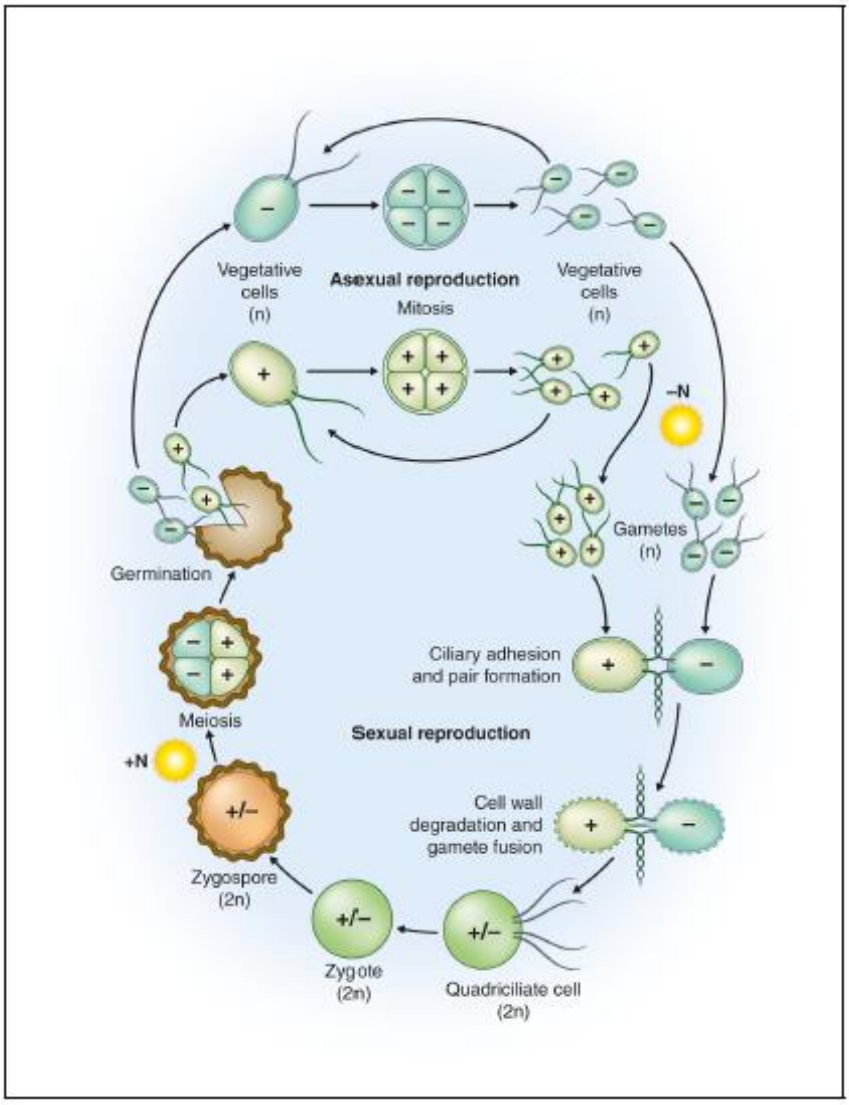

Figure 25: Life cycle of *Chlamydomonas reinhardtii* (from Sasso et al., 2018).

Studies on *C. reinhardtii* have provided many important results in different fields of the cell biology of flagella; we remind here, as significative examples, the discovery of IFT, and most part of the current knowledge on axonemal composition and function, including dyneins and the mechanisms of flagellar motility.

The benefits provided by *Chlamydomonas* as a model organism have been further increased by the advent of genetic transformation (Boynton et al., 1988; Remacle et al., 2006), the establishment of a full nuclear genome sequence (Merchant et al., 2007), the construction of a genome-wide library of mapped, indexed insertional mutants (Li et al., 2016) and by CRISPR-mediated targeted gene disruptions (Ferenczi et al., 2017). The nuclear and chloroplast genomes have been sequenced and annotated and organelles proteomes of *Chlamydomonas* are accessible. Based on genome sequences, proteins found in ciliates, including *C. reinhardtii,* were compiled in

the “Cilia Cut” list, consisting of 200 proteins (Li et al., 2004; Merchant et al., 2007). One major challenge will be to associate each protein with a function in cilia biogenesis and control, which will be aided by the availability of large mutant libraries (Li et al., 2016; Cheng et al., 2017), such as those deposited in *Chlamydomonas Resource Center* (*chlamycollection.org*).

2. Material and Methods

2.1 *Chlamydomonas reinhardtii* cultures

Chlamydomonas reinhardtii wild-type strain 137cc mt+, mutant strains *Roc22*, CC-5159 (*ift74-1*), CC-1919 (*fla10*), CC-1920 (*fla11*) were propagated on 2% agar (Bacto-Agar, Difco) plates prepared in Tris Acetate Phosphate (TAP) buffer (Gorman and Levine, 1965). Cells were then inoculated into liquid TAP medium for all experiments. The growth medium was prepared, with a final pH of 7.0, using the recipe schematized in the below summary table:

Solution	**Components**	**Molarity**
Tris Base (Trizma® base)	$NH_2C(CH_2OH)_3$	$2{,}00 \cdot 10^{-2}$ M
TAP-salts (Beijerinck salts)	NH_4Cl	$7{,}00 \cdot 10^{-3}$ M
	$MgSO_4 \cdot 7H_2O$	$8{,}30 \cdot 10^{-4}$ M
	$CaCl_2 \cdot 2H_2O$	$4{,}50 \cdot 10^{-4}$ M
Phosphate Buffer II	K_2HPO_4	$1{,}65 \cdot 10^{-3}$ M
	KH_2PO_4	$1{,}05 \cdot 10^{-3}$ M
Hutner's trace elements	$Na_2EDTA \cdot 2H_2O$	$1{,}34 \cdot 10^{-4}$ M
	$ZnSO_4 \cdot 7H_2O$	$1{,}36 \cdot 10^{-4}$ M
	H_3BO_3	$1{,}84 \cdot 10^{-4}$ M
	$MnCl_2 \cdot 4H_2O$	$4{,}00 \cdot 10^{-5}$ M
	$CoCl_2 \cdot 6H_2O$	$1{,}23 \cdot 10^{-5}$ M
	$CuSO_4 \cdot 5H_2O$	$1{,}00 \cdot 10^{-5}$ M
	$(NH4)_6MoO_3$	$4{,}44 \cdot 10^{-6}$ M
	$FeSO_2 \cdot 7H_20$	$3{,}29 \cdot 10^{-5}$ M
Glacial acetic acid	CH_3COOH	$1{,}74 \cdot 10^{-2}$ M

The liquid cultures were grown at 20-24°C, exposed at a cycle of 14 h of light and 10 h of dark, under a constant 5% CO_2 aeration (except for the strain CC-5159, which was grown without aeration).

For the temperature-sensitive strain *fla10* and *fla11*, the growth took place in medium at permissive temperature (22°C), then an aliquote of the culture was exposed to restrictive temperature (32°C) for 1,5 h.

2.2 Preparation of support film

For all the experiments reported in this study we utilized either Formvar® single slot (copper), or 75 mesh (nickel), or 300 mesh (copper and nickel) grids depending on sample and type of TEM analyses. Carbon-plastic (Formvar®) support films were produced by making – from a 2% Formvar® solution in 100% chloroform – a thin plastic film on the surface of a clean glass microscope slide. This plastic film was then released from the glass slide scratching its edges with a blade, and then leaving it to float on distilled water. Grids were then positioned individually onto the floating plastic sheet, with the opaque side of the grid facing down. The Formvar® film with the adhering grids was subsequently picked up using a piece of Parafilm.

Before use, 75 mesh and 300 mesh Formvar®-coated grids were carbon coated using a vacuum coating apparatus (Balzers' Union model MED 010). The thin carbon film made sample absorption on the grid more uniform, and improved the quality of the successive negative staining, providing an even background. Just before use, 300 mesh grids were treated with a solution of poly-L-lysine (MW 150-300 kDa, Sigma-Aldrich) to further improve the adhesion of biological material. The Formvar® carbon-coated grids were transferred for ~20 min on a small droplet (40 µl) of a solution of poly-L-lysine at a concentration of 2mg/ml, and subsequently washed 10x10 sec in H_2O_{dd}.

2.3 Negative staining and Immunolabeling

Suspensions of living cells of *Chlamydomonas,* harvested as described before and having full-length flagella, were centrifuged for 10 min at 900xg, in order to wash away the culture medium containing debris but, also, phosphate salts, which interfere with the use of uranyl salts. Pelleted cells were then resuspended in 10 mM HEPES, pH 7.4, at a final concentration of about $2x10^6$ cells/ml.

Chlamydomonas cells were left to adhere for 5 min onto Formvar® carbon-coated grids previously treated with poly-L-lysine (see above).

The experiments were then conducted using two inhibitors, W7 (A3281, Sigma-Aldrich) which inhibits Ca^{2+}/calmodulin-dependent protein kinases, and the 1294 compound (provided by Dr. Wesley Van Voorhis, Department of Medicine, University of Washington) which specifically inhibits protozoan CDPKs (Lendner et al., 2015). Both inhibitors were used in the presence of

adenylyl-imidodiphosphate (AMP-PNP), a nonhydrolyzable analogue of ATP, which stabilizes the binding of kinesin to MTs.

Cells, absorbed onto the grid, were exposed – by simply inverting the grid onto a drop of the inhibitor solution – to 5μM W7 (for a time of 30 sec), or to 5 μM 1294 (for 2 min); both inhibitors were dissolved in a solution of 10mM Hepes, 2mM $MgSO_4$, pH 7.4 (HM buffer), containing 2 mM AMP-PNP.

Grids were then transferred for 30 sec onto a droplet of HM buffer containing the nonionic detergent Nonidet P-40 (NP-40 0,1%), 2 mM AMP-PNP and 5μM W7 or 1294.

After 8x10 sec washes in HM buffer and 2x10 sec washes in H_2O_{dd} the grids were negatively stained with 2% uranyl acetate w/v in aqueous solution for 30 sec. During this exposure, the heavy metal-containing salt permeated the aqueous compartments surrounding the molecular components of the axoneme.

Excess staining solution was removed by gently blotting the edges of the grids with a piece of filter paper, then the grid was left to air-dry. The thin amorphous film of stain deposited on the grid by this procedure generated the differential electron scattering between the relatively electron-transparent biological material and the electron-opaque stain generating the negative contrast (Harris, 1997).

For the immunolabeling experiments, cells absorbed onto the grids were demembranated and washed as described above, then the grids were fixed for 30 min in 0,2% glutaraldehyde, 4% paraformaldehyde (IEM grade, diluted in the same buffer); grids were then washed again in HM buffer for 5 min and transferred in phosphate-buffered saline (PBS: NaCl 0,137 M; KCl 0,0027 M; Na_2HPO_4 0,01 M; KH_2PO_4 0,0018 M, pH 7.4) for 5 min.

In order to reduce aspecific signals, grids were sequentially incubated in glycine (0,1 M glycine, in PBS) for 15 min, and in Bovine Serum Albumin (0,1% BSA, in PBS) for 30 min, then washed again 2x5 min in PBS.

Primary antibodies utilized in this study:

- mouse monoclonal antibody specific for the IFT139 subunit of the IFT-A complex;
- rabbit polyclonal antibody specific for the IFT74 subunit of the IFT-B1 complex;
- mouse monoclonal antibody specific for the IFT81 subunit of the IFT-B1 complex;
- mouse monoclonal antibody, specific for the IFT172 subunit of the IFT-B2 complex;
- mouse monoclonal antibody, specific for the IFT57 subunit of the IFT-B2 complex.

All these antibodies were kindly gifted by Prof. Joel Rosenbaum, Yale University (USA).

Grids were incubated on a droplet of the antibody solution for 2 h; Antibodies were used at a 1:1 dilution. After the incubation with the primary antibody, the grids were washed 6x5 min

in PBS, and then incubated for 2 h with the gold-conjugated secondary antibody, i.e., an anti-rabbit and an anti-mouse antibody, respectively (10 nm gold-conjugated anti-rabbit IgG, Sigma G7402, and 10 nm gold-conjugated anti-mouse IgG, Sigma G7527). Secondary antibodies were used at a dilution of 1:20.

Finally, the grids were washed 6x5 min in PBS and 6x2 min in H_2O_{dd}, then negatively stained with 2% uranyl acetate w/v in aqueous solution for 30 sec.

2.4 Sample preparation and Epoxy Resin Infiltration of Flat-Embedded and of Centrifuged Cells (Pellet)

When *Chlamydomonas* cells are pelleted and then processed for transmission electron microscopy observations on thin sections, the flagella orient randomly and it is extremely laborious to find longitudinal sections over a long stretch of a flagellum. To circumvent this problem, Mitchell and Nakatsugawa (2004) set up an adequate and successful protocol: the flat-embedding.

The flat-embedding protocol allows to obtain *C. reinhardtii* samples displaying straight flagella on a flat surface, in order to facilitate their longitudinal sectioning.

All the following steps of the protocol were performed on glass coverslips treated with poly-L-lysine as regards the flat-embedding. Another set of experiments finalized to obtain cross sections of flagella was performed using cells pelleted in 2 ml-tubes. Samples for flat embedding and for pellet, were washed in HEPES 10 mM pH 7.4, fixed in glutaraldehyde solution 2,5% and incubated for 30 min at 4°C. The fixation was followed by 3 rinses with HEPES 10 mM pH 7.4. After that, osmium tetroxide at 1% in H_2O_{dd} was added followed by 30 min incubation at 4°C. After lipid stabilization and contrast by osmium postfixation, the samples were washed 3 times with H_2O_{dd}.

Successively, samples underwent through a serial dehydration steps, using a rising series of ethanol and they were then infiltrated with epoxy resin mixture (Glycid ether 100 cat. n°21045; 2-Dodecenylsuccinic-acid anhydride cat. n°20755; Methylnadic anhydride cat. n°29452;2-4,6 tris dimethyl-aminomethyl phenol cat. n°36975 by Serva Electrophoresis).

Resin on the coverslips carrying the sample was polymerized upside-down on a layer of Aclar film taking care of making a small chamber between Aclar and the coverslip to prevent cell squashing. The sample was set free from the glass coverslip, in order to correctly visualize the area of interest, and make possible the ultrathin sectioning at the ultramicrotome. Glass coverslip

could be removed from the embedded sample using two methods: an hydrofluoric acid bath or a freeze-shock with liquid nitrogen. After exposure to hydrofluoric acid the samples were processed by a second resin polymerization step for 24 h at 65°C.

As to the pelleted cells, the pellet was split in small pieces and each one was fixed, dehydrated, resin embedded and polymerized for 48h at 65°C in silicone molds.

2.5 Sample preparation- LW-Resin infiltration of Centrifuged Cells (Pellet)

In the post embedding immunogold-labeling technique, the biological material was first fixed, dehydrated, and embedded in acrylic resin able to preserve the antigenicity of the epitopes and the antibody reactions were performed on sectioned material.

The resin used for this experiment was the London White Resin (LWR), which is an acrylic, hydrophilic low viscosity embedding medium.

Chlamydomonas wild-type strain cells were centrifuged and resuspended in HEPES 10 Mm pH 7.4. The pellet was then fixed in HEPES 10 Mm pH 7.4 containing 0,2% glutaraldehyde and 4% paraformaldehyde (IEM grade), for 60 min at 4°C. Samples were rinsed with two, 5 min each, passages in HEPES 10 Mm pH 7.4, and finally washed twice in H_2O_{dd}.

Sample dehydration was performed by a graded series of ethanol, up to 90%. Pellet was infiltrated with LR Gold, it was then split up in smaller fragments which in turn were incubated in gelatin capsules.

Acrylic resins, as LRW, polymerization is inhibited by the presence of reacting oxygen species. To prevent this inconvenience, the capsules containing the pelleted fragments in resin were bubbled with gaseous nitrogen, paying attention to keep residual air bubble as small as possible by overfilling the capsule with gaseous nitrogen and LRW to convexity before closing the polymerization capsule.

Polymerization was then carried out at 25°C under UV light for at least 48 h and the capsule was removed by dissolving it in H_2O_{dd}.

2.6 Ultramicrotomy

Sections ~60 nm thick for standard TEM and 280/400 nm thick for tomography were cut from both pelleted and flat-embedded samples. Sections were obtained with a Diatome diamond knife type ultra 45°, mounted on an Ultracut-E Reichert-Jung ultramicrotome.

Sections, floating on H_2O_{dd}, were collected on formvar-coated single slot copper grids (or 75 mesh nickel grids for the post-embedding in LWR) and stained with 1% uranyl acetate in water and lead citrate (Reynolds, 1963).

For tomography, successively, a colloidal nanogold (10 nm) solution was applied for 60 sec on both sides of the resin slices.

2.7 Post-embedding Immunolabeling of LW-Resin Embedding Samples

After ultrathin sectioning of the LWR sample, sections harvested on 75 mesh grids were rehydrated by incubating them in PBS, saturated with BSA 3% in PBS for 2 hours and with Glycine 20 mM in PBS for 20 minutes, with the aim of avoiding non-specific antibody interactions with the sample.

After these steps, the grids were incubated overnight, at 4°C, with the primary antibody, a mouse monoclonal antibody specific for the IFT139 subunit of the IFT-A complex, diluted 1:1.

The next morning, the excess of antibody was removed with a wash in a droplet of PBS-Tween20 0,5% for 10 minutes, followed by 5 washes, 10 minutes each, in PBS.

Grids were then incubated in the secondary antibody (10 nm gold-conjugated anti-mouse IgG, Sigma G7527) used at a dilution of 1:20, for 2 hours at room temperature.

Finally, the grids were washed 5x10 minutes in PBS and 6x2 minutes in H_2O_{dd}, then stained with Reynolds method (see above).

2.8 Electron Tomography

Sections were observed and imaged by a Philips CM200 electron transmission microscope (TEM) fitted with a Field emission Electron Source and operating at an electron accelerating

voltage of 200kV. Imaging was performed by a CCD TVIPS F224HD camera. Series of tomographic images were collected using TVIPS EMMenu and EMTool software.

Serial samples projections were recorded every 1° of axis tilt rotation, from -60° to +60° (assuming as 0° the initial position of the sample), at magnification 27500x. After a first series was recorded, the grid was extracted by the microscope, rotated by 90° and a second tilt series was recorded along the orthogonal tilting axis.

IMOD software (http://bio3d.colorado.edu/imod/index.html) was used for image stakes alignment and tomograms assembly (Kremer et al., 1996). The signal-to-noise ratio was increased with mad_eed_3d software (Frangakis and Hegerl, 2001) from IMOD software.

The complete models were edited using UCSF Chimera (Pettersen et al., 2004).

2.9 Transmission Electron Microscopy of Thin sections

Samples were imaged by a FEI Tecnai G2 Spirit transmission electron microscope operating at an electron-accelerating voltage of 100 kV and fitted with a CCD camera 2K x 2K Veleta EMSIS, and ITEM software.

3. Results

3.1 The distal ciliary region is an ultrastructurally specialized district of the axoneme

Since the very first studies on *Chlamydomonas* flagella ultrastructure it appeared evident that the distal region of these organelles exhibits peculiar morphological features that distinguish it from the axonemal shaft (Ringo, 1967). These features, that later on were shown to be common also to cilia and flagella from other organisms (reviewed by Soares et al., 2019), essentially consist in the absence of the B-tubules and of all the components related to the genesis and control of motility, that is, the inner and outer dynein arms, the radial spokes and the central pair projections.

The level where the B-tubules terminate varies among individual doublets, and also the single A-tubules terminate one-by-one at random distances from the flagellar tip, while the two microtubules of the central pair persist almost to the very end of the flagellum. Hence, in about the last micron of its length, the flagellum decreases in diameter to form a blunt or slightly pointed tip. Concomitantly, an electrondense stripe of amorphous material – referred to as the "tip sheet" by Ringo (1967) - intercalates between the two central pair microtubules above the level where they have lost their projections. Located in the same district as the tip sheet, other authors have reported the occurrence of an helicoidal filament that surrounds the CP microtubules and is visible in negatively stained, demembranated *Chlamydomonas* flagella (Dentler and Rosenbaum, 1977). These observations have been recently confirmed and integrated by Lechtreck et al. (2013) in an accurate study on the de novo CP assembly along *Chlamydomonas* flagellar regeneration, that showed how the so-called tip sheet forms a sort of barrel-like element perpendicular to the CP plane, peculiar of the steady-state flagella but absent during early assembly stages.

We decided to start our investigations on the relationships that IFT components might establish with tip-specific structures during the conversion from the anterograde to the retrograde phase from an analysis *ex novo* of the organization of the distal region in *Chlamydomonas* flagella; the results we obtained on epoxy resin-flat-embedded flagella are reported in fig. 26. Here, the transition from the structural organization that is typical of the axonemal shaft, to that characterizing the distal tip region can be appreciated in longitudinal sections as a quite abrupt disappearance of the radial spokes (indicates by asterisks in A and B) and, consequently, to a clearer appearance of the flagellar matrix surrounding the CP. Sequential cross sections from proximal to distal flagellar regions (panels from C to F) illustrate, progressively, the disappearance of the B-tubules, the successive reduction in the number of the A-tubules, and, at the very distal flagellar tip,

the ends of the two CP tubules embedded in a plate of electrondense material. The “tip sheet” becomes progressively thicker towards the tip in longitudinal sections, and, in cross sections, appears as a barrel-like component with enlarged, often T-shaped ends protruding on both sides of the CP plane (white arrowheads). In both longitudinal and transversal sections, IFT trains can be identified as electrondense material located between the membrane and the doublet surface (black arrowheads). When found in the most distal flagellar region, IFT trains often seem to split into two components at a level approximately corresponding to the CP terminal plates (white arrows); the inner part of the train, originally adjacent to the doublet surface, appears to bend and contact the CP terminal plates, while the outer part of the train remains associated with the membrane even at levels above the plates (black arrowheads and black arrows in panel B, respectively).

These images suggested us the possibility that IFT trains, or at least part of them, could directly interact with the terminal CP capping structures.

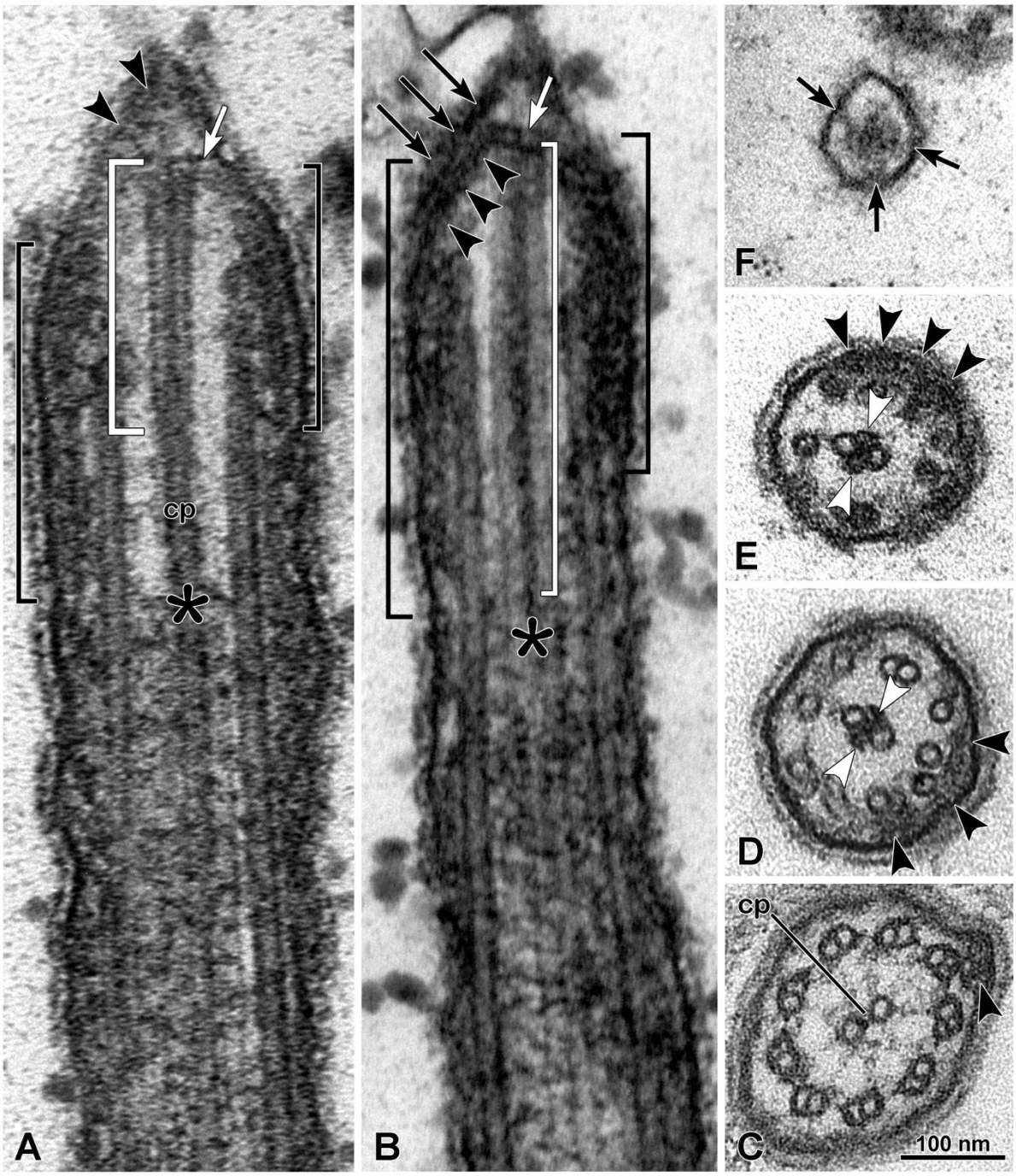

Figure 26: TEM micrographs of ultrathin sections of *Chlamydomonas* flagella. In **A-B**, the tip sheet is indicated by white squared bracket, while asterisk marks the end of radial spokes (RS) between the doublets and the CP. In **C-F**, distinct cross sections show the architectural modifications that occur along the flagellar length, from the very distal tip (**F**) down to the doublet region (**C**). White arrowheads indicate the electrondense tip sheet intercalated between the two microtubules of the central pair (**D-E**); black arrowheads in C indicate an electrondense IFT train and, more distally, IFT-like material that is located between the membrane and the A tubules (**E**) or remains associated with the membrane, distally to the terminal tip of the A tubules (black arrows in **F**). IFT trains, clearly visible in the longitudinal sections shown in **A-B** (black squared brackets), appear to split up in at least two components (black arrows, continuous with flagellar membrane and black arrowheads contacting the terminal plate of the central complex). The terminal plate of the CP is indicated by white arrows in **A-B**; at this level, cross section also shows links between the dense material underlying the membrane and the compact terminus of the CP (**F**).

3.2 Electron tomographic analysis of the flagellar tip

Electron tomographic procedures and 3D modeling protocols along with imaging analysis have provided a significant improvement and opened new possibilities for our understanding of the morphofunctional organization of cilia and flagella. Indeed, this approach has been employed for the study of several ciliary components, including dynein arms (Nicastro et al., 2006; reviewed by Ishikawa, 2013), radial spokes (reviewed by Ishikawa, 2013), the central pair projections and, more recently, for a detailed 3D reconstruction of doublet microtubules (Pigino et al., 2012).

Notwithstanding, the ciliary tip has till now escaped any analysis by means of advanced 3D electromicroscopy and computational approaches; this difficulty is probably due to the high complexity and structural variability that characterizes this district, thus impeding the subtomogram averaging required for the production of high-resolution ultrastructural data and 3D modeling.

To overcome this problem, we decided to perform our tomographic analysis on *single* flat-embedded flagellar tips. This methodological approach, that avoids any subtomogram averaging step, necessarily leads to a lower resolution but, even so, it can provide useful insights into the spatial relationships existing in situ between IFT trains and the CP capping structure.

The 3D model we obtained from one of such double tilt axis electron-tomographic reconstructions from thick sections of a flat-embedded flagellar tip is shown in fig. 27. This tomogram was selected among others for the occurrence of two IFT trains in proximity of the tip, which are indicated in figure 27A by brackets. The train on the left is about 50 nm wide and exhibits a highly compact organization; on this basis, it has been interpreted as an anterograde train (Pigino et al., 2009; Stepanek and Pigino, 2016). On the contrary, the train on the right shows a looser structure and the typical zig-zag pattern (the repeat of which is indicated in fig. 27A by dots) of the retrograde trains. The image substack shown in fig. 27B corresponds to the whole thickness of the flat-embedded section (see the substack shown in fig. 27C) and suggests that both the anterograde and the retrograde train establish a direct interaction with the distal end of the CP tubules.

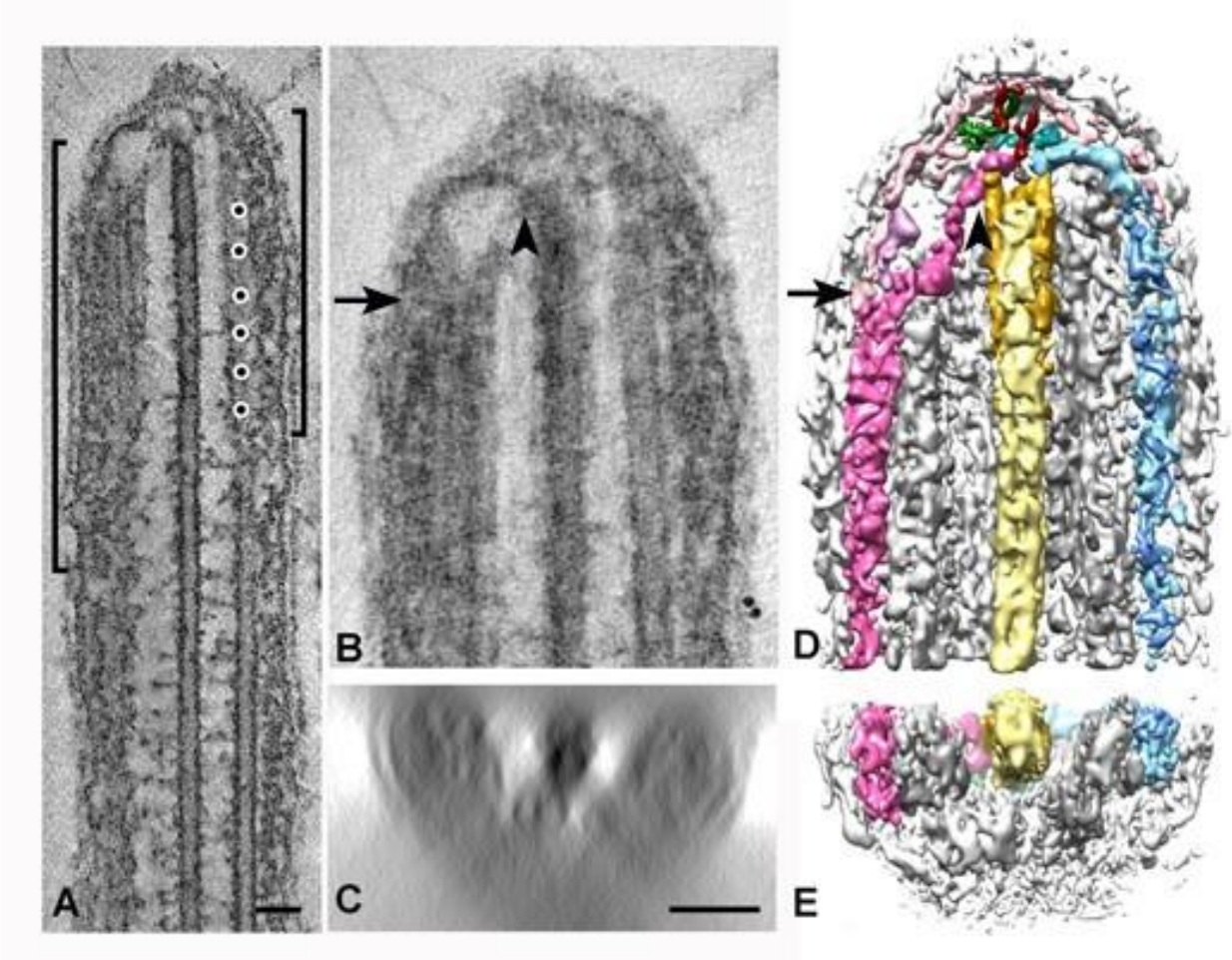

Figure 27: Tomogram of a flagellar tip of *Chlamydomonas reinhardtii.* In **A** is shown the presence of two IFT trains, indicated by the square brackets. The IFT train on the right, has the distinctive zig-zag periodicity of the retrograde train (dots). In **B-C** is shown the end of the tubule A (arrow) and the point of connection between the anterograde train and the CP (arrowhead). In **D-E**, the anterograde train is in pink, the retrograde one is in light blue. The two central tubules are in light yellow, the tip sheet is in gold yellow. Membrane and A tubules are, respectively, in white and in two alternated grey nuances. Bars in **A** and **C** = 50 nm.

The 3D model obtained by tomogram segmentation is shown in fig. 27D-E. It provides several information. First, the anterograde train, here depicted in different pink nuances, is confirmed to split at a level approximately corresponding to the end of the A-tubule; the outer part (light pink) of the train remains associated with the membrane and merge with the dense material that is sparcely with the membrane at the very distal tip district, the innermost one (hot pink) moves closer to the CP and contacts its distal end, while a third, intermediate mass (in plum) seems to terminate before reaching the very distal flagellar tip.

Second, the most distal tip district, which is located beyond the termination of the CP tubules and is expected to contain the CP capping structures described previously (Dentler and Rosenbaum, 1977; Dentler, 1980), appears to comprise multiple elongated elements (in dark green) (fig. 27); it is shown at a greater magnification and under different vantage points in fig. 28.

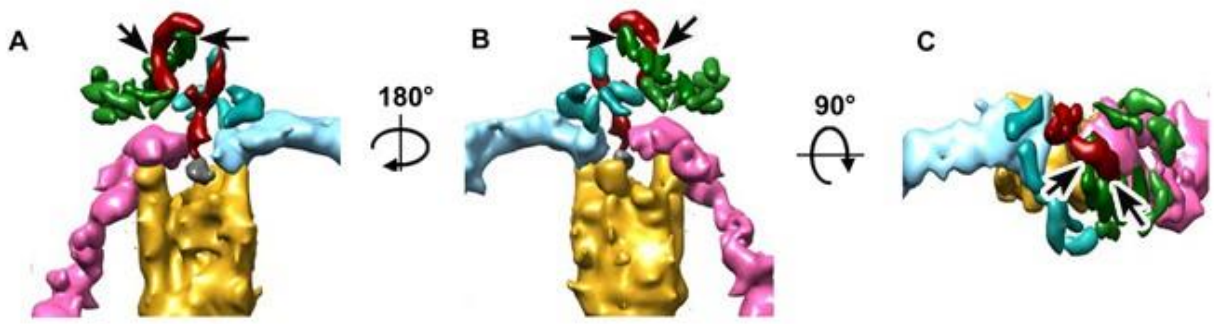

Figure 28 Tomogram analysis in details: the very distal tip components at a higher magnification, from different vantage points. A series of elongated elements (in dark green) appear to be closely associated with the ring (arrows); in light sea green are similar elements that are located on the side of the retrograde train.

The small elongated units are arranged roughly parallel each other in a sort of ribbon converging towards a central ring-like component (in red), that might correspond to the "sphere" described by Dentler (1980).

Third, the ring-like component and the innermost part of the anterograde trains contact the same restricted area above the distal end of the tip sheet, from which also the retrograde train emerges.

These data suggest that the terminal surface of the tip sheet might act as a hub for many components and might play a direct role in the anterograde to retrograde conversion.

3.3 Ultrastructure of the tip sheet

The electrontomographic results drew our interest towards the tip sheet, a till now uncharacterized flagellar component.

To get a better visualization, we looked for a procedure that could allow to expose the tip sheet completely. Among axonemal microtubules, the CP tubules are the most susceptible to depolymerization treatments. So, we treated whole *Chlamydomonas* cells, absorbed onto carbon-coated formvar grids, with a non-ionic detergent to remove both the membrane and the soluble matrix, and then, we exposed the demembranated cells to a cold temperature treatment (4°C, 1 hr).

After the sample was negatively stained, this protocol allowed us to visualize isolated ladder-like structures (LLS, from here on) that still maintain a continuity with the cap (terminal plates and the ring) (fig. 29) and are therefore likely to correspond to the tip sheet. LLSs consist of a central amorphous axis with thin lateral projections emerging on both sides; this morphology also

relates the LLS to the helicoidal filament reported to wrap around the distal CP region (Dentler and Rosenbaum, 1977). The latters are grouped in modules consisting each one of four projections; within each module, the first projection is separated from the second one by 10 nm, the second from the third one by 12 nm, and the third from the fourth by 16 nm (dots in fig. 29f). The number of modules observed in each LLS may vary from 1 to 3 with an interspace of about 25 nm between adjacent modules; hence we observed LLSs with an overall length up to 200 nm.

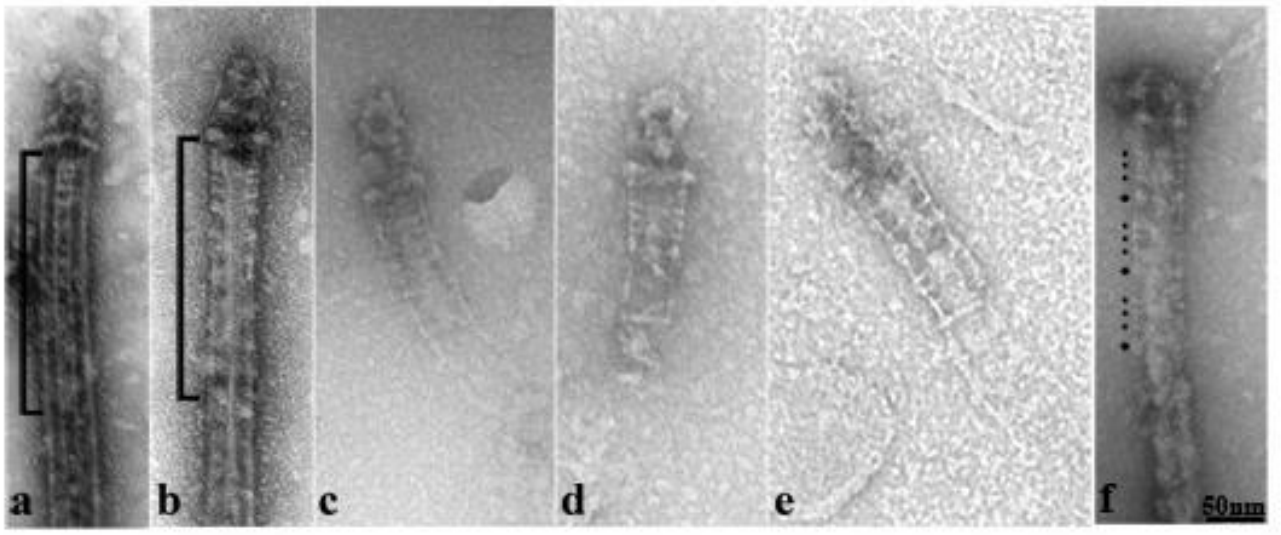

Figure 29: The ladder-like structure of the axonemal central pair microtubules. Negative staining samples of demembranated flagella. In **a-b** the structure, indicated by square brackets, is located transversally to the A tubules, enwrapping them. In **c,d,e** the LLS is well visible and isolated by cold treatment from the tubules, revealing an intimate connection within this structure and the capping structures. In **f** is reported the periodicity of the projections of the LLS.

These data induce to consider the electrondense tip sheet, or LLS, as a true component of the distal specialized region of *Chlamydomonas* axoneme, comprised of two distinct regions, i.e., a central amorphous axis and two lateral series of regularly arranged projections. It is interesting to note that the LLS seems to be continuous with the cap, since the proximal terminal plate – which does not consist of a unique plate, but rather is divided into two separated parts – is linked by thin filaments to the LLS, on one side, and to the ring, on the other side. Also, these observations exclude that the ring, or bead, derives from the membrane and has a lipidic composition, as was previously hypothesized (Dentler and Rosenbaum, 1977).

3.4 Protein kinase and protein phosphatase inhibitors block the dissociation of IFT particles and determine their accumulation on the CP capping structures

In order to confirm the interaction of IFT particles with the CP capping structures that had been suggested us by both electronmicroscopy of flagella flat-embedded thin sections and electrontomographic analysis, we first decided to check the effect that addition of protein kinase inhibitors might exert on the release of IFT particles during membrane removal.

The current information on the turnaround process, in fact, suggest that the molecular motor kinesin-2 dissociate from IFT particles at the ciliary tip as a consequence of a phosphorylation event, that in *Chlamydomonas* is mediated by the calcium-dependent kinase CDPK-1 and occurs on the S663 residue of the FLA8 subunit (Liang et al., 2014). The release of kinesin-2 from the anterograde train is thus an early event of the turnaround process, and its inhibition is expected to result in the block of the turnaround path at the flagellar tip. In addition, a putative protein phosphatase has been involved in the control of kinesin-2 dissociation from the anterograde train (Liang et al., 2014).

We tested two kinase inhibitors - W7, a general inhibitor for Ca^{++}-dependent kinases, and 1294, a synthetic compound specific for apicomplexan CDPK-1 that has been developed as a potential therapeutic drug (Johnson et al., 2012) – and a cocktail of protein phosphatase inhibitors. In our experiments, we added the inhibitor to the cell suspension briefly before detergent treatment for membrane removal; the grid-absorbed, demembranated cells were then processed for negative staining.

Both kinase and phosphatase inhibitors induce the accumulation of particles which maintain their association all around the cap also after detergent treatment (fig. 30). These piles contain both elongated and globular particles which, for their size and shape, might be reminiscent, respectively, of the IFT-B and the IFT-A complex (Jordan et al., 2018); sometimes, ring-like particles, reminiscent of dynein, can also be observed (E). It is possible to distinguish some elongated elements that insert directly onto the terminal plates (fig. 30D, arrowheads); also, the association of particles may not be limited to the cap region only, but may occur as well laterally, along the CP (square brackets in A-B) (fig.30).

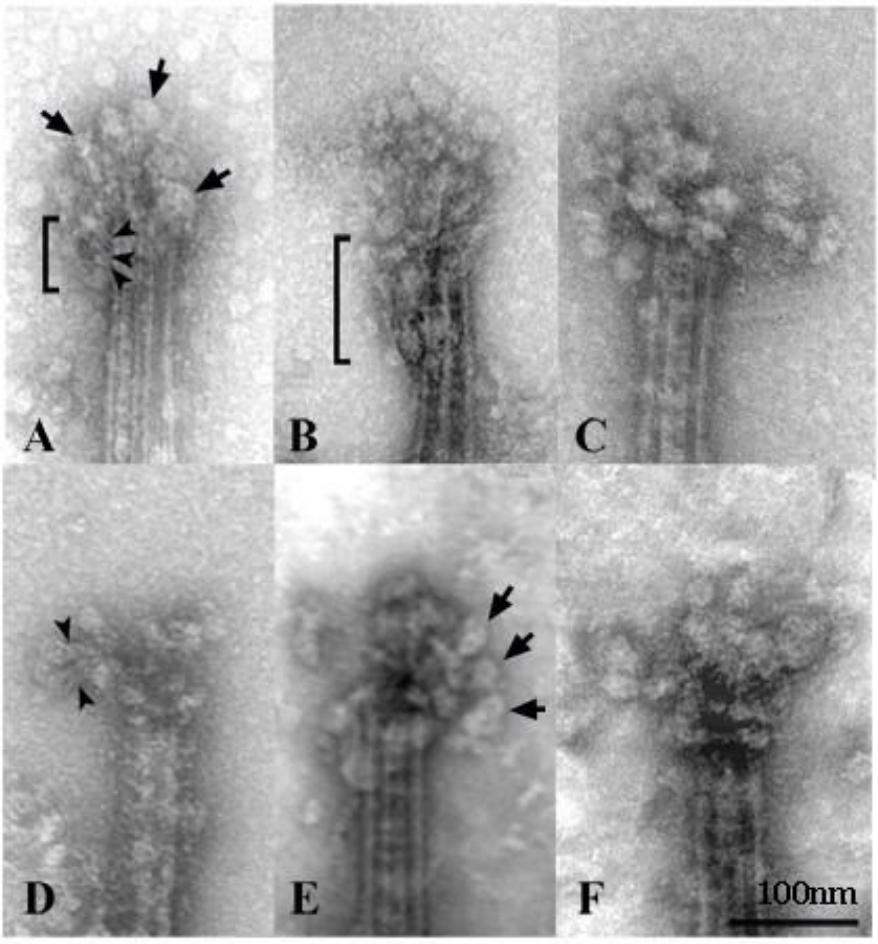

Figure 30: Effects of protein kinase and protein phosphatase inhibitors on IFT turnaround. Both inhibitors block IFT turnaround and induce the accumulation of IFT particles around the tip and the LLS (square brackets). Arrowheads indicate elongated elements and the arrows indicated other components associated with IFT.

These observations indicated us that the presence of calcium-dependent kinase or phosphatase inhibitors does not allow IFT particles to undergo a complete dissociation, and, furthermore, suggest that IFT particles establish a transient association with the distal CP structures during their anterograde to retrograde conversion.

3.5 IFT subcomplexes differentially interact with the distal CP district

We then performed a series of immunoelectronmicroscopy (IEM) observations on grid-absorbed demembranated cells, aimed at confirming that IFT components actually interact with the tip of the CP complex. These experiments were carried out in the absence of kinase or phosphatase

inhibitors, in order to avoid the piling of particles around the tip and to obtain a clearer visualization of the tip structures. We used antibodies for subunits of the complexes IFT-A (IFT139), IFT-B1 (IFT74, IFT81), and IFT-B2 (IFT172, IFT57). The results we obtained are reported in figg. 31-35.

Through repeated immunolocalization experiments carried out on demembranated cells, we were never able to observe any reactivity with the IFT139 antibody. This finding suggested us that the IFT-A complex might be solubilized by the detergent along with the membrane, and thus may be part of the membrane-associated material colored in light pink in fig. 27D. To get support to this hypothesis, we immunolocalized the IFT139 subunit on thin sections of LW-embedded cells, which still preserve the flagellar membrane. In these samples, IFT139 was found to localize close to the membrane (fig.31). These observations are in agreement with the position of the IFT-A complex indicated in the 3D model proposed by Jordan et al. (2018) as strictly apposed to the membrane and support the possibility that this complex is indeed completely solubilized during membrane removal.

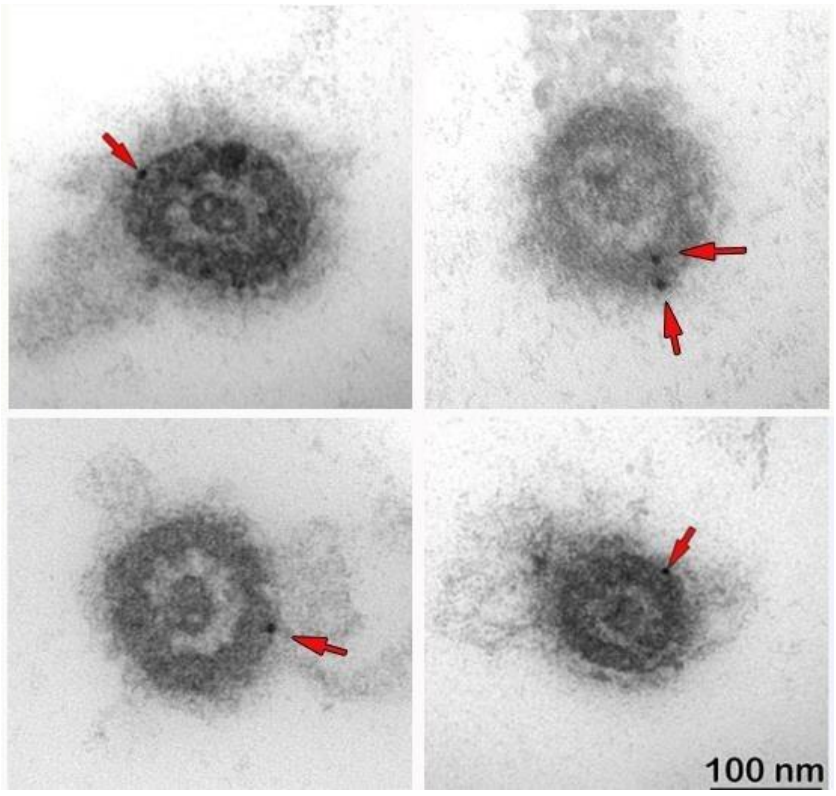

Figure 31: IEM carried out on LW-R embedded flagella. Cross sections showing the detection obtained with the IFT139 antibody (IFT-A complex), strictly localized to the membrane. Red arrows indicate the gold particles (10 nm).

On the contrary, all the antibodies against IFT-B1 and IFT-B2 subunits reacted positively with demembraneted flagella and marked the distal CP region. Interestingly, the IFT-B1 and IFT-B2 antibodies showed distinct spatial distributions. IFT172 revealed the most confined localization

(fig. 32), which approximately coincides with the length of the LLS. Gold particles were never found more distally to the terminal plates.

The peculiar IFT172 localization is in line with the reported interaction occurring between this subunit and EB1 (Pedersen et al., 2005), a plus-end microtubule binding protein with a comet-like distribution (Pedersen et al., 2003). Among IFT proteins, IFT172 is the only subunit the contains in its sequence the SxIP motif, known to identify proteins able to bind EB1 (Buey et al., 2012).

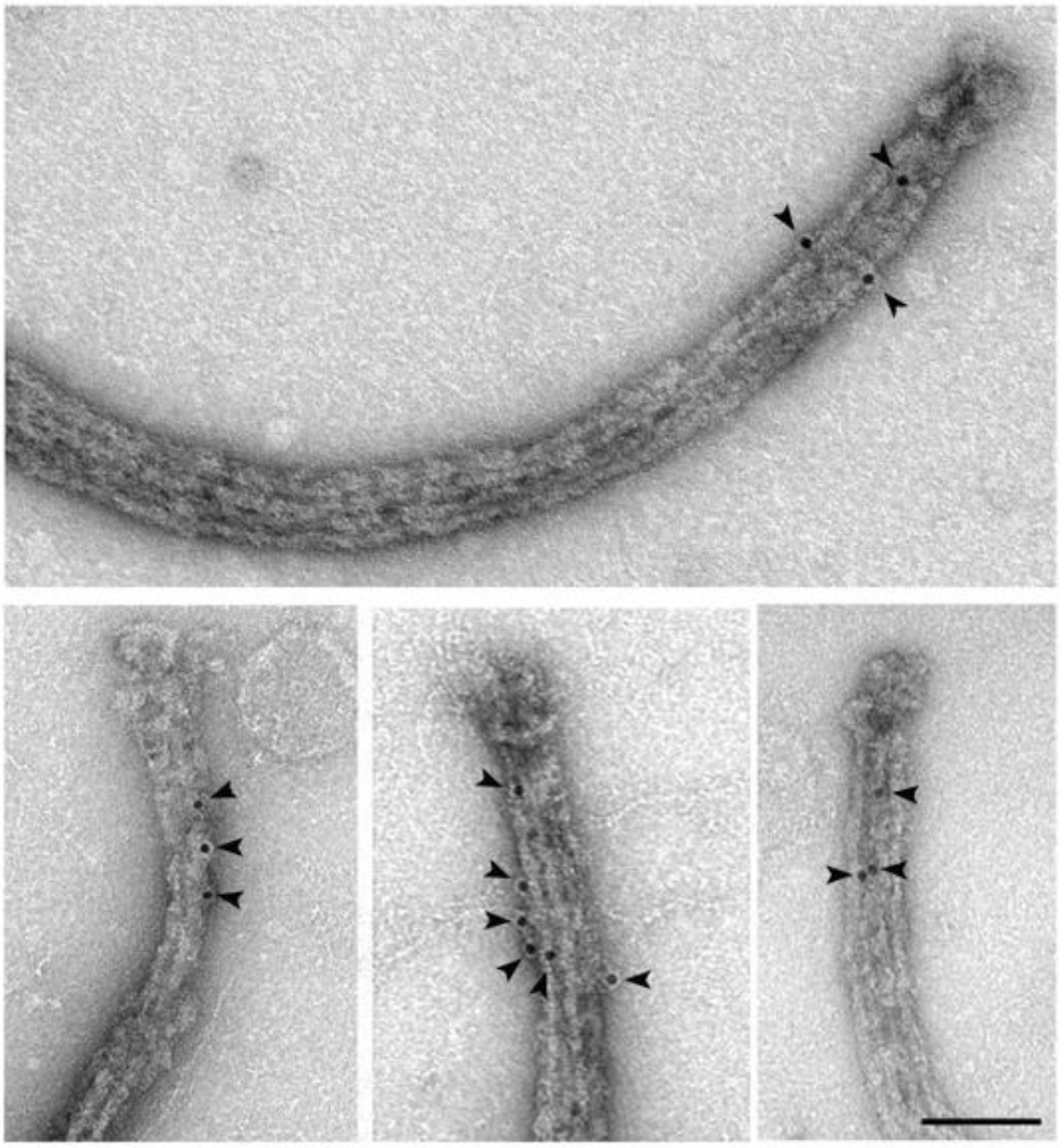

Figure 32: TEM micrographs of the distal portion of the CP complex, after immunolabeling with the IFT172 antibody and negative stain. Black arrowheads indicate the gold particles. Scalebar = 100 nm.

A similar gold particle localization was observed with the IFT57 antibody (fig. 33); in this case, however, the labeling was found to be much lower. This subunit has a direct role in the assembly of the subcomplex IFT-B2 (Jiang et al., 2017), and might be less accessible to the antibody.

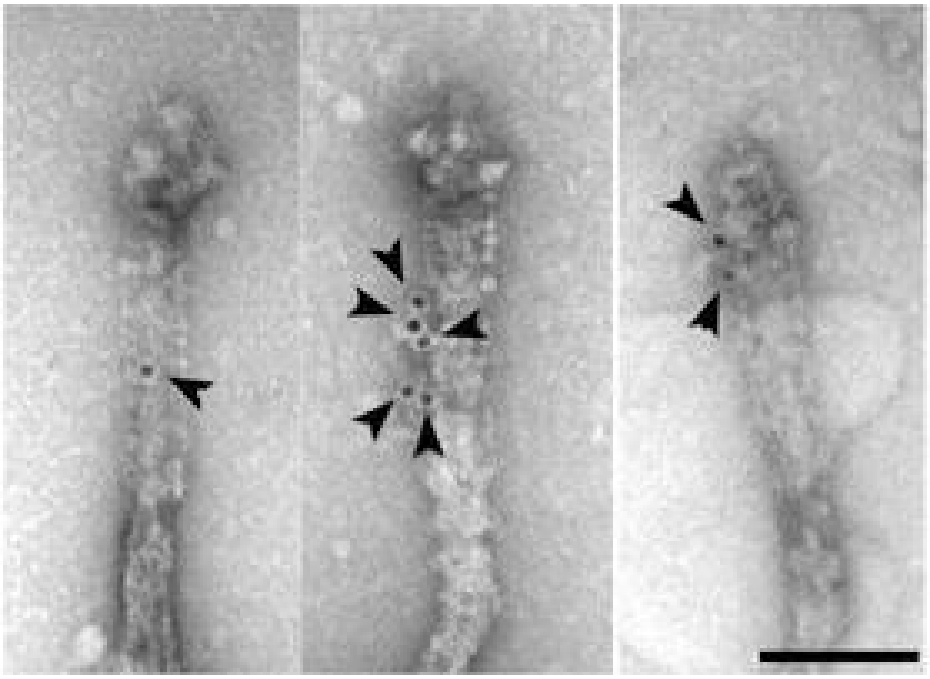

Figure 33: TEM micrographs of the distal portion of the CP complex, after immunolabeling with the IFT57 antibody and negative stain. Black arrowheads indicate the gold particles. Scalebar = 100 nm.

While the reactivity of the two antibodies for the IFT-B2 complex was restricted to the LLS-containing region of the CP, the antibodies for the IFT74 and IFT81 subunits of the IFT-B1 complex, on the contrary, were found to label mainly the cap structures (terminal plates and ring) (figg. 34-35). The overlapping labeling distribution observed with these two antibodies is in agreement with the involvement of the two IFT74 and IFT81 subunits in the formation of a heterodimer (Lucker et al., 2005).

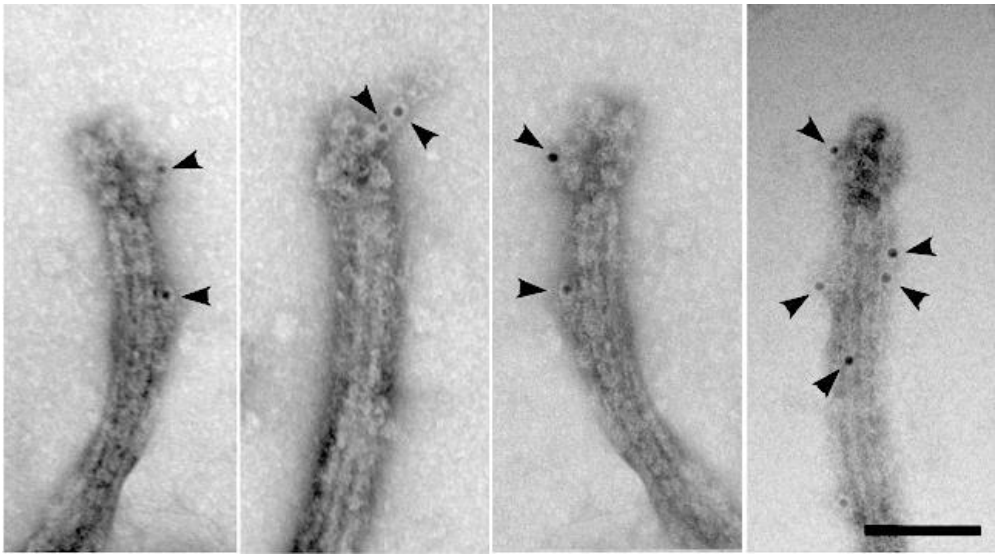

Figure 34: TEM micrographs of the distal portion of the CP complex, after immunolabeling with the IFT74 antibody and negative stain. Black arrowheads indicate the gold particles. Scalebar = 100 nm.

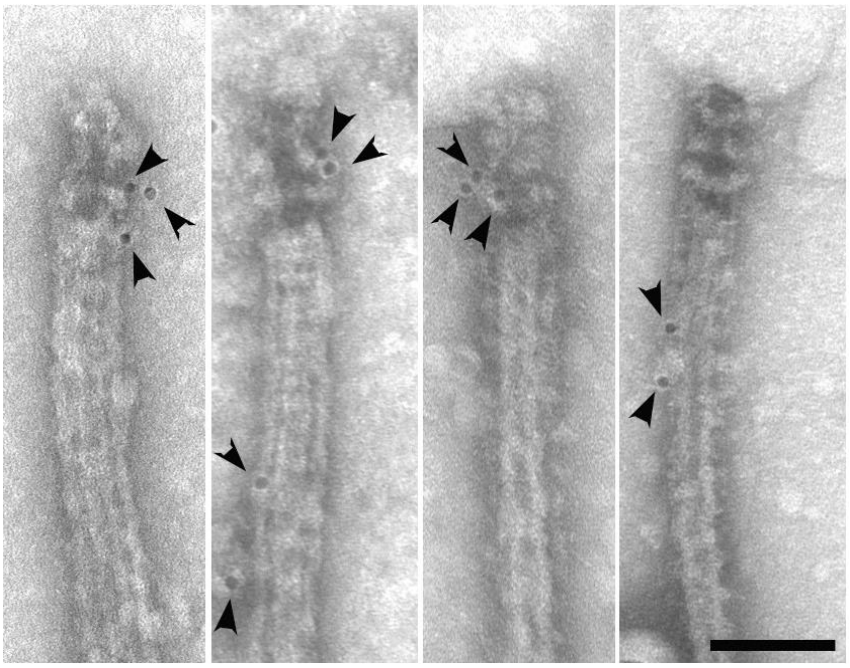

Figure 35: TEM micrographs of the distal portion of the CP complex, after immunolabeling with the IFT81 antibody and negative stain. Black arrowheads indicate the gold particles. Scalebar = 100 nm.

Fig. 36 reports the position of all the gold particles we have observed with each one of the four antibodies, thus allowing to directly compare the labeling distribution obtained with our antibodies.

The whole set of immunoelectronmicroscopy experiments clearly indicates that IFT-B1 and IFT-B2 differentially interact with the CP, with the latter interacting only with the LLS-containing CP region and the former also localized distally to the terminal plates, at the ring level.

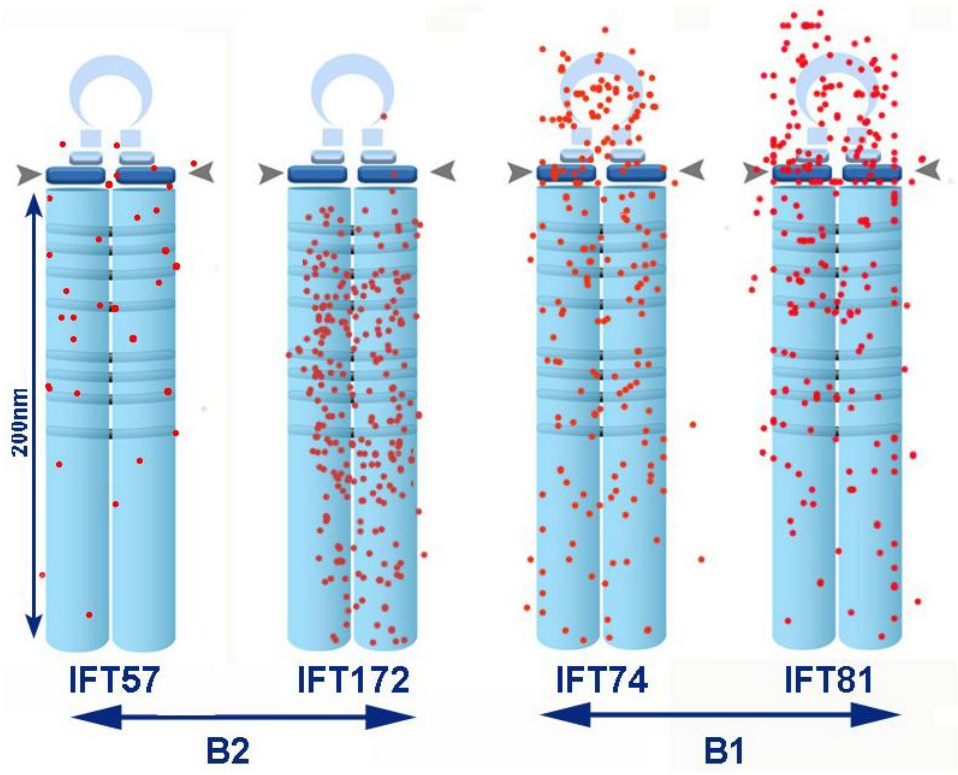

Figure 36: Schematic distribution of the gold particles localization observed in the IEM experiments.

3.6 Mutant *fla11*^{ts} flagella exhibit a reduced binding of IFT172 to the LLS region of the CP

Among the various IFT proteins, IFT172 exhibits a peculiar behavior, in that it is the most loosely associated subunit within the IFT-B complex (Lucker et al., 2005). It has been implicated in the turnaround process through the analysis of *fla11*^{ts}, a mutant strain that carries a single-point mutation resulting in the replacement of a conserved leucine with proline at residue 1615 of the IFT172 molecule (Pedersen et al., 2005). This mutant possesses a temperature sensitive phenotype, since at the restrictive temperature (32°C) it accumulates IFT proteins at the flagellar tip, a feature indicative of a defective turnaround.

Using the same immunolocalization protocol reported above, we analyzed IFT172 labeling in the *fla11*^{ts} mutant, at both the permissive and the restrictive temperature, and compared it with that observed in wild type flagella. Labeling was quantified by calculating average of gold particles found per CP; the results are reported in fig. 37, and show a significant reduction of labeling at the restrictive temperature of 32°C (about 50% respect to the wild type), and an intermediate decrease at the permissive temperature of 22°C. These values fit well with the restrictive and permissive phenotype described by Pedersen et al. (2005).

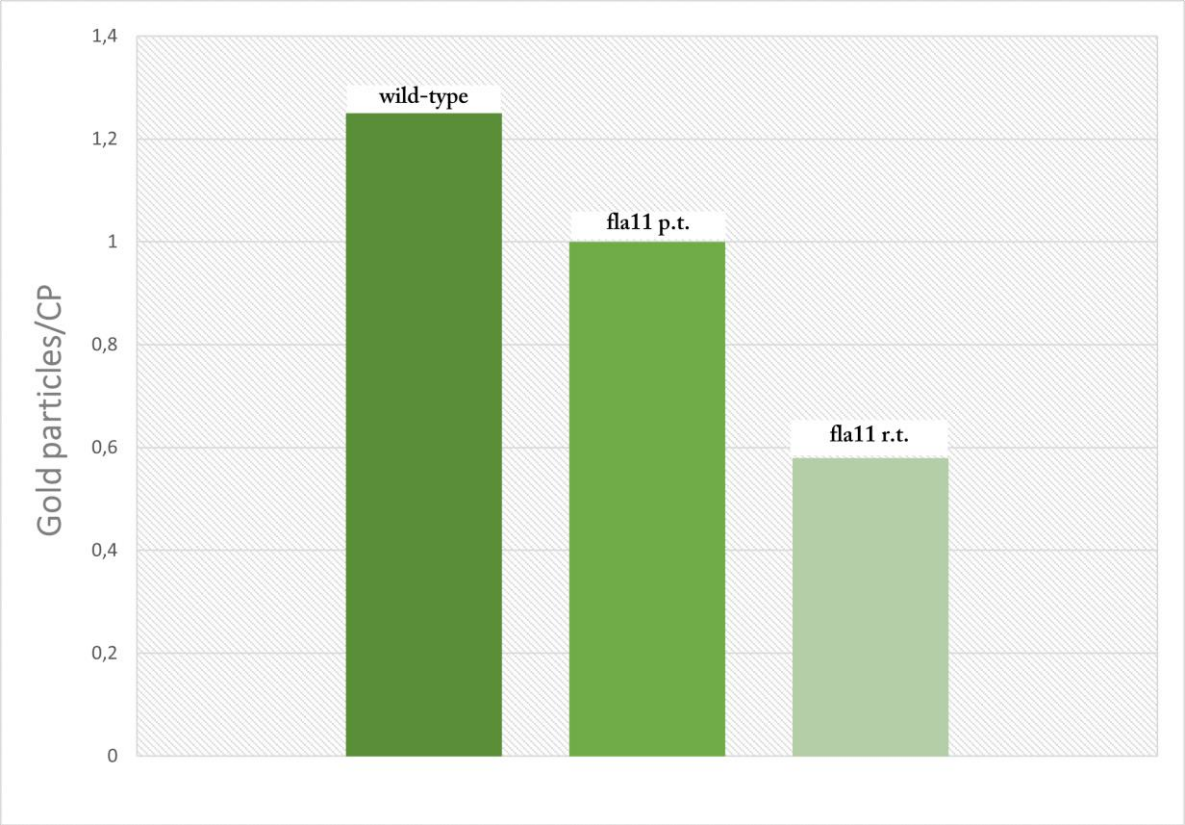

Figure 37: Average number of gold particles/CP found for each CP in wild-type and in *fla11*^{ts} flagella at permissive and restrictive temperature.

3.7 Is the IFT-B1 complex a main component of the cap?

The strong labeling observed with the IFT74 and IFT81 antibodies distally to the terminal CP plate suggested us the possibility that the IFT-B1 complex might be a main component of the cap.

We thus decided to compare our results with the 3D model of the IFT-B complex recently proposed by Jordan et al. (2018). In the anterograde train, the IFT-B complex is arranged as a series of parallel, elongated structural elements, that are associated on one side with the inactive dynein-1b; close to the flagellar tip, dynein dissociates from the train (Jordan et al., 2018).

We first compared the IFT-B 3D model (EMD-4303) with our tomographic results, overlapping each other. We noted that the part of the train (in plum and indicated by an arrow in fig. 38) that terminates before reaching the very distal tip region, is likely to correspond to dynein-1b. This correspondence can also underly the abrupt end of this part of the train, since the activation of dynein at the tip is expected to involve also its dissociation from the anterograde train (Jordan et al., 2018; Toropova et al., 2019). As a consequence, the part of the anterograde train that contacts the terminal plate/LLS region should consist of the IFT-B complex only. Along with the

immunoelectronmicroscopy findings, this observation indicates that only IFT-B, and specifically the IFT-B1 subcomplex, associates with, or is part of the CP capping structures.

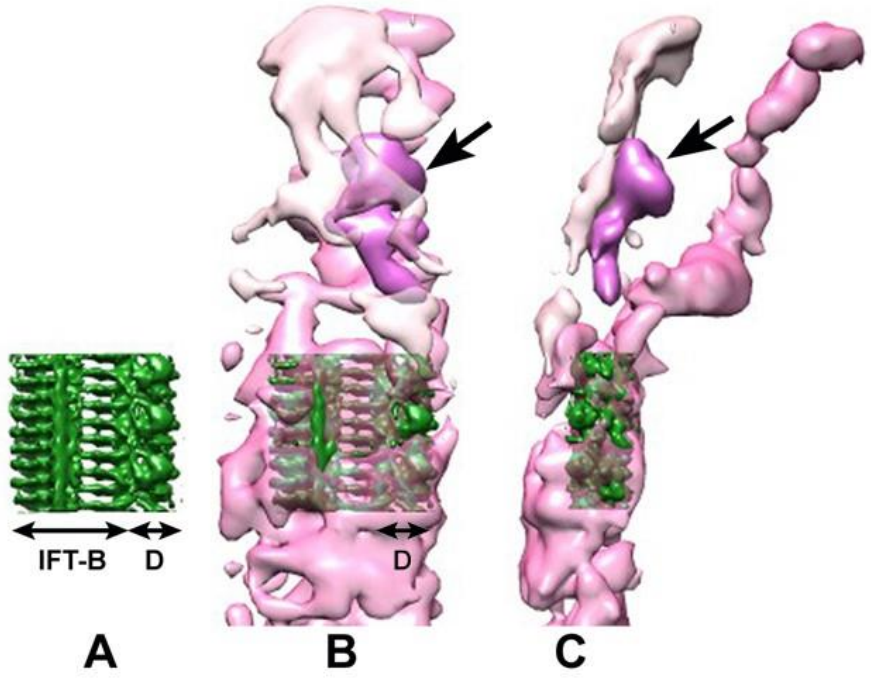

Figure 38: **A**. The model EMD-4303 (Jordan et al.,2018), which includes both the B complex (IFT-B) and inactive dynein (D), as indicated. **B-C**. Fitting of the Jordan's model into the distal part of our tomographic reconstruction of the anterograde train shown in fig. 27. **B**: view from the membrane; **C**: side view.

Searching for further support to this hypothesis, we compared the Jordan's IFT-B 3D model with our negatively stained images of the capping CP structures. The latters are characterized by a highly variable conformation (see for example the three conformations shown in fig.39), as it can be observed also in the original papers by Dentler and Rosenbaum (1977) and Dentler (1980); such variability may be further increased by the possible occurrence of other flagellar components that occasionally remain associated with the cap after detergent treatment (see for example the arrow in fig. 39A).

In our negatively stained samples, the cap was shown to consist of thin elongated elements, frequently with a sort of small knob at their mid region (arrowheads in fig. 39A-C).

We verified the possible fitting of the IFT-B 3D model (EMD-4303) deposited in the EMDB, to the capping structures. The dynein domain was removed from the model; the latter was then curved and torqued to adapt it to the underlying cap. Fig.39A'-B' shows three examples of how the elongated structure of the IFT-B model might fit with at least part of the cap structures, raising the possibility that part of this complex is indeed part of the cap.

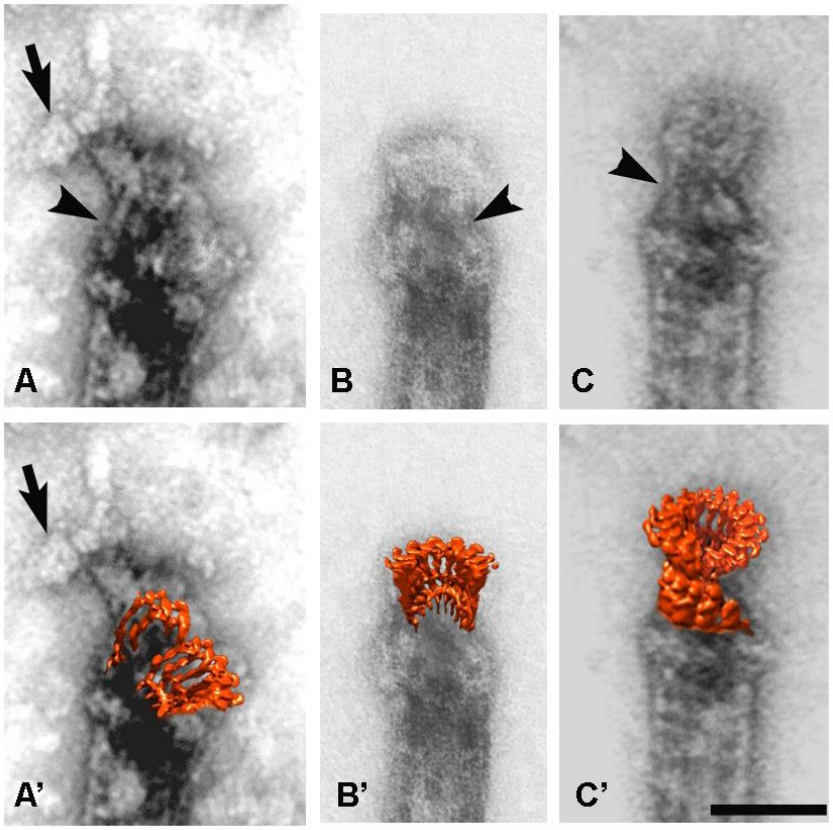

Figure 39: Overlapping of the IFT-B model (EMD-4303) deposited in the EMDB, on the capping structures. The three different cap conformations shown in this figure were selected since they were frequently observed, and might represent sequential steps leading to the ring-shaped cap. The black arrowheads indicate thin elongated elements, the arrow indicates accessory components associated with the cap. Scalebar = 50 nm.

3.8 Flagella of the mutant *ift74-1* do not show any cap structures

The above reported results suggest that - if in *Chlamydomonas* flagella the IFT-B1 complex is indeed part of the cap - the appearance of the capping structures might be linked to the presence of a functional IFT system.

To check this hypothesis, we analyzed the *Chlamydomonas ift74-1* mutant, which expresses a truncated IFT74 subunit, lacking 196 residues at the N-terminus (Brown et al., 2015). This mutant can assemble only half-length flagella which do not exhibit the cone-shaped tip typical of wild-type flagella, but are instead characterized by a flat tip (fig. 40). Longitudinal sections show that in this mutant the CP exhibits the same length as the doublets, and that the membrane is closely lining over the axoneme end, indicative of the absence of any capping structure. Interestingly, this phenotype is similar to that exhibited by the mutant *Roc22*, an insertional null mutant for FAP256/Cep104, a protein localized at the plus end of both the CP and the A tubules (Satish-Tammana et al., 2013) and reported to interact with IFT74 (Al-Jassar et al., 2017, fig S2).

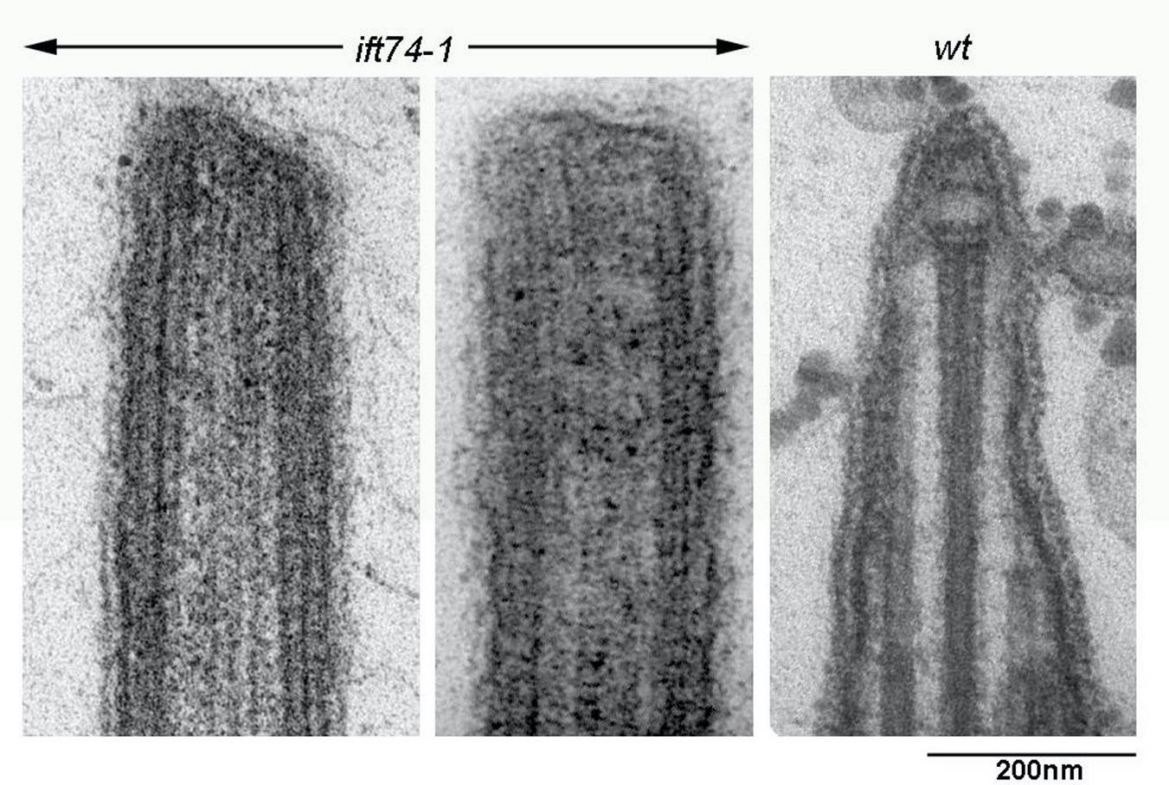

Figure 40: TEM micrographs of resin-embedded flagella from the *Chlamydomonas ift74-1* mutants (left and central panels) and the wild-type (right panel).

These findings support the requirement of an intact IFT-B1 subcomplex for the assembly of the capping structures and for a functional turnaround process.

3.9 IFT disruption leads to the disappearance of the ring component of the cap

We reasoned that – if the presence of the ring is indeed related to the establishment of an efficient IFT system – then the interruption of IFT transport should lead to the disappearance of the ring. We investigated this possibility using the *Chlamydomonas fla10* temperature sensitive mutant, that carries a point mutation at residue 329 of the FLA10 motor domain; in this strain IFT transport undergoes a complete cycle at the permissive temperature of 21°C, but is interrupted at the nonpermissive temperature of 32°C due to the block of anterograde transport (Kozminski et al., 1995).

The results we obtained clearly reveal that *fla10* flagella exhibit distinct phenotypes at the permissive or restrictive temperature (fig. 41).

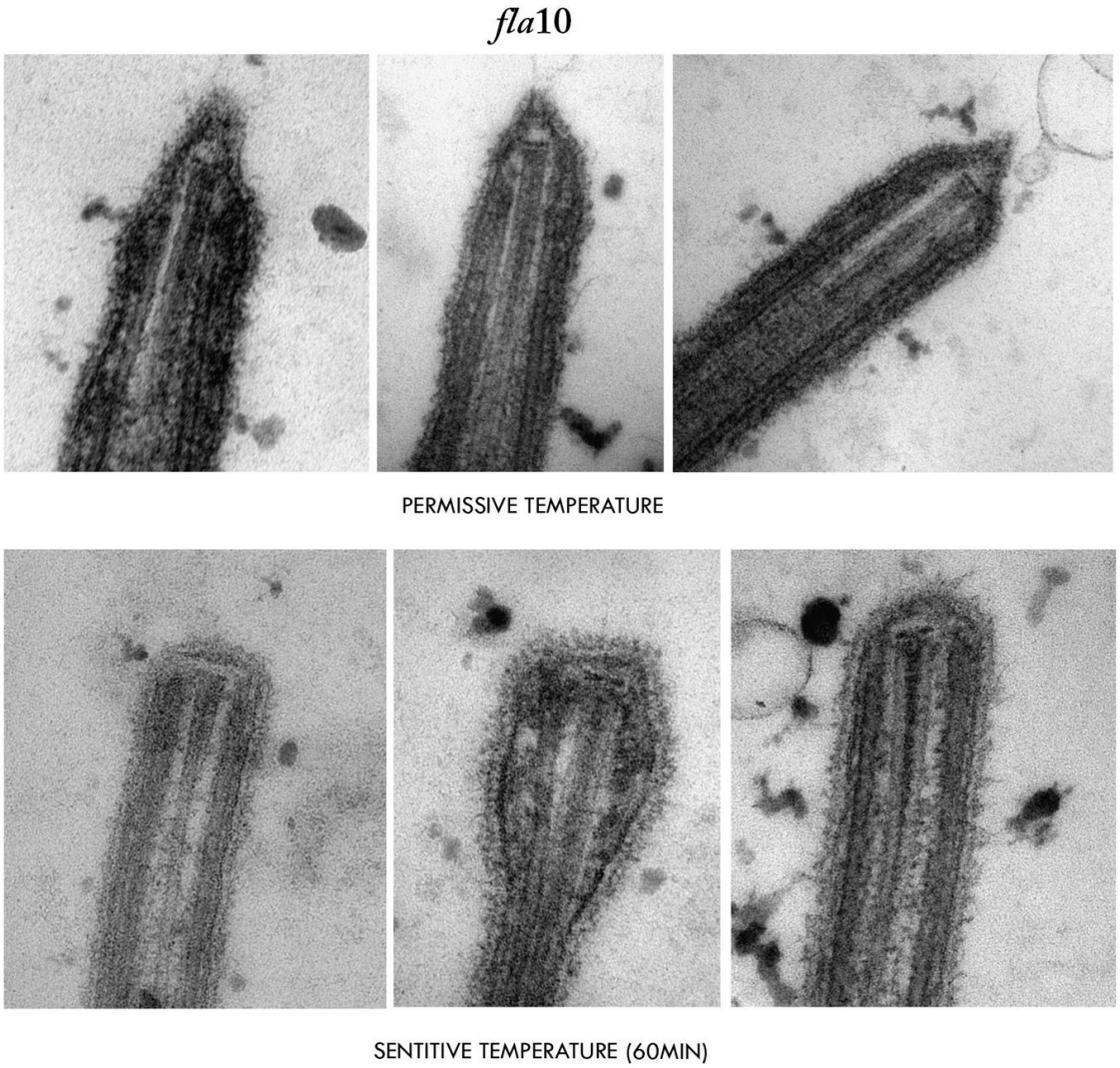

Figure 41: TEM micrographs of flat-embedded *fla10* mutant flagella. The top panel shows the phenotype observed at the permissive temperature (22°C), which is similar to that of the wt flagella; the bottom panel shows the flat tip phenotype observed at the restrictive temperature (32°C).

At the permissive temperature of 22°C, the tip of *fla10* flagella is almost the same as the tip in wild-type flagella, with the typical pointed shape. After *fla10* cells are incubated at the restrictive temperature (32°C) for 1 hr, IFT cycling is interrupted and flagellar resorption is just beginning. In such experimental conditions, flagella display a flat phenotype, indicative of the absence of the ring structure and the terminal plates are still present at the end of the CP.

As a whole, our results indicate that the ring disappears both in the case the defect occurs in proteins that are likely to be involved in the interaction between IFT and the CP distal segment (IFT74 in the IFT-B2 subcomplex, and Cep104 on the CP) and in the case the IFT process is disrupted due to a defective kinesin-2 motor.

3.10 The LLS and the cap ring are associated structures that assemble even in the absence of the CP

Our data indicate a close structural and functional association between IFT-B, the LLS (or tip sheet) and the capping structures located at the plus end of the CP complex. In order to verify if the assembly of the CP complex is an indispensable requisite for the presence of both LLS and the cap, we analyzed the *Chlamydomonas pf18* mutant strain; these cells are unable to assemble the CP complex, which is replaced by an amorphous central core (Lechtreck et al., 2013).

Surprisingly, we observed in the *pf18* flagella the presence of an ectopically assembled ladder-like structure, associated with one of the A tubules (stripes in fig.42A); also, ring-like arrangements could be evidenced at the tip of negatively stained demembranated flagella (arrows in fig. 42B).

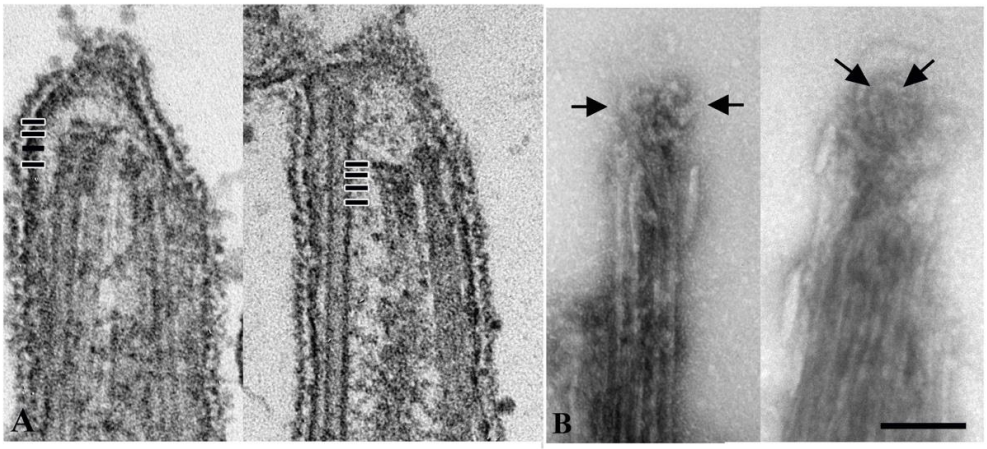

Figure 42: TEM micrographs of *pf18* mutant flagella. In panel **A**, resin-embedded flagella show an ectopic LLS; in panel **B**, demembranated and negatively stained flagella still show ring-like components (arrows).

To confirm that IFT components interact with (or are part of) the ring-like structure and the ectopic LLS of *pf18* flagella too, we performed an immunolocalization study with the IFT74 antibody, in order to compare flagella from this mutant strain with wild type cells; the results clearly indicate that the LLS, when ectopically formed, and the ring-like structures which are associated with the ectopic terminal plates are indeed labelled by the IFT74 antibody (fig. 43).

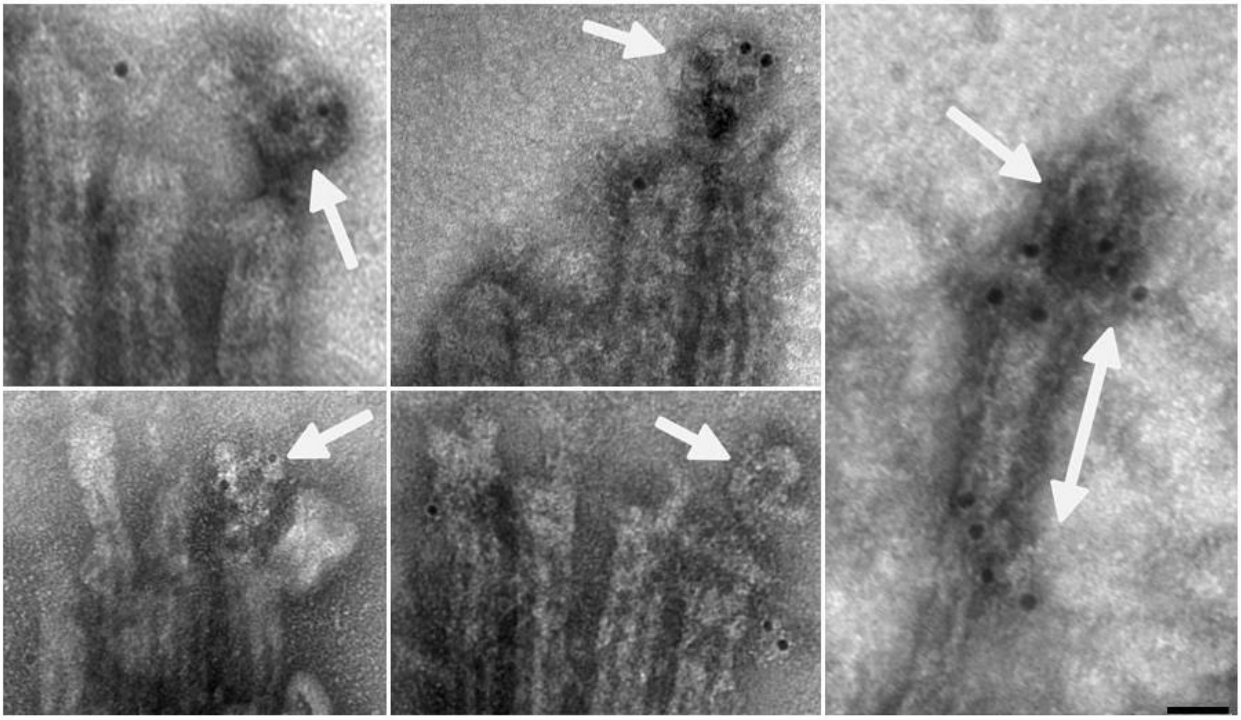

Figure 43: TEM micrographs of *pf18* mutants. The IFT74 antibody labels the ring-like structures and the ectopic LLS, which are indicated by the white arrows and the white double-ended arrow respectively. Scalebar = 50 nm.

These findings suggest that the conversion of anterograde into retrograde IFT transport can occur in this 9+0 mutant strain in a manner similar to that of wild type flagella, through the involvement of tubules other than those of the CP complex. Thus, the turnaround process is not strictly dependent on the presence of the CP tubules.

4. Discussion

As a trafficking process moving ciliary precursors and turnover products between the cell body and the ciliary compartment, the IFT process is continuously cycling between two terminals, the transition zone (TZ) at the ciliary base – which acts as a gate for the inbound/outbound transit of the IFT trains - and the ciliary tip, where the anterograde-to-retrograde conversion of IFT trains occurs. A considerable amount of information has been accumulated over the last years on the structural organization and the molecular composition of the transition zone (reviewed by Gonçalves and Pelletier, 2017; Okazaki et al., 2020). On the contrary, very little structural and molecular evidence is available on the ciliary tip and the mechanism of IFT turnaround, though the present knowledge on the architecture of anterograde and retrograde IFT trains indicate that a significant remodeling of IFT components must occur once the trains reach the flagellar tip.

The current model for IFT turnaround is based on the results obtained by Pedersen et al. (2006) (see fig. 11). On the basis of biochemical analyses carried out on a variety of *Chlamydomonas* mutants, these authors proposed that IFT remodeling at the tip involves both the dissociation of IFT complexes A and B and the release of the associated motors, in a model for IFT turnaround consisting of three steps, i) the dissociation of IFT-A and IFT-B complexes and the release of inactive dynein-1b, ii) the binding of the IFT-A complex to active dynein-1b, and iii) the reassociation of the IFT-A and IFT-B complexes to form the retrograde train. The turnaround point was suggested to be localized distal to the B-tubule end. According to this model, the tip district is expected to contain soluble IFT components (the two A and B complexes, and the two motors kinesin-2 and dynein-1b), while they are mostly bound to each other along the flagellar shaft, associated into the assembled anterograde and retrograde trains. These events occur very rapidly, because there is no build-up of IFT particles in the tips of wild type flagella.

This model has gained further support from studies on the *in vivo* dynamics of IFT turnaround, which have confirmed both the dissociation of the two IFT complexes at the tip, and the requirement of IFT-A for the retrograde transport. In *C.elegans*, single molecule fluorescence microscopy revealed that IFT-A particles turn around quickly at the ciliary tip (600 ms) whereas IFT-B particles linger longer as they reside at the tip for an average of 3 s before returning to the base by retrograde IFT (Mijalkovic et al., 2017). Furthermore, in *dyf2/IFT144* worm mutants the anterograde transport is regularly functioning and both IFT-A and IFT-B can reach the cilia tip; however, only IFT-A can perform retrograde IFT, while IFT-B fails to reassociate with IFT-A prior to retrograde IFT, and is accumulated at the tip (Wei et al., 2012). These results indicate that IFT-A

plays a crucial role for the assembly of the retrograde trains, while the association of IFT-B with kinesin-2 only is strictly required for IFT entering the flagellum.

The regulatory mechanisms controlling the disassembly of IFT trains at the tip are not completely clear, but, interestingly, the available information suggests that similar – but reverse - molecular processes might be implicated for IFT turnaround at the tip and for IFT assembly at the flagellar base.

At the tip, a FLA8 phosphorylation event by the calcium-dependent kinase CDPK-1 has been shown in *Chlamydomonas* to release kinesin-2 from the IFT-B complex (Liang et al., 2014); similarly, other calcium-dependent protein kinases have been implicated in the phosphorylation of KIF3B and in IFT turnaround in mammalian cells (Guillaud et al., 2008). Thus, kinesin-2 phosphorylation at a specific motor subunit site is likely to be an early event of IFT remodeling at the tip occurring in evolutionarily distant organisms.

At the basis of *Chlamydomonas* flagella, IFT proteins are recruited and assembled sequentially into anterograde trains, and bona fide IFT trains are only seen near the distal end of basal bodies, just before they are released into the cilium upon completion. Assembly is a stepwise process that commences with the arrival of IFT-A complexes, followed by the association of IFT-B2, then IFT-B1, and finally the kinesin-2 motor, which is necessary for entering the TZ (Wingfield et al., 2018). Hence, IFT proteins at the flagellar base are gathered as subcomplexes, rather than as entire IFT particles. Accordingly with such a temporal pattern, IFT proteins show distinct distributions at the basal body, with kinesin-2 and the IFT-B proteins located more distally along the basal body axis, closer to the TZ, and IFT-A located deeper and at a more peripherally position. Inactive IFT dynein, which is a cargo of anterograde IFT trains, is loaded just before the trains are dispatched to the flagellum. Each of the nine basal body triplets with its associated structures might assist to assemble complete IFT trains. The nascent trains move upwards along the triplet blades combining with additional IFT subcomplexes, and queue in various stages of assembly for sequential release into the cilium. There seems not to be any interdependence among IFT-A and IFT-B recruitment during train assembly; in mutants knocked out for IFT-A subunits the IFT-B complex is still able to bind kinesin-2 and enter the flagellum, though thereafter it accumulates at the tip, due to the lack of retrograde traffic (Hirano et al., 2017).

As it occurs at the tip, the binding of kinesin-2 to IFT-B is regulated by phosphorylation at the flagellar base too, where FLA8 phosphorylation disrupts the interaction between kinesin-2 and IFT-B and inhibits IFT entry (Liang et al., 2014). In fact, the phosphomimetic (S663D) mutated FLA8 subunit is not able to enter the flagellum, while the phosphodefective (S663A) FLA8 mutant accumulated both IFT-B1 and IFT-B2 proteins at the tip, but not IFT-A, indicating that inhibition of

FLA8 phosphorylation at the flagellar tip prevents dissociation of IFT particles from kinesin-2 and leads to an abnormal accumulation of IFT proteins. The whole set of data is therefore indicative that FLA8 phosphorylation acts as a molecular switch to control both IFT entry and turnaround.

It is interesting to note that the kinesin-2 binding site is located on the connecting tetramer that constitutes the interface between the IFT-B1 core and the IFT-B2 peripheral subcomplex and comprises the IFT52 and IFT88 subunits from the core subcomplex, and the IFT38 and IFT57 subunits from the peripheral subcomplex (Funabashi et al., 2018). The possibility that kinesin-2 might trigger the complete IFT-B assembly by clamping the two subcomplexes at the ciliary base is therefore somewhat intriguing, though still devoid of experimental evidence.

Calcium-dependent kinases are not the only molecular actors that have been implicated in IFT assembly at the ciliary base. Recently, the IFT-B holocomplex has been shown to be the effector of the sGTPase RABL2 (Lo et al., 2012; Kanie et al., 2017; Nishijima et al., 2017). Interaction mapping revealed that RABL2 binds to the IFT-B1 heterodimer IFT74/IFT81, and that this binding is indispensable for initiating IFT; in fact, mice knocked out for RABL2 exhibit a deficit in the number of trains entering the primary cilia (Kanie et al., 2017), and in *Chlamydomonas* the disruption of the RABL2 gene leads to a non-flagellated phenotype (Nishijima et al 2017). RABL2 is also present in the list of putative *Chlamydomonas* tip proteins proposed by Satish-Tammana et al., (2013), and has been implicated in the outbound trafficking of GPCRs (Dateyama et al., 2019; Duan et al., 2021).

In vivo analysis of IFT turnaround in *Chlamydomonas* flagella has revealed that a single anterograde train gives raise to multiple retrograde trains at the tip and, also, that multiple anterograde trains dissociate and mix up together to form retrograde trains (Chien et al., 2017). Kinetic analysis of the tip resting time revealed also that disassembly of anterograde trains and reassembly of the retrograde trains is a multistep process regulated by extracellular calcium and the concentration of active dynein motors (Chien et al., 2017).

Due to this sort of “traffic jam” at the turnaround zone and the resulting ultrastructural variability, how IFT trains are remodeled in the turnaround zone cannot be easily determined by conventional imaging.

Our approach, combining electrontomographic and immunoelectronmicroscopy, allowed us to get some insights into the IFT turnaround pathway in *Chlamydomonas* flagella, which are here below discussed following a point-by-point order.

First, we obtained a clear evidence that in this model organism the turnaround process occurs in the vicinity of the CP complex and directly involves its terminal district. This conclusion is supported by both flat-embedded thin section observations and single-tip electron tomographic

analyses, and is further confirmed by the piling up of IFT-like particles we observed around the CP terminus in the presence of calcium dependent protein kinases inhibitors. We correlate this finding with the peculiar ultrastructure exhibited by the terminal CP segment, which is clearly differentiated from the CP architecture along the axonemal shaft. The two ultrastructurally differentiated regions of the CP are assembled in distinct phases during ciliogenesis: an earlier phase during which the CP microtubules are assembled along with their specific projections, but do not extend over the A tubules, the flagellar tip is rounded and the electron-opaque tip sheet is still absent, and a later phase, when the CP microtubules exceed the axoneme, the tip tapers and the LLS, or tip sheet, is formed (Lechtreck et al., 2013). The latter phase begins when the flagellum is about half-length, a critical time point at which the activity of some protein kinases implicated in flagellar assembly shows significant changes (Pan et al., 2004; Luo et al., 2011; Wilson and Lefebvre, 2004), and the number of IFT particles assembled in the short, moving IFT trains equals that of the long trains (Vannuccini et al., 2016), that have been reported to be stationary trains (Stepanek et al., 2016). On this basis, we can reason that a continuous, cycling IFT trafficking might be established only when the regenerating flagellum reaches its half-lenght, a time coincident with the appearance of the LLS.

The LLS is shown here to consist not only of an amorphous, electrondense longitudinal core, as previously observed in resin-embedded flagellar sections (Ringo, 1967; Lechtreck et al., 2013), but to comprise also two lateral series of thin, T-shaped projections that are arranged in regularly disposed repeats. Such a peculiar architecture could reasonably be related to a definite function for LLS, which hence should not be considered as just the simple accumulation of material in the space between the two CP tubules.

Second, our data indicate that, close to the end of the A-tubule, the anterograde train splits into three parts, an outer part remaining associated with the membrane, an intermediate part that soon interrupts, and an inner part that proceeds onwards and turns to contact the CP. Comparison of our tomographic reconstruction with the 3D model obtained by Jordan et al. (2019) suggests that these three branches of the train may be assigned, respectively, to the IFT-A complex, to dynein-1b, and to the IFT-B complex. This conclusion is supported by the following considerations: i) the possibility that the membrane-associated branch consists of IFT-A is confirmed by the labeling pattern we obtained on sections of resin-embedded samples as well as by the absence of any IFT-A labeling found on detergent-treated flagella, in agreement with the strict association described between this complex and the membrane (Jordan et al., 2018); ii) dynein-1b travels in an inactive form as a cargo of anterograde IFT until the flagellar tip, where it is activated by an unknown mechanism to initiate retrograde IFT. The inactive-to-active transition occurs through an intermediate conformation (Toropova et al., 2017; Jordan et al., 2018); at the tip, dynein molecules

in such an intermediate conformation have been observed completely disassociated from IFT trains (Jordan et al., 2018), suggesting that dynein-1b may indeed become transiently soluble during its activation and before it re-associates to the retrograde train.

The pathway followed at the tip by the IFT-B complex appears to be more complex and – as suggested by our immunolabeling results – to involve both an interaction with the CP and the split of IFT-B2 from IFT-B1.

IFT-B2 labeling is selectively localized in the distal 200 nm of the CP complex, a length that approximately coincides with that of the singlet zone and of the LLS. Such observation is in agreement with the finding that IFT172 can bind to the plus-end microtubule binding protein EB1, since the two proteins can be coimmunoprecipitated (Pedersen et al., 2005); IFT172 is the only IFT protein containing the EB1-binding motif SxIP (Buey et al., 2012). Only a soluble IFT172 pool that is not complexed with the other IFT subunits IFT139 (IFT-A) and IFT81/74 (IFT-B1) was immunoprecipitated by the anti-EB1 antibodies, suggesting that EB1 interacts with a fraction of IFT172 that is not associated with other IFT polypeptides. However, in this study the presence of other IFT-B2 subunits in the immunoprecipitate was not tested, thus leaving open the possibility that the interaction with EB1 involves the whole IFT-B2 subcomplex, rather than the single IFT172 subunit.

Our data indicate the distal segment of the CP, including the LLS, as the site of IFT-B dissociation into its two subcomplexes B1 and B2, and suggest that it might also act as an anchoring site for IFT-B2, given that only the IFT-B1 subcomplex is found distally to the CP terminal plates.

We note that, in the flagella of mutants lacking the CP, this is always replaced by an amorphous core, which was shown to contain IFT proteins (Lechtreck et al., 2013); these flagella are about 60-70% in length with respect to the wild type, and are still able to undergo IFT turnaround, though less efficiently than wild type flagella (Lechtreck et al., 2013). It seems likely that in wild type flagella the accumulation of IFT-B proteins in the distal space between the two CP tubules is part of, or is the consequence of, the normal turnaround process and that - in the absence of the CP and with a defective turnaround – such a process proceeds to originate the amorphous core that extends throughout the whole axonemal length.

This role of the terminal CP segment in IFT turnaround is further supported by the results we obtained on the *fla11*^{ts} mutant strain. *fla11*^{ts} flagella exhibit an anterograde trafficking with normal rate and frequency, a reduced frequency in the retrograde transport and the accumulation of IFT proteins at the tip, indicative of a defective turnaround (Pedersen et al., 2005). This phenotype is due to the expression of a mutated IFT172 protein, in which a conserved leucine residue at position 1615 is replaced by proline (Pedersen et al., 2005). Our results reveal that, with respect to

wild type, the efficiency of IFT172 binding to the LLS-containing segment of the CP is diminished in *fla11*^{ts} flagella at the permissive temperature and reduced to about 50% at the restrictive temperature. These observations confirm the involvement of IFT172 and its binding to the distal CP segment in IFT turnaround and validate the accuracy of our experimental approach.

The whole set of data is coherent with the available evidence on the dynamics of IFT at the tip, showing a different and quicker rate of turnaround for the IFT-A complex, while the IFT-B complex turns around more slowly and dwells at the tip for a longer time, as it would be expected for this complex to dissociate and interact with the CP.

Our immunolocalization results also suggest that the IFT-B1 subcomplex may be an integral component of the CP capping structures. Among all the IFT proteins, the IFT74/81 coiled-coil heterodimer constitutes the only structurally elongated component (Lucker et al., 2005), and might well contribute to the assembly of the series of parallel rods that form part of the 6 nm IFT-B repeat (Jordan et al., 2018). When we torqued the IFT-B 3D model from Jordan's et al. (2018) and overlapped it with images of negatively stained CP cap, we found quite a good fitting. It seems thus possible that, during IFT turnaround, the ribbon formed by IFT-B1 subcomplexes interacts with the distal CP ends, possibly at the level of the terminal plates, then folds on itself to give raise to the ring. This hypothesis appears likely when we consider the phenotypes exhibited by the mutants *ift74-1* (Brown et al., 2015) and *fla10*^{ts}. Flagella of the *ift74-1* strain, which expresses a truncated IFT-74 protein and assembles very short flagella (< 4 mm), have a flat tip devoid of the CP ring. In the *fla10*^{ts} strain, in which IFT stops after exposure at the restrictive temperature, the ring is also no longer present at the CP terminus when cells are maintained at 32°C. These observations suggest that the presence of the ring requires an intact IFT-B1 subcomplex, and that this structure of the CP cap only forms when a cycling IFT system is established.

Our results are indicative for the implication of the CP capping structures in the anterograde-to-retrograde IFT conversion. We can speculate that some flagellar-tip proteins may be involved in regulating the dissociation/association of IFT-B subcomplexes at the flagellar tip. The first event might be the detachment of kinesin-2 from the IFT-B complex, followed by the interaction of the two IFT-B subcomplexes with some tip component. A possible candidate could be CEP104, which is a plus-end protein with a TOG domain located at both the flagellar basis, where it is involved in the initiation of flagellar assembly, and at the tip (Satish-Tammana et al., 2013; Al-Jassar et al., 2017; Yamazoe et al., 2020); it is interesting that CEP104 deficient flagella also are shorter and possess flat tips (Satish-Tammana et al., 2013). Another tip protein that might be a good candidate for a regulatory role in this process is RABL2. It has been shown that this sGTPase controls the assembly of the anterograde train at the flagellar base (Kanie et al., 2017; Nishijima et

al., 2017), and that this process depends on IFT74 (Brown et al., 2015). Given that RABL2 has been also localized at the flagellar tip (Satish-tammana et al., 2013), it may be that in this district is involved in the reverse process.

Our results may suggest the hypothetical model of IFT turnaround shown in fig. 44, in which we assume that the assembly of the retrograde train begins with the reassociation of IFT-A - that has undergone its own pathway tethered to the membrane - to the now-activated dynein and to the IFT-B complex coming out from the CP.

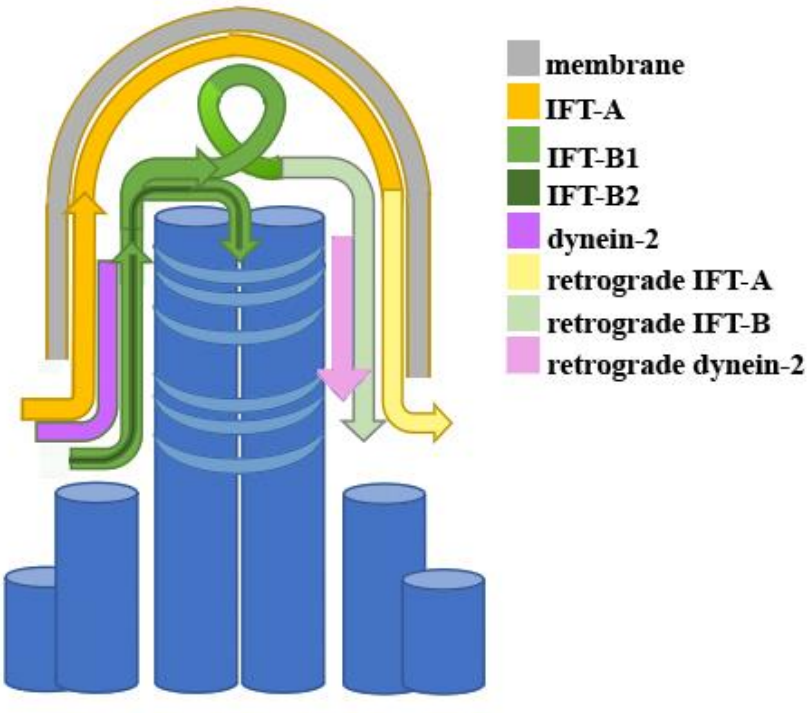

Figure 44: This schematic proposes a provisional model for IFT turnaround in *Chlamydomonas* flagella based on the results presented in this thesis.

This model, based on the presence of the CP complex, raises the question of how IFT turnaround takes place in 9+0 cilia, e.g. in primary cilia. In this respect, we think that our observations on flagella of the *pf18* mutant cells, which are devoid of the CP, are particularly relevant. We have documented in *pf18* flagella the presence of ectopically-assembled structures that closely resemble the LLS component of the CP but are instead associated with one of the A-tubules. Ring-like structures can be evidenced by negative staining at the distal end of these axoneme too, and, once again, these structures are labelled by IFT-B1 antibodies. On this basis, we retain likely that in primary cilia the IFT turnaround process may occur at the end of each single A-tubule sharing the same basic mechanism and molecular components as the 9+2 flagella of *Chlamydomonas* flagella.

References

- Afzelius B. A. (1976). A human syndrome caused by immotile cilia. *Science*, 193: 317–319.
- Akella J. S., Carter S. P., Nguyen K., Tsiropoulou S., Moran A. L., Silva M., Rizvi F., Kennedy B. N., Hall D. H., Barr M. M., Blacque O. E. (2020). Ciliary Rab28 and the BBSome negatively regulate extracellular vesicle shedding. *Elife,* 9.
- Al-Jassar C., Andreeva A., Barnabas D. D., McLaughlin S. H., Johnson C. M., Yu M., van Breugel M. (2017). The Ciliopathy-Associated Cep104 Protein Interacts with Tubulin and Nek1 Kinase. *Structure*, 25: 146-156.
- Anderson R. G. (1972). The three-dimensional structure of the basal body from the rhesus monkey oviduct. *Journal of Cell Biology,* 54: 246–265.
- Anvarian Z., Mykytyn K., Mukhopadhyay S., Pedersen L. B., Christensen S. T. (2019). Cellular signalling by primary cilia in development, organ function and disease. *Nature Reviews Nephrology*, 15: 199–219.
- Bahe S., Stierhof Y. D., Wilkinson C. J., Leiss F., Nigg E. A. (2005). Rootletin forms centriole-associated filaments and functions in centrosome cohesion. *The Journal of Cell Biology,* 171: 27-33.
- Berbari N. F., O'Connor A. K., Haycraft C. J., Yoder B. K. (2009). The primary cilium as a complex signaling center. *Current Biology,* 19: R526-R535.
- Berman S. A., Wilson N. F., Haas N. A., Lefebvre P. A. (2003). A novel MAP kinase regulates flagellar length in *Chlamydomonas. Current Biology*, 13: 1145–1149.
- Bertiaux E., Mallet A., Fort C., Blisnick T., Bonnefoy S., Jung J., Lemos M., Marco S., Vaughan S., Trépout S., Tinevez J.-Y., Bastin P. (2018). Bidirectional intraflagellar transport is restricted to two sets of microtubule doublets in the *trypanosome* flagellum. *The Journal of Cell Biology*, 217: 4284–4297.
- Besschetnova T. Y., Kolpakova-Hart E., Guan Y., Zhou J., Olsen B. R., Shah J. V. (2010). Identification of Signaling Pathways Regulating Primary Cilium Length and Flow-Mediated Adaptation. *Current Biology,* 20: 182–187.
- Blacque O. E., Reardon M. J., Li C., McCarthy J., Mahjoub M. R., Ansley S. J., Badano J. L., et al. (2004). Loss of *C. elegans* BBS-7 and BBS-8 protein function results in cilia defects and compromised intraflagellar transport. *Genes & Development*, 18, 1630–1642.
- Blaineau C., Tessier M., Dubessay P., Tasse L., Crobu L., Pagès M., Bastien P. (2007). A Novel Microtubule-Depolymerizing Kinesin Involved in Length Control of a Eukaryotic Flagellum. *Current Biology*, 17: 778–782.
- Bloch M. A., Johnson K. A. (1995). Identification of a molecular chaperone in the eukaryotic flagellum and its localization to the site of microtubule assembly. *Journal of Cell Science,* 108: 3541–3545.
- Blum J. J. (1971). Existence of a break point in cilia and flagella. *Journal of Theorical Biology,* 33: 257-63.
- Bhogaraju S., Cajanek L., Fort C., Blisnick T., Weber K., Taschner M., Mizuno N., Lamla S., Bastin P., Nigg E. A., Lorentzen E. (2013). Molecular basis of tubulin

transport withinmthe cilium by IFT74 and IFT81. *Science,* 341: 1009-1012.

- Bhogaraju S., Taschner M., Morawetz M., Basquin C., Lorentzen E. (2011). Crystalstructure of the intraflagellar transport complex 25/27. *The EMBO Journal*, 30: 1907-1918.
- Bhogaraju S., Weber K., Engel B. D., Lechtreck K. F., Lorentzen E. (2014). Getting tubulin to the tip of the cilium: One IFT train, many different tubulin cargo-binding sites? *BioEssays*, 36: 463–467.
- Boynton J. E., Gillham N. W., Harris E. H., Hosler J. P., Johnson A. M., Jones A. R., Randolph-Anderson B. L., et al. (1988). Chloroplast transformation in *Chlamydomonas* with high velocity microprojectiles. *Science,* 240: 1534–1538.
- Breslow D. K., Hoogendoorn S., Kopp A. R., Morgens D. W., Vu B. K., Kennedy M. C., Han K., Li A., Hess G.T., Bassik M. C., et al. (2018). A CRISPR-based screen for Hedgehog signaling provides insights into ciliary function and ciliopathies. *Nature Genetics*, 50: 460–471.
- Brown J. M., Cochran D. A., Craige B., Kubo T., Witman G. B. (2015). Assembly of IFT trains at the ciliary base depends on IFT74. *Current Biology*, 25: 1583-1593.
- Brown J. M., Witman G. B. (2014). Cilia and Diseases. *BioScience*, 64: 1126-1137.
- Brown A., Zhang R. (2020). Primary Cilia: A Closer Look at the Antennae of Cells. *Current Biology*, 30: R1494-R1496.
- Brunnbauer M., Mueller-Planitz F., Kosem S., Ho T. H., Dombi R., Gebhardt J. C. M., Rief M., Okten Z. (2010). Regulation of a heterodimeric kinesin-2 through an unprocessive motor domain that is turned processive by its partner. *Proceedings of the National Academy of Sciences of USA,* 107: 10460–10465.
- Buey M. R., Sen I., Kortt O., Mohan R., Gfeller D., Veprintsev D., Kretzschmar I., et al. (2012). Sequence determinants of a microtubule tip localization signal (MtLS). *Journal of Biological Chemistry*, 287: 28227-42.
- Chaya T., Omori Y., Kuwahara R., Furukawa T. (2014). ICK is essential for cell type-specific ciliogenesis and the regulation of ciliary transport. *The EMBO Journal,* 33: 1227–1242.
- Cheshire J. L., Keller L. R. (1991). Uncoupling of *Chlamydomonas* flagellar gene expression and outgrowth from flagellar excision by manipulation of Ca^{2+}. *Journal of Cell Biology,* 115: 1651–1659.
- Chien A., Shih S. M., Bower R., Tritschler D., Porter M. E., Yildiz A. (2017). Dynamics of the IFT machinery at the ciliary tip. *ELife,* 6: e28606.
- Chih B., Liu P., Chinn Y., Chalouni C., Komuves L. G., Hass P. E., Sandoval W., Peterson A. S. (2011). A ciliopathy complex at the transition zone protects the cilia as a privileged membrane domain. *Nature Cell Biology,* 14: 61–97.
- Cole D. G., Diener D. R., Himelblau A. L., Beech P. L., Fuster J. C., Rosenbaum J. L. (1998). *Chlamydomonas* kinesin-II–dependent intraflagellar transport (IFT): IFT particles contain proteins required for ciliary assembly in *Caenorhabditis elegans* sensory neurons. *The Journal of Cell Biology*, 141: 993-1008.
- Cordier A. C. (1975). Ultrastructure of the cilia of thymic cysts in “nude” mice. *The Anatomical Record*, 181: 227–249.
- Craft J. M., Harris J. A., Hyman S., Kner P., Lechtreck K. F. (2015). Tubulin transport

by IFT is upregulated during ciliary growth by a cilium-autonomous mechanism. *The Journal of Cell Biology*, 208: 223–237.

- Currie A. R., Wheatley D. N. (1966). Cilia of a Distinctive Structure (9+0) in Endocrine and other Tissues. *Postgraduate Medical Journal*, 42: 403.
- Dabdoub A., Kelley M.W. (2005). Planar cell polarity and a potential role for a Wnt morphogen gradient in stereociliary bundle orientation in the mammalian inner ear. *Journal of Neurobiology,* 64: 446-57.
- van Dam T. J. P., Townsend M. J., Turk M., Schlessinger A., Sali A., Field M. C., Huynen M. A. (2013). Evolution of modular intraflagellar transport from a coatomer-like progenitor. *Proceedings of the National Academy of Sciences of USA,* 110: 6943-6948.
- Daems M., Peacock H. M., Jones E. A. V. (2020). Fluid flow as a driver of embryonic morphogenesis. *Development (Cambridge, England)*, 147: dev185579.
- Dateyama I., Sugihara Y., Chiba S., Ota R., Nakagawa R., Kobayashi T., Itoh H. (2018). RABL2 positively controls localization of GPCRs in mammalian primary cilia. *Journal of Cell Science*, 132: jcs224428.
- Davis E. E., Katsanis N. (2012). The ciliopathies: a transitional model into systems biology of human genetic disease. *Current Opinion in Genetics & Development,* 22: 290–303.
- Dawson, S. C., Sagolla M. S., Mancuso J. J., Woessner D. J., House, S. A., Fritz-Laylin, L., Cande W. Z. (2007). Kinesin-13 Regulates Flagellar, Interphase, and Mitotic Microtubule Dynamics in Giardia intestinalis. *Eukaryotic Cell*, 6: 2354–2364.
- Dean S., Moreira-Leite F., Varga V., and Gull K. (2016). Cilium transition zone proteome reveals compartmentalization and differential dynamics of ciliopathy complexes. *Proceedings of National Academy of Sciences of USA,* 113: E5135-5143.
- Deane J. A., Cole D. G., Seeley E.S., Diener D. R., Rosenbaum J. L. (2001). Localization of intraflagellar transport protein IFT52 identifies basal body transitional fibers as the docking site for IFT particles. *Current Biology*, 11: 1586–1590.
- Dentler W. L. (1980). Structures linking the tips of ciliary and flagellar microtubules to the membrane. *Journal of Cell Science,* 42: 207-220.
- Dentler W. L., LeCluyse E. L. (1982). Microtubule capping structures at the tips of tracheal cilia: Evidence for their firm attachment during ciliary bend formation and the restriction of microtubule sliding. *Cell Motility*, 2: 549–572.
- Dentler W. L., Rosenbaum J. L. (1977). Flagellar elongation and shortening in *Chlamydomonas.* III. structures attached to the tips of flagellar microtubules and their relationship to the directionality of flagellar microtubule assembly. *The Journal of Cell Biology*, 74: 747-759.
- Desai A., Verma S., Mitchison T. J., Walczak C. E. (1999). Kin I kinesins are microtubule-destabilizing enzymes. *Cell*, 96: 69–78.
- Diener D. L., Lupetti P., Rosenbaum J. L. (2015). Proteomic analysis of isolated ciliary transition zones reveals the presence of ESCRT proteins. *Current Biology*, 25: 379-384.
- Dirksen E. R., Satir P. (1972). Ciliary activity in the mouse oviduct as studied by transmission and scanning electron microscopy. *Tissue and Cell*, 4: 389–403.
- Dossou S. J. Y., Bré M.-H., Hallworth R. (2007). Mammalian cilia function is

independent of the polymeric state of tubulin glycylation. *Cell Motilility and the Cytoskeleton*, 64: 847–855.

- Duan S., Li H., Zhang Y., Yang S., Chen Y., Qiu B., Huang C., et al. (2021). Rabl2 GTP hydrolysis licenses BBSome-mediated export to fine-tune ciliary signaling. *The EMBO Journal*, 40: e105499.
- Eguether T., San Agustin J. T., Keady B. T., Jonassen J. A., Liang Y., Francis R., Tobita K., Johnson C. A., Abdelhamed Z. A., Lo C. W. (2014). IFT27 links the BBSome to IFT for maintenance of the ciliary signaling compartment. *Developmental Cell,* 31: 279–290.
- Falk N., Lösl M., Schröder N., Gießl A. (2015). Specialized cilia in mammalian sensory systems. *Cells*, 4: 500-519.
- Fan Z. C., Behal R. H., Geimer S., Wang Z., Williamson S. M., Zhang H., Cole D. G., Qin H. (2010). *Chlamydomonas* IFT70/CrDYF-1 is a core component of IFT particle complex B and is required for flagellar assembly. *Molecular Biology of the Cell*, 21: 2696-2706.
- Fawcett D. W., Porter K. R. (1954). A study of the fine structure of ciliated epithelia. *Journal of Morphology*, 94: 221–281.
- Ferenczi A., Pyott D. E., Xipnitou A., Molnar A. (2017). Efficient targeted DNA editing and replacement in *Chlamydomonas reinhardtii* using Cpf1 ribonucleoproteins and single-stranded DNA. *Proceedings of National Academy of Sciences of USA,* 114: 13567–13572.
- Ferkol T. W., Leigh M. W. (2012). Ciliopathies: the central role of cilia in a spectrum of pediatric disorders. *The Journal of Pediatrics*, 160: 366–371.
- Fisch C., Dupuis-Williams P. (2011) Ultrastructure of Cilia and Flagella - Back to the Future! *Biology of the Cell*, 103: 249–270.
- Flock A., and Duvall 3rd A. J. (1965). The ultrastructure of the kinocilium of the sensory cells in the inner ear and lateral organs. *The Journal of Cell Biology,* 25: 1-8.
- Fliegauf M., Omran H. (2006). Novel tools to unravel molecular mechanisms in cilia-related disorders. *Trends in Genetics,* 22: 241-5.
- Follit J.A., Xu F., Keady B.T., Pazour G.J. (2009). Characterization of mouse IFT complex B. *Cell Motility and the Cytoskeleton*. 66: 457–468.
- Frangakis A., Hegerl R. (2001). Noise reduction in electron tomographic reconstruction using non linear anistropic diffusion. *Journal of Structural Biology,* 135: 239-205.
- Funabashi T., Katoh Y., Okazaki M., Sugawa M., Nakayama K. (2018). Interaction of heterotrimeric kinesin-II with IFT-B–connecting tetramer is crucial for ciliogenesis. *The Journal of Cell Biology*. 217: 2867–2876.
- Garcia-Gonzalo F. R., Corbit K. C., Salome Sirerol-Piquer M., Ramaswami G., Otto E. A., Noriega T. R., Seol A. D., Robinson J. F., Bennett C. L., Josifova D. J., Manuel Garcia-Verdugo J., Katsanis N., Hildebrandt F., Reiter J. F. (2011). A transition zone complex regulates mammalian ciliogenesis and ciliary membrane composition. *Nature Genetics,* 43: 776–788.
- Garcia-Gonzalo F. R., Reiter J. F. (2012). Scoring a backstage pass: mechanisms of ciliogenesis and ciliary access. *The Journal of Cell Biology*, 197: 697-709.
- Gibbons B. H., Asai D. J., Tang W. J., Hays T. S., Gibbons I. R. (1994). Phylogeny and

expression of axonemal and cytoplasmic dynein genes in sea urchins. *Molecular Biology of the Cell,* 5: 57–70.

- Gigante E. D., Caspari T. (2020). Signaling in the primary cilium through the lens of the Hedgehog pathway. *Wiley Interdisciplinary Reviews. Developmental Biology,* 9: e377.
- Goetz S. C., Anderson K. V. (2010). The primary cilium: A signalling centre during vertebrate development. *Nature Reviews Genetics*, 11: 331–344.
- Gonçalves J., Pelletier L. (2017). The Ciliary Transition Zone: Finding the Pieces and Assembling the Gate. *Molecules and Cells*, 40: 243-253.
- Goodenough U., Lin H., Lee J-H. (2007). Sex determination in *Chlamydomonas*. *Seminars in Cell and Developmental Biology,* 18: 350–361.
- Guillaud L., Wong R., Hirokawa N. (2008). Disruption of KIF17–Mint1 interaction by CaMKII-dependent phosphorylation: a molecular model of kinesin–cargo release. *Nature Cell Biology*, 10: 19–29.
- Gupta M. L., Carvalho P., Roof D. M., Pellman D. (2006). Plus end-specific depolymerase activity of Kip3, a kinesin-8 protein, explains its role in positioning the yeast mitotic spindle. *Nature Cell Biology*, 8: 913–923.
- Gorman D. S., Levine R. P. (1965). Cytochrome f and plastocyanin: their sequence in the photosynthetic electron transport chain of *Chlamydomonas reinhardtii*. *Proceedings of the National Academy of Sciences of USA*, 54: 1665-1669.
- Han S., Miyoshi K., Shikada S., Amano G., Wang Y., Yoshimura T., Katayama T. (2019). TULP3 is required for localization of membrane-associated proteins ARL13B and INPP5E to primary cilia. *Biochemical and Biophysical Research Communications* 509: 227-234.
- Hao L., Thein M., Brust-Mascher I., Civelekoglu-Scholey G., Lu Y., Acar S., Prevo B., Shaham S., Scholey J. M. (2011). Intraflagellar transport delivers tubulin isotypes to sensory cilium middle and distal segments. *Nature Cell Biology,* 13: 790–798.
- Harris E. H. (2001). *Chlamydomonas* as a Model Organism. *Annual Review of Plant Physiology and Plant Molecular Biology,* 52: 363-406.
- He M., Agbu S., Anderson K.V. (2017). Microtubule Motors Drive Hedgehog Signaling in Primary Cilia. *Trends in Cell Biology,* 27: 110–125.
- Hirano T., Katoh Y., Nakayama K. (2017). Intraflagellar transport-A complex mediates ciliary entry and retrograde trafficking of ciliary G protein–coupled receptors. *Molecular Biology of the Cell,* 28: 429–439.
- Hou Y., Witman G. B. (2015). Dynein and intraflagellar transport. *Experimental Cell Research*. 334: 26–34.
- Howard P. W., Jue S. F., Maurer R. A. (2013). Interaction of mouse TTC30/DYF-1 with multiple intraflagellar transport complex B proteins and KIF17. *Experimental Cell Research*, 319: 2275–2281.
- Huet D., Blisnick T., Perrot S., Bastin P. (2019) IFT25 is required for the construction of the trypanosome flagellum. *Journal of Cell Science*, 132: jcs228296.
- Huet D., Blisnick T., Perrot S., Bastin P. (2014) The GTPase IFT27 is involved in both anterograde and retrograde intraflagellar transport. *Elife,* 3: e02419.
- Ichinose S., Ogawa T., Hirokawa N. (2015). Mechanism of Activity-Dependent Cargo Loading via the Phosphorylation of KIF3A by PKA and CaMKIIa. *Neuron,* 87: 1022-

1035.

- Iomini C., Li L., Esparza J. M., Dutcher S. K. (2009). Retrograde Intraflagellar Transport Mutants Identify Complex A Proteins with Multiple Genetic Interactions in *Chlamydomonas reinhardtii. Genetics*, 183: 885–896.
- Ishikawa T. (2013). 3D structure of eukaryotic flagella/cilia by cryo-electron tomography. *BIOPHYSICS (Nagoya-shi, Japan)*, 9: 141–148.
- Ishikawa H., Ide T., Yagi T., Jiang X., Hirono M., Sasaki H., Yanagisawa H., Wemmer K. A., Stainier D. Y. R., Qin H., Kamiya R., Marshall W. F. (2014). TTC26/DYF13 is an intraflagellar transport protein required for transport of motility-related proteins into flagella. *ELife,* 3: 1-24.
- Ishikawa H., Kubo A., Tsukita S. (2005). Odf2-deficient mother centrioles lack distal/subdistal appendages and the ability to generate primary cilia. *Nature Cell Biology*, 7: 517–524.
- Ishikawa H., Marshall W. F. (2011). Ciliogenesis: building the cell's antenna. *Nature Reviews. Molecular Cell Biology,* 12: 222-234.
- Izawa I., Goto H., Kasahara K., Inagaki M. (2015). Current topics of functional links between primary cilia and cell cycle. *Cilia*, 4: 12.
- Jana S. C., Mendonça S., Machado P., Werner S., Rocha J., Pereira A., Maiato H., Bettencourt-Dias M. (2018). Differential regulation of transition zone and centriole proteins contributes to ciliary base diversity. *Nature Cell Biology,* 20: 928–941.
- Jeffery P. K., Reid L. (1975). New observations of rat airway epithelium: A quantitative and electron microscopic study. *Journal of Anatomy*, 120: 295–320.
- Jékely G., Arendt D. (2006). Evolution of intraflagellar transport from coated vesicles and autogenous origin of the eukaryotic cilium. *Bioessay*, 28: 191-8.
- Jensen V. L., Leroux M. R. (2017). Gates for soluble and membrane proteins, and two trafficking systems (IFT and LIFT), establish a dynamic ciliary signaling compartment. *Current Opinion in Cell Biology,* 47: 83–91.
- Jiang X., Hernandez D., Hernandez C., Ding Z., Nan B., Aufderheide K., Qin H. (2017). IFT57 stabilizes the assembled intraflagellar transport complex and mediates transport of motility-related flagellar cargo. *Journal of Cell Science*, 130: 879-891.
- Jiang K., Toedt G., Montenegro Gouveia S., Davey N. E., Hua S., van der Vaart B., Grigoriev I., Larsen J., Pedersen L. B., Bezstarosti K., et al. (2012). A Proteome-wide Screen for Mammalian SxIP Motif-Containing Microtubule Plus-End Tracking Proteins. *Current Biology*, 22: 1800–1807.
- Jin H., White S. R., Shida T., Schulz S., Aguiar M., Gygi S. P., Bazan J. F., Nachury M. V. (2010). The Conserved Bardet-Biedl Syndrome Proteins Assemble a Coat that Traffics Membrane Proteins to Cilia. *Cell,* 141: 1208–1198.
- Jordan M. A., Diener D. R., Stepanek L., Pigino G. (2018). The cryo-EM structure of intraflagellar transport trains reveals how dynein is inactivated to ensure unidirectional anterograde movement in cilia. *Nature Cell Biology*, 20: 1250–1255.
- Kamiya R. (2002). Functional diversity of axonemal dyneins as studied in *Chlamydomonas* mutants. *International Review of Citology,* 219:115-55.

- Kanie T., Abbott K. L., Mooney N. A., Plowey E., D., Demeter J., Jackson P. K. (2017). The CEP19-RABL2 GTPase Complex Binds IFT-B to Initiate Intraflagellar Transport at the Ciliary Base. *Developmental Cell*, 42: 22-36.
- Kar A., Phadke S. R., Das Bhowmik A., Dalal A. (2018). Whole exome sequencing reveals a mutation in ARMC9 as a cause of mental retardation, ptosis, and polydactyly. *American Journal of Medical Genetics Part A*, 176: 34–40.
- Katoh Y., Nozaki S., Hartanto D., Miyano R., Nakayama K. (2015). Architectures of multisubunit complexes revealed by a visible immunoprecipitation assay using fluorescent fusion proteins. *Journal of Cell Science,* 128: 2351–2362.
- Kiesel P., Alvarez Viar G., Tsoy N., Maraspini R., Gorilak P., Varga V., Honigmann A., Pigino G. (2020). The molecular structure of mammalian primary cilia revealed by cryo-electron tomography. *Nature Structural & Molecular Biology,* 27: 1115-1124.
- Kim S., Lee K., Choi J. H., Ringstad N. Dynlacht B. D. (2015). Nek2 activation of Kif24 ensures cilium disassembly during the cell cycle. *Nature Communications*, 6: 8087.
- Klink B. U., Zent E., Juneja P., Kuhlee A., Raunser S., Wittinghofer A. (2017). A recombinant BBSome core complex and how it interacts with ciliary cargo. *Elife,* 6: e27434.
- Knowles M. R., Zariwala M., Leigh M. (2016). Primary ciliary dyskinesia. *Clinics in Chest Medicine,* 37: 449–461.
- Ko H. W., Norman R. X., Tran J., Fuller K. P., Fukuda M., Eggenschwiler J. T. (2010). Broad-Minded Links Cell Cycle-Related Kinase to Cilia Assembly and Hedgehog Signal Transduction. *Developmental Cell,* 18:237–247.
- Kobayashi T., Dynlacht B. D. (2011). Regulating the transition from centriole to basal body. *The Journal of Cell Biology*, 193: 435–444.
- Kobayashi T., Gengyo-Ando K., Ishihara T., Katsura I., Mitani S. (2007). IFT-81 and IFT-74 are required for intraflagellar transport in *C. elegans*. *Genes to Cells*, 12: 593–602.
- Kobayashi T., Ishida Y., Hirano T., Katoh Y., Nakayama K. (2021). Cooperation of the IFT-A complex with the IFT-B complex is required for ciliary retrograde protein trafficking and GPCR import. *Molecular Biology of the Cell*, 32: 45-56.
- Kobayashi T., Tsang W. Y., Li J., Lane W. and Dynlacht B. D. (2011). Centriolar kinesin Kif24 interacts with CP110 to remodel microtubules and regulate ciliogenesis. *Cell,* 145: 914–925.
- Komsic-Buchmann K., Wöstehoff L., Becker B. (2014). The contractile vacuole as a key regulator of cellular water flow in *Chlamydomonas reinhardtii*. *Eukaryotic Cell,* 13: 1421–1430.
- Kozminski K. G., Beech P. L., Rosenbaum J. L. (1995). The *Chlamydomonas* Kinesin-like Protein FLA10 is involed in motility associated with the flagellar membrane. *The Journal of Cell Biology*, 6: 1517-1527.
- Kozminski K. G., Johnson K. A., Forscher P., Rosenbaum J. L. (1993). A motility in the eukaryotic flagellum unrelated to flagellar beating. *Proocedings of the National Academy of Sciences of USA,* 90: 5519-5523.
- Kremer J. R., Mastronarde D. N., McIntosh J. R. (1996). Computer visualization of three-dimensional image data using IMOD. *Journal of Structural Biology,* 116: 71-76.

- Kubo T., Brown J. M., Bellve K., Craige B., Craft J. M., Fogarty K., Lechtreck K. F., Witman G. B. (2016). Together, the IFT81 and IFT74 N-termini form the main module for intraflagellar transport of tubulin. *Journal of Cell Science*, 129: 2106-2119.
- Kubo A., Yuba-Kubo A., Tsukita S., Tsukita S., Amagai M. (2008). Sentan: A Novel Specific Component of the Apical Structure of Vertebrate Motile Cilia. *Molecular Biology of the Cell*, 19: 5338–5346.
- Kuhn C., Engleman W. (1978). The structure of the tips of mammalian respiratory cilia. *Cell and Tissue Research*, 186: 491–498.
- Kwon R.Y., Temiyasathit S., Tummala P., Quah C. C., Jacobs C. R. (2010). Primary cilium-dependent mechanosensing is mediated by adenylyl cyclase 6 and cyclic AMP in bone cells. *The FASEB Journal,* 24: 2859–2868.
- Larsen J., Grigoriev I., Akhmanova A., Pedersen L. B. (2013). Analysis of Microtubule Plus-End-Tracking Proteins in Cilia. *Methods in Enzymology*, 524: 105–122.
- Lechtreck K. F. (2015). IFT–Cargo Interactions and Protein Transport in Cilia. *Trends in Biochemical Sciences,* 40: 765–778
- Lechtreck K. F., Gould T. J., Witman G. B. (2013). Flagellar central pair assembly in *Chlamydomonas reinhardtii. Cilia,* 2: 15.
- Lechtreck K. F., Johnson E. C., Sakai T., Cochran, D., Ballif B. A., Rush J., Pazour G. J., Ikebe M., Witman, G. B. (2009). The *Chlamydomonas reinhardtii* BBSome is an IFT cargo required for export of specific signaling proteins from flagella. *The Journal of Cell Biology*, 187: 1117-1132.
- van Leeuwenhoek A. (1677). Concerning little animals observed in rain-, well-, sea- and snow-water; as also in water wherein pepper had lain infused. *Philosophical Transactions of the Royal Society*, 12: 821–831.
- Lee K. L., Guevarra M. D., Nguyen A. M., Chua M. C., Wang Y., Jacobs C. R. (2015). The primary cilium functions as a mechanical and calcium signaling nexus. *Cilia,* 4: 7.
- Lendner M., Böttcher D., Delling C., Ojo K. K., Van Voorhis W. C., Daugschies A. (2015). A novel CDPK1 inhibitor—a potential treatment for cryptosporidiosis in calves? *Parasitology Research*, 114: 335–336.
- Lewin R. A., Lee K. W. (1985). Autotomy of algal flagella: Electron microscope studies of *Chlamydomonas (Chlorophyceae)* and *Tetraselmis (Prasinophyceae)*. *Phycologia,* 24: 311–316.
- Li J. B., Gerdes J. M., Haycraft C. J., Fan Y., Teslovich T. M., May-Simera H., Li H., et al. (2004). Comparative genomics identifies a flagellar and basal body proteome that includes the *BBS5* human disease gene. *Cell,* 117: 541–552.
- Li X., Zhang R., Patena W., Gang S. S., Blum S. R., Ivanova N., Yue R., et al. (2016). An indexed, mapped mutant library enables reverse genetics studies of biological processes in *Chlamydomonas reinhardtii*. *The Plant Cell,* 28: 367–387.
- Liang Y., Pang Y., Wu Q., Hu Z., Han X., Xu Y., Deng H. Pan J. (2014). FLA8/KIF3B phosphorylation regulates kinesin-II interaction with IFT-B to control IFT entry and turnaround. *Developmental Cell,* 30: 585-597.
- Liew G. M., Ye F., Nager A. R., Murphy J. P., Lee J. S., Aguiar M., Breslow D. K., Gygi S. P., Nachury M. V. (2014). The intraflagellar transport protein IFT27 promotes BBSome exit from cilia through the GTPase ARL6/BBS3. *Developmental Cell,* 31: 265– 278.

- Liu P., Lechtreck K. F. (2018). The Bardet-Biedl syndrome protein complex is an adapter expanding the cargo range of intraflagellar transport trains for ciliary export. *Proceedings of the National Academy of Sciences of USA,* 115: E934-E943.
- Liu Q., Tan G., Levenkova N., Li T., Pugh E. N., Rux J. J., Speicher D. W., Pierce E. A. (2007). The Proteome of the Mouse Photoreceptor Sensory Cilium Complex. *Molecular and Cellular Proteomics*, 6: 1299–1317.
- Lo J. C. Y., Jamsai D., O'Connor A., E, Borg C., Clark B. J., Whisstock J. C., Field M. C., et al. (2012). RAB-like 2 has an essential role in male fertility, sperm intra-flagellar transport, and tail assembly. *PLOS Genetics*, 8: e1002969.
- Lohret T. A., Zhao L., Quarmby L. M. (1999). Cloning of *Chlamydomonas* p60 katanin and localization to the site of outer doublet severing duringdeflagellation. *Cell Motility and the Cytoskeleton,* 43: 221–231.
- Loktev A. V., Zhang Q., Beck J. S., Searby C. C., Scheetz T. E., Bazan J. F., Slusarski D. C., Sheffield V. C., Jackson P. K., Nachury M. V. (2008). A BBSome subunit links ciliogenesis, microtubule stability, and acetylation. *Developmental Cell,* 15: 854–865.
- Long H., Zhang F., Xu N., Liu G., Diener D. R., Rosenbaum J. L., Huang K. (2015). Comparative Analysis of Ciliary Membranes and Ectosomes. *Current Biology*, 26: 3327-3335.
- Luo M., Cao M., Kan Y., Li G., Snell W., Pan J. (2011). The phosphorylation state of an aurora-like kinase marks the length of growing flagella in *Chlamydomonas*. *Current Biology*, 21: 586-91.
- Louka P., Vasudevan K. K., Guha M., Joachimiak E., Wloga D., Tomasi F.-X., Baroud C. N., Dupuis-Williams P., Galati D. F., Pearson C. G.; et al. (2018). Proteins that control the geometry of microtubules at the ends of cilia. *The Journal of Cell Biology*, 217: 4298–4313.
- Lucker B. F., Behal R. H., Qin H., Siron L. C., Taggart W. D., Rosenbaum J. L., Cole D. G. (2005). Characterization of the intraflagellar transport complex B core: Direct interaction of the IFT81 and IFT74/72 subunits. *The Journal of Biological Chemistry*, 280: 27688–27696.
- Lucker B. F., Miller M. S., Dziedzic S. A., Blackmarr P. T., Cole D. G. (2010). Direct interactions of intraflagellar transport complex B proteins IFT88, IFT52, and IFT46. *The Journal of Biological Chemistry,* 285: 21508–21518.
- Ludington W. B., Wemmer K. A., Lechtreck K. F., Witman G. B., Marshall W. F. (2013). Avalanche-like behavior in ciliary import. *Proceedings of the National Academy of Sciences of USA,* 110: 3925–3930.
- Megías M., Molist P., Pombal M. A. (2019). Animal tissues. Atlas of Plant and Animal Histology.
- Merchant S. S., Prochnik S. E., Vallon O., Harris E.H., Karpowicz S. J., Witman G. B., Terry A., et al. (2007). The *Chlamydomonas* genome reveals the evolution of key animal and plant functions. *Science,* 318: 245–251.
- McGlashan S. R.,Jensen C. G., Poole C. A. (2006). Localization of Extracellular Matrix Receptors on the Chondrocyte Primary Cilium. *Journal of Histochemistry & Cytochemistry,* 54: 1005–1014.

- Mijalkovic J., Prevo B., Oswald F., Mangeol P., Peterman E. J. G. (2017). Ensemble and single-molecule dynamics of IFT dynein in *Caenorhabditis elegans* cilia. *Nature Communications*, 8: 14591.
- Miller J. M., Wang W., Balczon R., Dentler W. L. (1990). Ciliary Microtubule Capping Structures Contain a Mammalian Kinetochore Antigen. *The Journal of Cell Biology*, 110: 703–714.
- Mirvis M., Stearns T., Nelson W. J. (2018). Cilium structure, assembly, and disassembly regulated by the cytoskeleton. *The Biochemical Journal*, 475: 2329-2353.
- Mitchison H. M., Valente E. M. (2017). Motile and non-motile cilia in human pathology: from function to phenotypes. *The Journal of Pathology,* 241: 294–309.
- Miyamoto T., Hosoba K., Ochiai H., Royba E., Izumi H., Sakuma T., et al. (2015). The microtubule-depolymerizing activity of a mitotic kinesin protein KIF2A drives primary cilia disassembly coupled with cell proliferation. *Cell Reports*, 10: 664–673.
- Morris R. L., Scholey J. M. (1997). Heterotrimeric Kinesin-II Is Required for the Assembly of Motile 9+2 Ciliary Axonemes on Sea Urchin Embryos. *The Journal of Cell Biology*, 138: 1009–1022.
- Mueller J., Perrone C. A., Bower R., Cole D. G., Porter M. E. (2005). The FLA3 KAP subunit is required for localization of kinesin-2 to the site of flagellar assembly and processive anterograde intraflagellar transport. *Molecular Biology of the Cell*, 16: 1341-1354.
- Mukhopadhyay S., Wen X., Chih B., Nelson C. D., Lane W. S., Scales S. J., Jackson P. K. (2010). TULP3 bridges the IFT-A complex and membrane phosphoinositide to promote trafficking of G protein-coupled receptors into primary cilia. *Genes & Development*, 24: 2180-2193.
- Mukhopadhyay S., Wen X., Ratti N., Loktev A., Rangell L., Scales S. J., Jackson P. K. (2013). The ciliary G-protein-coupled receptor Gpr161 negatively regulates the Sonic Hedgehog pathway via cAMP signaling. *Cell,* 152: 210–223.
- Mykytyn K., Mullins R. F., Andrews M., Chiang A. P., Swiderski R. E.,Yang B.,Braun T., Casavant T., Stone E. M., Sheffield V.C. (2004). Bardet-Biedl syndrome type 4 (BBS4)-null mice implicate Bbs4 in flagella formation but not global cilia assembly. *Proceedings of the National Academy of Sciences of USA,* 101: 8664–8669.
- Nachury M.V., Mick D.U. (2019). Establishing and regulating the composition of cilia for signal transduction. *Nature Reviews Molecular Cell Biology,* 20: 389–405.
- Nachury M. V., Loktev A.V., Zhang Q., Westlake C. J., Peränen J., Merdes A., Slusarski D. C., Scheller R. H., Bazan J. F., Sheffield V. C., Jackson P. K. (2007). A core complex of BBS proteins cooperates with the GTPase Rab8 to promote ciliary membrane biogenesis. *Cell*, 129: 1201-1213.
- Nakayama K., Katoh Y. (2020). Architecture of the IFT ciliary trafficking machinery and interplay between its components. *Critical Reviews in Biochemistry and Molecular Biology*, 55: 179-196.
- Nauli S. M., Alenghat F. J., Luo Y., Williams E., Vassilev P., Li X., Elia A. E. H., Lu W., Brown E. M., Quinn S. J., et al. (2003). Polycystins 1 and 2 mediate mechanosensation in the primary cilium of kidney cells. *Nature Genetics,* 233: 129–137.
- Nicastro D., Schwartz C., Pierson J., Gaudette R., Porter M. E., McIntosh J. R. (2006).

The Molecular Architecture of Axonemes Revealed by Cryoelectron Tomography. *Science,* 313: 944-8.

- Nishijima Y., Hagiya Y., Kubo T., Takei R., Katoh Y., Nakayama K. (2017). RABL2 interacts with the intraflagellar transport-B complex and CEP19 and participates in ciliary assembly. *Molecular Biology of the Cell*, 28: 1652-1666.
- Niwa S., Nakajima K., Miki H., Minato Y., Wang D., Hirokawa N. (2012). KIF19A Is a Microtubule-Depolymerizing Kinesin for Ciliary Length Control. *Developmental Cell*, 23: 1167–1175.
- Nonaka S., Tanaka Y., Okada Y., Takeda S., Harada A., Kanai Y., Kido M., Hirokawa N. (1998). Randomization of left–right asymmetry due to loss of nodal cilia generating leftward flow of extraembryonic fluid in mice lacking KIF3B motor protein. *Cell*, 95: 829- 837.
- Nozaki S., Castro Araya R.F., Katoh Y., Nakayama K. (2019). Requirement of IFT-B–BBSome complex interaction in export of GPR161 from cilia. *Biology Open,* 8: bio043786.
- Nozaki S., Katoh Y., Kobayashi T., Nakayama K. (2018). BBS1 is involved in retrograde trafficking of ciliary GPCRs in the context of the BBSome complex. *PLOS ONE,* 13: e0195005.
- Nozawa Y. I., Lin C., Chuang P.-T. (2013). Hedgehog signaling from the primary cilium to the nucleus: an emerging picture of ciliary localization, trafficking and transduction. *Current Opinion in Genetics & Development*, 23: 429–437.
- Oda T., Yagi T., Yanagisawa H., Kikkawa M. (2013). Identification of the outer-inner dynein linker as a hub controller for axonemal dynein activities. *Current Biology,* 23: 656-64.
- Oh Y. S., Wang E. J., Gailey C. D., Brautigan D. L., Allen B. L., Fu Z. (2019). Ciliopathy-Associated Protein Kinase ICK Requires Its Non-Catalytic Carboxyl-Terminal Domain for Regulation of Ciliogenesis. *Cells,* 8: 677.
- Okazaki M., Kobayashi T., Chiba S., Takei R., Liang L., Nakayama K., Katoh Y. (2020). Formation of the B9-domain protein complex MKS1-B9D2-B9D1 is essential as a diffusion barrier for ciliary membrane proteins. *Molecular Biology of the Cell,* 31: 2259-2268.
- Omori Y., Chaya T., Katoh K., Kajimura N., Sato S., Muraoka K., Ueno S., Koyasu T., Kondo M., Furukawa T. (2010). Negative regulation of ciliary length by ciliary male germ cell associated kinase (MAK) is required for retinal photoreceptor survival. *Proceedings of the National Academy of Sciences of USA,* 107: 22671–22676.
- Orback R., Howard J. (2019). The dynamic and structural properties of axonemal tubulins support the high length stability of cilia. *Nature Communications*, 10: 1838.
- Ou G., Blacque O. E., Snow J. J., Leroux M. R., Scholey J. M. (2005). Functional coordination of intraflagellar transport motors. *Nature,* 436: 583-587.
- Paintrand M., Moudjou M., Delacroix H., Bornens M. (1992). Centrosome organization and centriole architecture: their sensitivity to divalent cations. *Journal of Structural Biology*, 108: 107-128.
- Paul B. M., Vanden Heuvel G. B. (2014). Kidney: polycystic kidney disease. *WIREs Developmental Biology*, 3: 465–487.
- Pazour G. J., Agrin N., Leszyk J., Witman G. B. (2005). Proteomic analysis of a

eukaryotic cilium. *The Journal of Cell Biology,* 170: 103–113.

- Pazour G. J., Dickert B. L., Vucica Y, Seeley E. S., Rosenbaum J. L., Witman G. B., Cole D. G. (2000). *Chlamydomonas* IFT88 and its mouse homologue, polycystic kidney disease gene tg737, are required for assembly of cilia and flagella. *The Journal of Cell Biology*, 151: 709-718.
- Pazour G. J., Wilkerson C. G., Witman G. B. (1998). A dynein light chain is essential for the retrograde particle movement of intraflagellar transport (IFT). *The Journal of Cell Biology*, 141: 979–992.
- Pedersen L. B., Geimer, S., Rosenbaum, J. L. (2006). Dissecting the molecular mechanisms of Intraflagellar Transport in *Chlamydomonas. Current Biology*, 16: 450-459.
- Pedersen L. B., Geimer S., Sloboda R. D., Rosenbaum, J. L. (2003). The Microtubule plus end-tracking protein EB1 is localized to the flagellar tip and basal bodies in *Chlamydomonas reinhardtii*. *Current Biology,* 13: 1969–1974.
- Pedersen L. B., Miller M. S., Geimer S., Leitch J. M., Rosenbaum J. L., Cole, D. G. (2005). *Chlamydomonas* IFT172 is encoded by FLA11, interacts with CrEB1, and regulates IFT at the flagellar tip. *Current Biology,* 15: 262-266.
- Pedersen L. B., Schrøder J. M., Satir P., Christensen S. T. (2012). The Ciliary Cytoskeleton. *Comprehensive Physiology*, 2: 779–803.
- Perkins L. A., Hedgecock E. M., Thomson J. N., Culotti J. G. (1986). Mutant sensory cilia in the nematode *Caenorhabditis elegans. Developmental Biology*, 117: 456-87.
- Pettersen, E. F., Goddard T. D., Huang C. C., Couch G. S., Greenblatt D. M., Meng E. C., Ferrin T. E. (2004). UCSF Chimera? A visualization system for exploratory research and analysis. *Journal of Computational Chemistry*, 25: 1605–1612.
- Piao T., Luo M., Wang, L., Guo Y., Li D., Li P., Pan J., Snell W. J. (2009). A microtubule depolymerizing kinesin functions during both flagellar disassembly and flagellar assembly in *Chlamydomonas. Proceedings of National Academy of Sciences of USA*, 106: 4713–4718.
- Pigino G., Geimer S., Lanzavecchia S., Paccagnini E., Cantele F., Diener D. R., Rosenbaum J. L., Lupetti, P. (2009). Electron-tomographic analysis of intraflagellar transport particle trains in situ. *The Journal of Cell Biology*, 187: 135-148.
- Pigino G., Maheshwari A., Huy Bui K., Shingyoji C., Kamimura S., Ishikawa T. (2012). Comparative structural analysis of eukaryotic flagella and cilia from *Chlamydomonas*, *Tetrahymena*, and sea urchins. *Journal of Structural Biology,* 178: 199-206.
- Piperno G., Mead K. (1997). Transport of a novel complex in the cytoplasmic matrix of *Chlamydomonas* flagella. *Proceedings of the National Academy of Sciences of USA,* 94: 4457–4462.
- Plotnikova O. V., Nikonova A. S., Loskutov Y. V., Kozyulina P. Y., Pugacheva E. N., Golemis E. A. (2012). Calmodulin activation of Aurora-A kinase (AURKA) is required during ciliary disassembly and in mitosis. *Molecular Biology of the Cell,* 23: 2658–2670.
- Porter M. E., Bower R., Knott J. A., Byrd P., Dentler W. (1999). Cytoplasmic dynein heavy chain 1b is required for flagellar assembly in *Chlamydomonas. Molecular Biology of the Cell,* 10: 693–712.
- Powles-Glover N. (2014). Cilia and ciliopathies: classic examples linking phenotype

and genotype-An overview. *Reproductive Toxicology (Elmsford, N. Y.),* 48: 98–105.

- Praetorius H. A., Spring K. R. (2003). Removal of the MDCK cell primary cilium abolishes flow sensing. *Journal of Membrane Biology,* 191: 69-76.
- Praetorius H. A., Spring K. R. (2001). Bending the MDCK cell primary cilium increases intracellular calcium. *Journal of Membrane Biology,* 184: 71-79.
- Prevo B., Mangeol P., Oswald F., Scholey J. M., Peterman E. J. (2015). Functional differentiation of cooperating kinesin-2 motors orchestrates cargo import and transport in *C. elegans* cilia. *Nature Cell Biology*, 17: 1536-1545.
- Pröschold T., Darienko T., Krienitz L., Coleman A.W. (2018). *Chlamydomonas schloesseri* sp. nov. (*Chlamydophyceae, Chlorophyta*) revealed by morphology, autolysin cross experiments, and multiple gene analyses. *Phytotaxa,* 362: 21–38.
- Pugacheva E. N., Jablonski S. A., Hartman T. R., Henske E. P., Golemis E. A. (2007). HEF1-dependent aurora A activation induces disassembly of the primary cilium. *Cell,* 129: 1351–1363.
- Qin H., Diener D. R., Geimer S., Cole D. J., Rosenbaum J. L. (2004). Intraflagellar transport (IFT) cargo: IFT transports flagellar precursors to the tip and turnover products to the cell body. *The Journal of Cell Biology*, 164: 255-266.
- Quarmby L. M. (2004). Cellular deflagellation. *International Review of Citology,* 233: 47-91.
- Rasi M. Q.,Parker J. D. K., Feldman J. L., Marshall W. F., Quarmby L. M. (2009). Katanin Knockdown Supports a Role for Microtubule Severing in Release of Basal Bodies before Mitosis in *Chlamydomonas*. *Molecular Biology of the Cell,* 20: 379–388.
- Rezabkova L., Kraatz S. H. W., Akhmanova A., Steinmetz M. O., Kammerer R. A. (2016). Biophysical and Structural Characterization of the Centriolar Protein Cep104 Interaction Network. *The Journal of Biological Chemistry*, 291: 18496–18504.
- Reiter J. F., Blacque O. E., Leroux M. R. (2012). The base of the cilium: roles for transition fibres and the transition zone in ciliary formation, maintenance and compartmentalization. *EMBO Reports*, 13: 608-18.
- Reiter J. F., Leroux M. R. (2017). Genes and molecular pathways underpinning ciliopathies. *Nature Reviews Molecular Cell Biology*, 18: 533–547.
- Remacle C., Cardol P., Coosemans N., Gaisne M., Bonnefoy N. (2006). High-efficiency biolistic transformation of *Chlamydomonas* mitochondria can be used to insert mutations in complex I genes. *Proceedings of National Academy of Sciences of USA,* 103: 4771–4776.
- Reynolds E. S. (1963). The use of lead citrate at high pH as an electron-opaque stain in electron microscopy. *The Journal of Cell Biology*, 17: 208-2012.
- Ringo D. L. (1967). Flagella motion and fine structure of the flagellar apparatus in *Chlamydomonas. The Journal of Cell Biology,* 33: 543-571.
- Rogowski M., Scholz D., Geimer S. (2013) Chapter Fourteen—Electron Microscopy of Flagella, Primary Cilia, and Intraflagellar Transport in Flat-Embedded Cells. *Methods in Enzymology,* 524: 243-263.
- Sanders M. A, Salisbury J. L. (1994). Centrin plays an essential role in microtubule severing during flagellar excision in *Chlamydomonas reinhardtii*. *Journal of Cell Biology*, 124: 795–805.

- Sanders M. A., Salisbury J. L. (1989). Centrin-mediated microtubule severing during flagellar excision in *Chlamydomonas reinhardtii*. *Journal of Cell Biology*, 108: 1751–1760.
- Sang L., Miller J. J., Corbit K. C., Giles R. H., Brauer M. J., Otto E. A., Baye L. M., et al. (2011). Mapping the NPHP-JBTS-MKS protein network reveals ciliopathy disease genes and pathways. *Cell,* 145: 513-528.
- Santos N., Reiter J. F. (2008). Building it up and taking it down: The regulation of vertebrate ciliogenesis. *Developmental Dynamics,* 237: 1972–1981.
- Sasso S., Stibor H., Mittag M., Grossman A. R. (2018). From molecular manipulation of domesticated *Chlamydomonas reinhardtii* to survival in nature. *Elife*, 7: e39233.
- Satir P., Christensen S. T. (2007). Overview of Structure and Function of Mammalian Cilia. *Annual Review of Physiology*, 69: 377–400.
- Satir P., Mitchell D. R., Jékely G. (2008). How Did the Cilium Evolve? *Current Topics in Developmental Biology,* 85: 63–82.
- Satish-Tammana T. V., Tammana D., Diener D. R., Rosenbaum J. L. (2013). Centrosomal protein CEP104 (*Chlamydomonas* FAP256) moves to the ciliary tip during ciliary assembly. *Journal of Cell Science*, 126: 5018-5029.
- Schmidt K. N., Kuhns S., Neuner A., Hub B., Zentgraf H., Pereira G. (2012). Cep164 mediates vesicular docking to the mother centriole during early steps of ciliogenesis. *The Journal of Cell Biology*, 199: 1083–1101.
- Scholey J. M. (2013). Kinesin-2: a family of heterotrimeric and homodimeric motors with diverse intracellular transport functions. *Annual Review of Cell and Developmental Biology*, 29: 443–69.
- Schrøder J. M., Larsen J., Komarova Y., Akhmanova A., Thorsteinsson R. I., Grigoriev I., Manguso R., Christensen S.T., Pedersen S. F., Geimer S., et al. (2011). EB1 and EB3 promote cilia biogenesis by several centrosome-related mechanisms. *Journal of Cell Science*, 124: 2539–2551.
- Seixas C., Casalou C., Melo L. V., Nolasco S., Brogueira P., Soares H. (2003). Subunits of the chaperonin CCT are associated with Tetrahymena microtubule structures and are involved in cilia biogenesis. *Experimental Cell Research*, 290: 303–321.
- Seixas C., Cruto T., Tavares A., Gaertig J., Soares H. (2010). CCT and CCT Chaperonin Subunits Are Essential and Required for Cilia Assembly and Maintenance in Tetrahymena. *PLoS ONE*, 5: e10704.
- Signor D., Wedaman K. P., Orozco J. T., Dwyer N. D., Bargmann C. I., Rose L. S., Scholey J. M. (1999). Role of a class DHC1b dynein in retrograde transport of IFT motors and IFT raft particles along cilia, but not dendrites, in chemosensory neurons of living *Caenorhabditis elegans. The Journal of Cell Biology,* 147: 519–530.
- Soares H., Carmona B., Nolasco S., Melo L. V., Gonçalves J. (2019). Cilia Distal Domain: Diversity in Evolutionarily Conserved Structures. *Cells*, 8: 160.
- Sonar P., Youyen W., Cleetus A., Wisanpitayakorn P., Mousavi S. I., Stepp W. L., Hancock W. O., Tüzel E., Ökten Z. (2020). Kinesin-2 from *C. reinhardtii* Is an Atypically Fast and Auto-inhibited Motor that Is Activated by Heterotrimerization for Intraflagellar Transport. *Current Biology*, 30: 1160-1166.
- Sorokin S. (1968). Reconstructions of centriole formation and ciliogenesis in mammalian lungs. *The Journal of Cell Biology*, 3: 207–230.

- Sorokin S. (1962). Centrioles and the formation of rudimentary cilia by fibroblasts and smooth muscle cells. *The Journal of Cell Biology*, 15: 363-377.
- Stepanek L., Pigino G. (2016). Microtubule doublets are double-track railways for intraflagellar transport trains. *Science,* 352: 721-724.
- Stephens R. E., Lemieux N. A. (1999). Molecular chaperones in cilia and flagella: Implications for protein turnover. *Cell Motility and the Cytoskeleton*, 44: 274–283.
- Su X., Driscoll K., Yao G., Raed A., Wu M., Beales P. L., Zhou J. (2014). Bardet–Biedl syndrome proteins 1 and 3 regulate the ciliary trafficking of polycystic kidney disease 1 protein. *Human Molecular Genetics*, 23: 5441–5451.
- Sun S., Fisher R. L., Bowser S. S., Pentecost B. T., Sui H. (2019). Three-dimensional architecture of epithelial primary cilia. *Proceedings of the National Academy of Sciences of USA,* 116: 9370–9379.
- Sung C.-H., Leroux M. R. (2013). The roles of evolutionarily conserved functional modules in cilia-related trafficking. *Nature Cell Biology,* 15: 1387–1397.
- Swiderski R. E., Nakano Y., Mullins R. F., Seo S., Bànfi L. (2014). A mutation in the mouse ttc26 gene leads to impaired hedgehog signaling. *PLoS Genetics,* 10: e1004689.
- Takei R., Katoh Y., Nakayama K. (2018). Robust interaction of IFT70 with IFT52–IFT88 in the IFT-B complex is required for ciliogenesis. *Biology Open,* 7: bio033241.
- Tam L. W., Wilson N. F., Lefebvre P. A. (2007). A CDK-related kinase regulates the length and assembly of flagella in *Chlamydomonas*. *The Journal of Cell Biology*, 176: 819–829.
- Tanos B. E., Yang H.-J., Soni R., Wang W.-J., Macaluso F. P., Asara J.M., Tsou M.-F.B. (2013). Centriole distal appendages promote membrane docking, leading to cilia initiation. *Genes & Development*, 27: 163–168.
- Taschner M., Bhogaraju S., Lorentzen E. (2012). Architecture and function of IFT complex proteins in ciliogenesis. *Differentiation,* 83: S12–S22.
- Taschner M., Bhogaraju S., Vetter M., Morawetz M., Lorentzen E. (2011). Biochemical Mapping of Interactions within the Intraflagellar Transport (IFT) B Core Complex. *Journal of Biological Chemistry*, 286: 26344–26352.
- Taschner M., Kotsis F., Braeuer P., Kuehn E. W., Lorentzen E. (2014). Crystal structures of IFT70/52 and IFT52/46 provide insight into intraflagellar transport B core complex assembly. *The Journal of Cell Biology*, 207: 269–282.
- Taschner M., Lorentzen E. (2016). The Intraflagellar Transport Machinery. *Cold Spring Harbor Perspectives in Biology,* 8: a028092.
- Taschner M., Weber K., Mourão A., Vetter M., Awasthi M., Stiegler M., Bhogaraju S., Lorentzen E. (2016). Intraflagellar transport proteins 172, 80, 57, 54, 38, and 20 form a stable tubulin-binding IFT-B2 complex. *The EMBO Journal*, 35: 773-790.
- Tobin J. L., Beales P. L. (2009). The nonmotile ciliopathies. *Genetics in Medicine*, 11: 386–402.
- Toropova K., Mladenov M., Roberts A. J. (2017). Intraflagellar transport dynein is autoinhibited by trapping of its mechanical and track-binding elements. *Nature Structural & Molecular Biology*. 24: 461–468.
- Toropova K., Zalyte R., Mukhopadhyay A. G., Mladenov M., Carter A. P., Roberts A. J. (2019). Structure of the dynein-2 complex and its assembly with intraflagellar

transport trains. *Nature Structural & Molecular Biology*, 26: 823–829.

- Treier U., Fuchs S., Weber M., Wakarchuk W. W., Beck C. F. (1989). Gametic differentiation in *Chlamydomonas reinhardtii*: light dependence and gene expression patterns. *Archives of Microbiology,* 152: 572–577.
- Tsao C. C., Gorovsky M. A. (2008). Tetrahymena IFT122A is not essential for cilia assembly but plays a role in returning IFT proteins from the ciliary tip to the cell body. *Journal of Cell Science,* 121: 428–436.
- Tucker R. W., Pardee A. B., Fujiwara K. (1979). Centriole ciliation is related to quiescence and DNA synthesis in 3T3 cells. *Cell,* 17: 527-35.
- Vannuccini E., Paccagnini E., Cantele F., Gentile M., Dini D., Fino F., Diener D., Mencarelli C., Lupetti P. (2016). Two classes of short intraflagellar transport train with different 3D structures are present in *Chlamydomonas* flagella. *Journal of Cell Science*, 129: 2064-2074.
- Wachter S., Jung J., Shafiq S., Basquin J., Fort C., Bastin P., Lorentzen E. (2019). Binding of IFT22 to the intraflagellar transport complex is essential for flagellum assembly. *The EMBO Journal,* 38: e101251.
- Wallmeier J., Nielsen K. G., Kuehni C. E., Lucas J. S., Leigh M. W., Zariwala M. A., Omran H. (2020). Motile Ciliopathies. *Nature Reviews. Disease Primers,* 6: 77.
- Walther Z., Vashishtha M., Hall J. L. (1994). The *Chlamydomonas* FLA10 gene encodes a novel kinesin-homologous protein. *The Journal of Cell Biology*, 126: 175–188.
- Wang L., Dynlacht B.D. (2018). The regulation of cilium assembly and disassembly in development and disease. *Development*, 145: dev151407.
- Wang Z., Fan Z. C., Williamson S. M., Qin H. (2009). Intraflagellar transport (IFT) protein IFT25 is a phosphoprotein component of IFT complex B and physically interacts with IFT27 in *Chlamydomonas*. *PLoS ONE*, 4: e5384.
- Wang Y., Ren Y., Pan J. (2019). Regulation of flagellar assembly and length in *Chlamydomonas* by LF4, a MAPK-related kinase. *The FASEB Journal,* 33: 6431–6441.
- Waters A. M., Beales P. L. (2011). Ciliopathies: an expanding disease spectrum. *Pediatric Nephrology,* 26: 1039–1056.
- Webb S., Mukhopadhyay A. G., Roberts A. J. (2020). Intraflagellar transport trains and motors: Insights from structure. *Seminars in Cell & Developmental Biology,* 107: 82–90.
- Wedaman K. P., Meyer D. W., Rashid D. J., Cole D. G., Scholey D. G. (1996). Sequence and submolecular localization of the 115-kD accessory subunit of the heterotrimeric kinesin-II (KRP85/95) complex. *The Journal of Cell Biology,* 132: 371–380.
- Wei Q., Zhang Y., Li Y., Zhang Q., Ling K., Hu J. (2012). The BBSome controls IFT assembly and turnaround in cilia. *Nature Cell Biology,* 14: 950–957.
- Wheatley D. N. (1969). Cilia in cell-cultured fibroblasts. I. On their occurrence and relative frequencies in primary cultures and established cell lines. *Journal of Anatomy*, 105: 351–362.
- Wheway G., Lord J., Baralle D. (2019). Splicing in the pathogenesis, diagnosis and treatment of ciliopathies. *Biochimica and BiophysicaActa. Gene Regulatory*

Mechanisms, 1862: 194433.

- Williams C. L., McIntyre J. C., Norris S. R., Jenkins P. M., Zhang L., Pei Q., Verhey K., Martens J. R. (2014). Direct evidence for BBSome-associated intraflagellar transport reveals distinct properties of native mammalian cilia. *Nature Communications*, 5: 5813.
- Wiegering A., Rüther U., Gerhardt C. (2019). The Role of Primary Cilia in the Crosstalk between the Ubiquitin–Proteasome System and Autophagy. *Cells*, 8: 241.
- Wilson N. F., Lefebvre P. A. (2004). Regulation of flagellar assembly by glycogen synthase kinase 3 in *Chlamydomonas reinhardtii*. *Eukaryotic Cell,* 3: 1307–1319.
- Wingfield J. L., Mengoni I., Bomberger H., Jiang Y. Y., Walsh J. D., Brown J. M., Picariello T., Cochran D. A., Zhu B., Pan J. et al. (2017). IFT trains in different stages of assembly queue at the ciliary base for consecutive release into the cilium. *ELife*, 6: e26609.
- Wood C., Rosenbaum J. (2014). Proteins of the Ciliary Axoneme Are Found on Cytoplasmic Membrane Vesicles during Growth of Cilia. *Current Biology,* 24: 1114–1120.
- Xue B., Liu Y.-X., Don B., Wingfield J. L., Wu M., Sun J., Lechtreck K. F., Fan Z-C. (2020). Intraflagellar transport protein RABL5/IFT22 recruits the BBSome to the basal body through the GTPase ARL6/BBS3. *Proceedings of the National Academy of Sciences of USA,* 117: 2496–2505.
- Yamazoe T., Nagai T., Umeda S., Sugaya Y., Mizuno K. (2020). Roles of TOG and jelly-roll domains of centrosomal protein CEP104 in its functions in cilium elongation and Hedgehog signaling. *Journal of Biological Chemistry*, 295: 14723-14736.
- Ye F., Nager A. R., Nachury M. V. (2018). BBSome trains remove activated GPCRs from cilia by enabling passage through the transition zone. *The Journal of Cell Biology,* 217:1847-1868.
- Zhao C., Malicki J. (2011). Nephrocystins and MKS proteins interact with IFT particle and facilitate transport of selected ciliary cargos. *The EMBO Journal,* 30: 2532–2544.
- Zimmerman K. W. (1898). Beitrage zur kenntnis einiger Drusen und Epithelien. *Archiv für mikroskopische Anatomie,* 52: 552–706.
- Zhu X., Wang J., Li S., Lechtreck K., Pan J. (2020). IFT54 directly interacts with kinesin-II and IFT dynein to regulate anterograde intraflagellar transport. *The EMBO Journal*, e105781.